

Frederik Weber

Reaktionen von Methanol auf  
Pd(111), Pd/Zn- und Pd/ZnO-  
Oberflächen

**DIPLOMARBEIT**

zur Erlangung des akademischen Grades  
Diplom-Ingenieur

Diplomstudium Technische Physik



**Technische Universität Graz**

Betreuer:

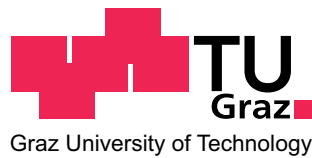
Ao.Univ.Prof.Mag.Dr.rer.nat. Robert Schennach  
Institut für Festkörperphysik

Graz, April 2010

Frederik Weber

Reactions of methanol on Pd(111),  
Pd/Zn- and Pd/ZnO- surfaces

DIPLOMA THESIS



Graz University of Technology

Adviser:

Ao.Univ.Prof.Mag.Dr.rer.nat. Robert Schennach  
Institut of Solid State Physics

Graz, April 2010

Deutsche Fassung:  
Beschluss der Curricula-Kommission für Bachelor-, Master- und Diplomstudien vom 10.11.2008  
Genehmigung des Senates am 1.12.2008

## EIDESSTÄTLICHE ERKLÄRUNG

Ich erkläre an Eides statt, dass ich die vorliegende Arbeit selbstständig verfasst, andere als die angegebenen Quellen/Hilfsmittel nicht benutzt, und die den benutzten Quellen wörtlich und inhaltlich entnommene Stellen als solche kenntlich gemacht habe.

Graz, am .....

.....  
(Unterschrift)

Englische Fassung:

## STATUTORY DECLARATION

I declare that I have authored this thesis independently, that I have not used other than the declared sources / resources, and that I have explicitly marked all material which has been quoted either literally or by content from the used sources.

.....  
date

.....  
(signature)

## Danksagung

Diese Diplomarbeit entstand unter der Leitung von Herrn Ao.Univ.-Prof.Dr. Robert Schennach am Institut für Festkörperphysik der Technischen Universität Graz. Hiermit möchte ich mich für die überaus freundschaftliche und kompetente Betreuung von Herrn Professor Schennach bedanken. Mein ganz besonderer Dank gilt auch Herrn Dr. DI Hans Peter Koch, Herrn DI Gunther Weirum, sowie Herrn DI Jörg Killmann, die mir mit Rat und Tat zur Seite standen.

Weiters gebührt mein Dank auch allen anderen Angehörigen des Institutes, allen voran: DI Eduard Gilli, B.Sc. Mario Djak, Prof. Dr. Manfred Leisch, Prof. Dr. Adolf Winkler. Schlußendlich soll auch die tatkräftige Unterstützung von Herrn Martin Kornschöber hier nicht unerwähnt bleiben.

## Abstract

During this diploma thesis the methanol desorption from Pd(111), Pd/Zn, Pd/ZnO with partly oxidized ZnO and Pd/ZnO with fully oxidized ZnO has been studied by thermal desorption experiments (TDS) and reflection absorption infrared spectroscopy (RAIRS). Furthermore it was investigated if ZnO shows a wurzit structure on Pd(111). If this is the case there would be different terminations, depending on the oxidation of the ZnO layers. To check if this theory is right, pyridine was exposed to Pd/ZnO because pyridine goes into physisorption with oxygen and chemisorption with metal atoms. The different strength of bond type has to lead to a shift of the peaks in the IR- and TPD-spectrum. After pyridine was adsorbed on the surface, several TDS and RAIRS measurements of pyridine desorption from Pd/ZnO were done to draw conclusions from the bond type of pyridine on Pd/ZnO. Hence information of the structure of ZnO on Pd(111) are obtained. The measurements have shown that there is no shift of the peaks (neither IR-peaks nor TDS-peaks). Therefore it seems that there is always the same surface structure or rather termination independent from the oxidation level of the surface. According to the DFT-theory ZnO does not form a wurzit structure but a bor-nitride-structure up to 4 ML. TDS measurements of methanol desorption from Pd/Zn or rather Pd/ZnO yielded the result that methanol dissociation takes place at the interfaces of Pd and Zn/ZnO. Furthermore, methanol desorption leads to a zinc desorption if the Zn coverage is below 1 ML. RAIRS measurements of methanol desorption from Pd(111), Pd/Zn and Pd/ZnO have shown that the reaction process is much more complicated than expected. The whole process is sensitive to the temperature where methanol adsorption takes place. More detailed information about the reaction paths were not received because of the complexity of the whole system. Therefore further investigations are necessary.

## Zusammenfassung

Während dieser Diplomarbeit wurde die Methanoldesorption von Pd(111), Pd/Zn, Pd/ZnO mit schwach oxidiertem ZnO und Pd/ZnO mit stark oxidiertem ZnO, mittels der Thermodesorptionsspektroskopie (TDS) und Reflektions-Absorption-Infrarot-Spektroskopie (RAIRS) untersucht. Weiters wurde überprüft, ob ZnO eine Wurzitstruktur auf Pd(111) bildet. Wäre dies der Fall, würde es je nach Oxidierungsgrad der ZnO Schichten zu unterschiedlichen Terminierungen der Oberfläche kommen. Zur Überprüfung dieser Hypothese wurde Pyridin auf Pd/ZnO mit unterschiedlich oxidierten ZnO Schichten adsorbiert, da Pyridin auf Sauerstoff physisorbiert und auf Metallatomen chemisorbiert. Durch die unterschiedlichen Bindungsarten mit ihren unterschiedlichen Bindungsstärken muss es zu einer Verschiebung der Peaks im IR- und TDS-Spektrum kommen, sofern unterschiedliche Terminierungen gegeben sind. Nach der Pyridinadsorption wurden nun TDS, sowie RAIRS Messungen durchgeführt, um Rückschlüsse auf die Bindungsart von Pyridin auf der Probenoberfläche ziehen zu können. Daraus konnte wiederum auf die Struktur von ZnO auf Pd geschlossen werden. Es stellte sich heraus, dass ZnO auf Pd(111) offenbar keine Wurzitstruktur wie angenommen bildet, da es zu keiner Peakverschiebung gekommen ist. Der DFT-Theorie zufolge bildet ZnO keine Wurzitstruktur auf Pd(111), sondern eine Bor-Nitrid Struktur, bis zu einer Bedeckung von 4 ML. Dies würde mit den erhaltenen Ergebnissen zusammen passen. Die TDS Messungen der Methanoldesorption enthüllten, dass die Methanolzersetzung an den Grenzflächen Pd/Zn bzw. Pd/ZnO stattfindet. Weiters führt die Methanolzersetzung zu einer Zinkdesorption, wenn die Zinkbedeckung der Probe unter 1 ML ist. Die RAIRS Messungen der Methanoldesorption von Pd(111), Pd/Zn und Pd/ZnO haben gezeigt, dass der Reaktionsablauf auf der Oberfläche komplizierter ist als angenommen. Der gesamte Prozess ist empfindlich von der Temperatur abhängig, bei der Methanol adsorbiert wird. Genauere Aussagen über die Reaktionswege konnten auf Grund der Komplexität des gesamten Systems nicht gewonnen werden. Daher sind weitere Untersuchungen notwendig, um die genauen Reaktionswege zu ermitteln.

# Contents

|   |            |
|---|------------|
| <b>1. Motivation</b>  | <b>2</b>   |
| <b>2. Experimental Setup</b>  | <b>4</b>   |
| 2.1. The Measuring Equipment . . . . .                                      | 4          |
| 2.1.1. The Sample and Sample Mounting . . . . .                             | 9          |
| 2.2. LEED . . . . .   | 10         |
| 2.2.1. LEED - set up . . . . .  | 10         |
| 2.2.2. LEED - theoretical background . . . . .                              | 12         |
| 2.3. XPS . . . . .  | 14         |
| 2.4. QMS . . . . .  | 16         |
| 2.5. FTIR . . . . .   | 18         |
| 2.6. Thermal Desorption Spectroscopy . . . . .                              | 20         |
| 2.7. Sputter gun . . . . .  | 23         |
| 2.8. Zn Evaporator . . . . .  | 23         |
| <b>3. Adsorption of pyridine on ZnO films on Pd(111)</b>                    | <b>24</b>  |
| 3.1. Sample cleaning . . . . .  | 24         |
| 3.2. ZnO deposition on Pd(111) . . . . .                                    | 25         |
| 3.3. Pyridine adsorption on ZnO . . . . .                                   | 29         |
| <b>4. TDS - study of methanol desorption from Pd(111), Pd/Zn and Pd/ZnO</b> | <b>32</b>  |
| 4.1. TDS - Results . . . . .  | 32         |
| 4.1.1. 1 <sup>st</sup> Measurement series . . . . .                         | 34         |
| 4.1.2. 2 <sup>nd</sup> Measurement series . . . . .                         | 49         |
| 4.1.3. 3 <sup>rd</sup> Measurement series . . . . .                         | 56         |
| 4.2. TDS - Summary . . . . .  | 62         |
| <b>5. IR - study of methanol desorption from Pd(111), Pd/Zn and Pd/ZnO</b>  | <b>63</b>  |
| 5.1. IR - Results . . . . .   | 63         |
| 5.1.1. Methanol desorption from Pd(111) . . . . .                           | 63         |
| 5.1.2. Methanol desorption from Pd/Zn . . . . .                             | 66         |
| 5.1.3. Methanol desorption from Pd/ZnO . . . . .                            | 79         |
| 5.2. IR - Summary . . . . .   | 101        |
| <b>6. IR/TDS - Comparison</b>   | <b>102</b> |
| 6.1. Introduction . . . . .   | 102        |

---

|   |            |
|---|------------|
| 6.2. Discussion . . . . .   | 103        |
| 6.2.1. IR/TDS-results: Methanol . . . . .                         | 103        |
| 6.2.2. IR/TDS-results: Formaldehyde . . . . .                     | 104        |
| 6.2.3. IR/TDS-results: Formate . . . . .                          | 104        |
| 6.2.4. IR/TDS-results: Carbon dioxide . . . . .                   | 105        |
| 6.2.5. IR/TDS-results: Remaining species . . . . .                | 105        |
| <b>7. Summary</b>   | <b>106</b> |
| 7.1. Pyridine adsorption on Pd/ZnO . . . . .                      | 106        |
| 7.2. Methanol desorption from Pd(111), Pd/Zn and Pd/ZnO . . . . . | 107        |
| <b>A. Appendix - Matlab Program and Calculated Values</b>         | <b>115</b> |

# 1. Motivation

Nowadays alternative energy resources instead of oil are becoming more and more of interest. Especially hydrogen has the potential to replace fossil fuels. Hydrogen as an energy carrier could be used as fuel in hydrogen fuel cells. This technology is expected to achieve a cleaner and much more flexible energy system in the near future.

An archetypal example of a fuel cell is the so called Proton Exchange Membrane Fuel Cell (PEMFC) which is schematically shown in figure 1.1. A fuel cell consists of electrodes which are separated from each other by a proton-conducting electrolyte membrane. Hydrogen is applied to the anode where it dissociates into protons and electrons. Because of the electronically insulating membrane the electrons are forced to travel in an external circuit where they perform electric work. The protons migrate through the membrane to the cathode. At the cathode the electrons which have travelled through the external circuit react with oxygen molecules. These negative charged oxygen molecules react with the protons to form water.

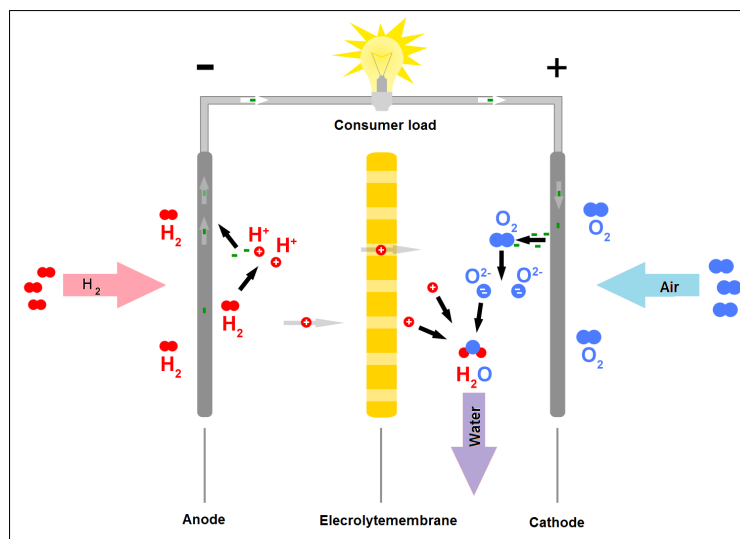
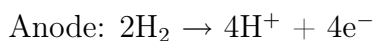


Figure 1.1.: Schematic description of a PEMFC; adapted from [1]

The following reaction equations apply for PEMFCs:

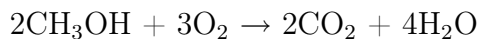


In order to make this technology commercially useable, the production and storage of hydrogen in an efficient and economic way is an important issue. This is why several groups are working on different ways to gain hydrogen. One way to obtain hydrogen is by steam reforming methanol. For this a catalytic system is needed. Several catalyst systems have been studied in the last few years. First different copper systems were in use but as the melting point of Pd is higher than that of Cu nowadays Pd is the favorite substrate. Especially two systems have shown superior catalytic performance, Pd/Zn and Pd/ZnO [2, 3, 4, 5].

Methanol can then be used in Direct Methanol Fuel Cells (DMFC) as the power source for mobile phones or laptops. DMFCs use hydrogen which is produced by the dehydrogenation reaction of methanol. The following reaction equations apply for DMFCs which are based on the oxidation of methanol on a catalyst layer to form carbon dioxide and hydrogen:



This results in following net reaction:



Although Pd/Zn and Pd/ZnO were investigated in the last decade, the reaction mechanism of methanol dissociation are not known in detail. This diploma thesis deals with TDS and RAIRS investigations of the methanol decomposition on Pd(111), Pd/Zn and Pd/ZnO to get an overview of the reactivity of each compound. Moreover, the structure-hypothesis, stemming from STM results of ZnO submonolayers on a Pd(111) crystal, were studied via pyridine adsorption and desorption.

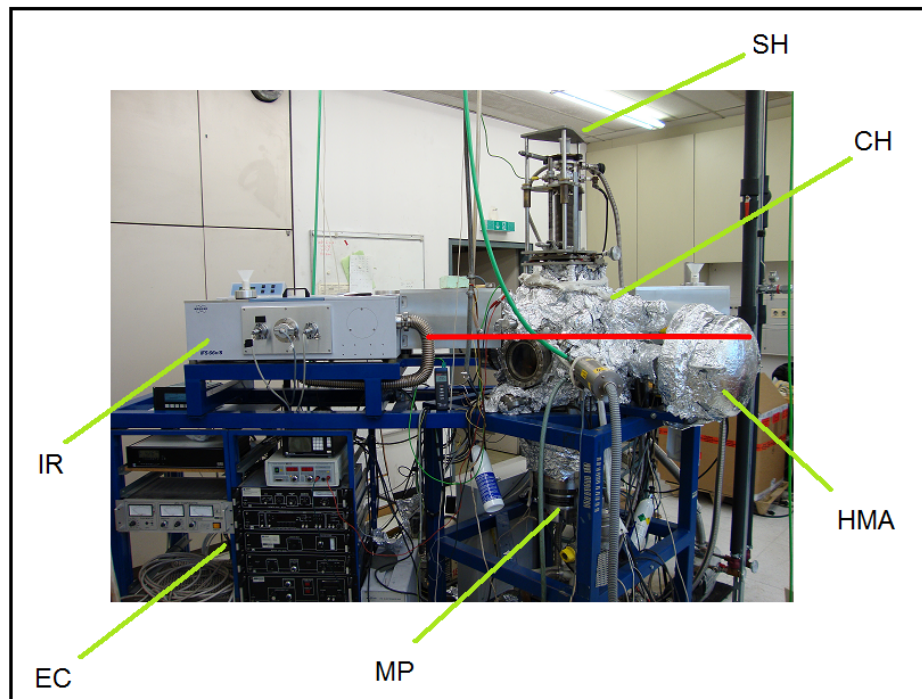
## 2. Experimental Setup

### 2.1. The Measuring Equipment

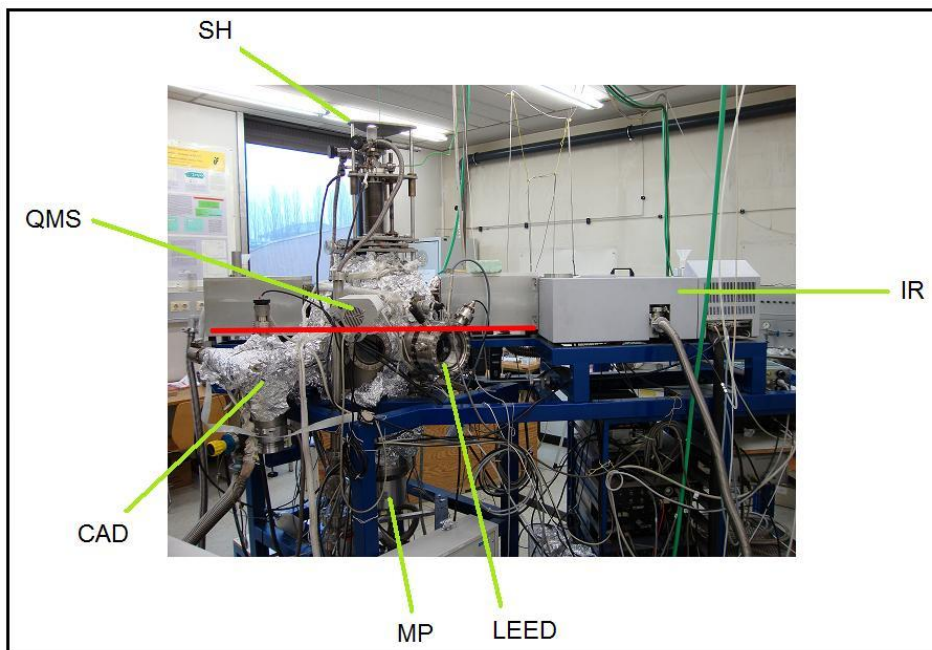
The experiments were done in an ultrahigh vacuum chamber (UHV) which is shown in figure 2.1, figure 2.2 and figure 2.3. UHV is needed to keep the sample surface clean from adsorbates of the residual gas. The time till the sample surface is covered with atoms and molecules from the residual gas depends on the pressure and the sticking probability. At a pressure of  $\leq 10^{-10}$  mbar the cleanliness of the surface was assured for at least three hours. So several experiments can be done without sample cleaning. Whereas the two pictures in figure 2.1 give an overview of the hole machine, a schematic view of the two levels is given in figure 2.2 and figure 2.3.

Figure 2.1 exhibits the whole machine from both sides (front side and back side). The UHV chamber (CH in figure 2.1) consists of the sample mounted on a manipulator (SH) and the analytical devices which are organized in two levels around the chamber. Figure 2.1(a) shows the front side of the machine. There the infrared spectrometer (IR) is seen. Beneath the infrared spectrometer there are the electric controls (EC) of the measurement devices. Beneath the measurement chamber (CH) and next to the electric controls the main pump (MP) can be seen. The hemispherical mirror analyser (HMA) which was used for XPS-measurements is seen on the right hand side of figure 2.1(a).

Figure 2.1(b) shows the back side of the machine. There the sample holder/manipulator (SH), the infrared spectrometer (IR) and the main pump (MP) are seen again. Additionally the low energy electron diffraction (LEED), the capillar array doser (CAD) and the quadrupole mass spectrometer (QMS) are seen in this figure. The red line in figure 2.1 symbolizes the borderline between higher level and lower level.



(a) Front side of the machine



(b) Back side of the machine

Figure 2.1.: UHV-chamber; Red line divides the machine into lower and higher level

- SH - sample holder
- CH - UHV-chamber
- IR - infrared spectrometer
- EC - electric control
- MP - main pump
- HMA - hemispherical mirror analyser
- LEED - low energy electron diffraction
- QMS - quadrupole mass spectrometer
- CAD - capillar array doser

A detailed view of the machine is given in figure 2.2 where a schematic of the lower level is shown. The chamber is mainly pumped by two turbo molecular pumps (Pfeifer TPU 1501 P, 1450 l/s, TMP1; Pfeifer Balzers TPH 170, 170 l/s, TMP2) which are connected in a serial adjustment with a rotary vane pump (Leybold Trivac D253, 25  $m^3/h$ , RVP1) as a fore-vacuum pump. This configuration ensures a better exhausting rate. The total pressure in the chamber is measured by a Bayard-Alpert ion gauge (Leybold Ionivasc IM 520, IG in figure 2.2) and by an extractor (EXT in figure 2.2).

On the top of this picture you can see the x-ray-source (XA) and the hemispherical mirror analyser (HMA) for XPS-measurements. Auger electron spectroscopy is possible with the electron gun (EG) in combination with the HMA.

Next to the electron gun the capillar array doser (CAD), which was used to dose pyridine or methanol (depending on the experiment), is seen. An additional turbo molecular pump (TMP4) with a rotary vane pump (RVP2) is connected to the CAD to ensure a stable exhausting rate. A side arm with an angle valve is connected to the CAD. This valve was always open for pyridine/methanol dosing. The methanol as well as the pyridine was cleaned by several freeze and thaw cycles. Beneath the CAD the used gases (argon and oxygen) and next to the gases the low energy electron diffraction (LEED in figure 2.2; Specs ErLEED 150) are shown. Argon was used for sputtering, oxygen for ZnO fabrication.

About fifteen centimeters above the lower level the upper level hosts the other measuring and manipulating instruments. At the higher level (figure 2.3) the sputter gun (Perkin Elmer PHI Model 04-161 Sputter Ion Gun; SG in figure 2.3) which is mounted at a distance of 5 cm to the sample, can be found. To the right of the sputter gun the infrared source (Bruker IFS 66 v/S FTIR; IRS in figure 2.3) is seen. A description of the infrared source is found in chapter 2.5. Above the IRS, the zinc evaporator (ZE) can be seen, which was used for zinc evaporation. On the top of figure 2.3 the quartz microbalance (QMB) can be found. Next to the QMB the infrared detector, an external nitrogen cooled mercury-cadmium-telluride (MCT) detector, (IRD in figure 2.3) is shown. At last there is the used quadrupol-mass-spectrometer (Pfeiffer QMS 200; QMS). The red line in figure 2.3 symbolizes the infrared beam coming from the IRS. The beam is reflected from the sample and hits the IRD.

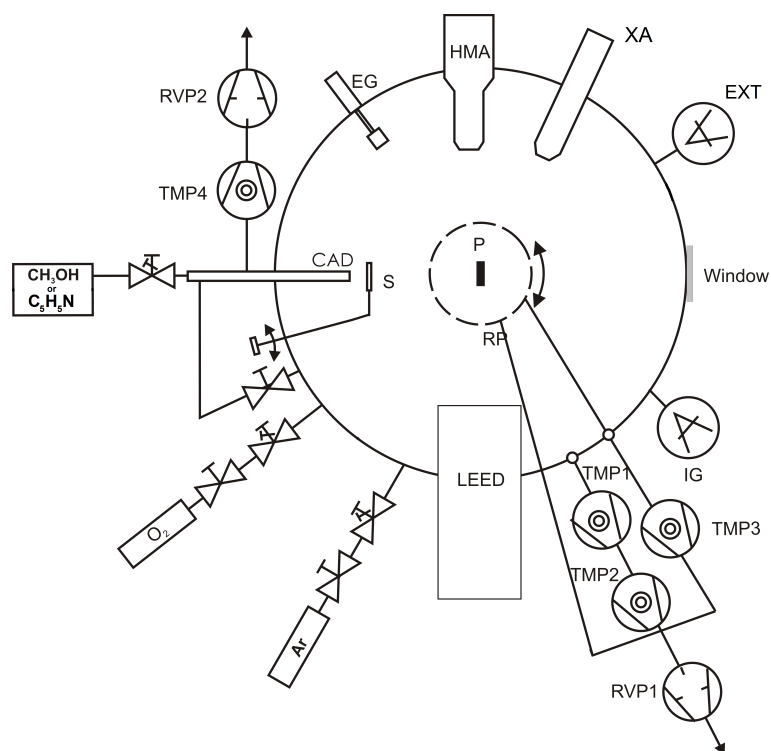


Figure 2.2.: UHV chamber and measuring instruments at lower level; adapdet from [6]

- CAD - capillary array doser
- EG - electron gun
- EXT - extractor
- GFG - gas friction gauge
- HMA - hemispherical mirror analyser
- IG - ionisation gauge
- P - sample
- RP - rotatable platform
- S - shutter
- XA - X-ray anode
- LEED - Low Energy Electron Diffraction
- TMP - turbo molecular pump
- RVP - rotary vane pump.

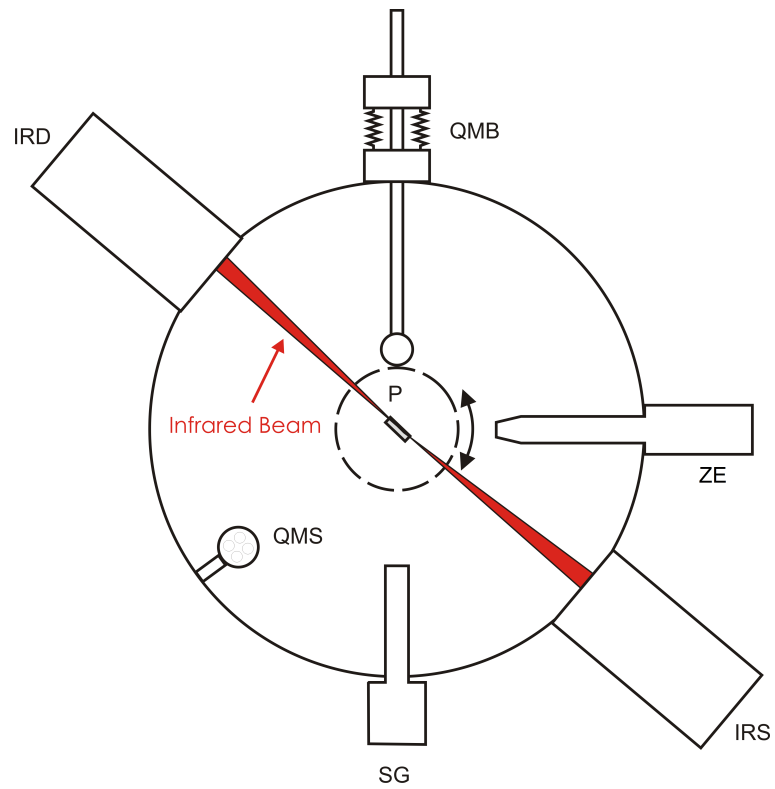
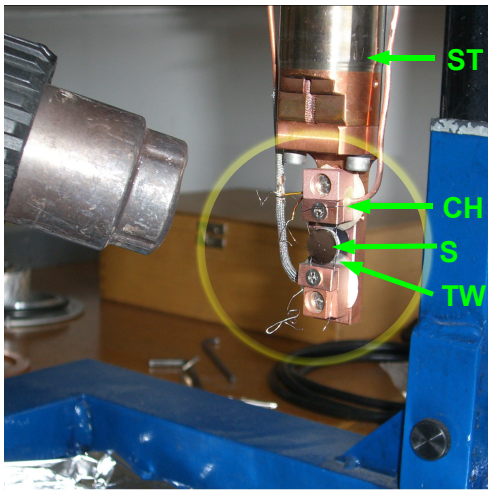


Figure 2.3.: UHV Chamber and measuring instruments at upper level; adapted from [6]

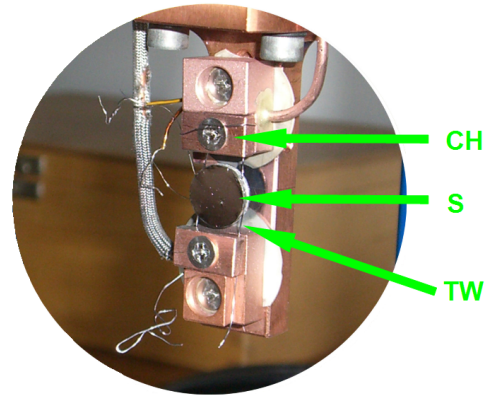
ZE - zinc evaporator,  
IRS - infrared source,  
IRD - infrared detector  
P - sample,  
QMB - quartz microbalance,  
QMS - quadrupole mass spectrometer,  
SG - sputter gun

### 2.1.1. The Sample and Sample Mounting

The sample was mounted on a manipulator (described in the PhD thesis of G.Krenn [7] in detail). It enables to change the sample position  $\pm 3$  cm in x- and y-direction and 20 cm in z-direction. The rotation of the manipulator is restricted to  $270^\circ$ . The sample (S) mounted on the manipulator is shown in figure 2.4. The sample disc provides a groove. So the sample is fixed to the copper holder by tantalum wires (CH and TW in the right picture of figure 2.4) which are fit into this groove, forming two intricate loops and enable resistive heating of the sample. Furthermore, these wires are responsible for the cooling by thermal conduction. The main part of the manipulator is a hollow steel tube (ST) which was filled with liquid nitrogen for sample-cooling.



(a) Sample and manipulator



(b) Sample and copper holder

Figure 2.4.: The Pd(111) sample, mounted on the manipulator

ST - Steel tube

CH - copper holder

S - sample

TW - tantalum wire

## 2.2. LEED

### 2.2.1. LEED - set up

Low Energy Electron Diffraction (LEED) was used for surface structure analysis. This measuring method allows structure determination of thin films and of clean and adsorbate covered crystal surfaces. A short overview is given below (for further descriptions and technical data of the used Specs ErLEED 150 see [8] or [9])

A schematic diagram of a LEED-system is shown in figure 2.5 and figure 2.6 as well as a schematic diagram of the used ErLEED 150 optics with the LEED flange in figure 2.7.

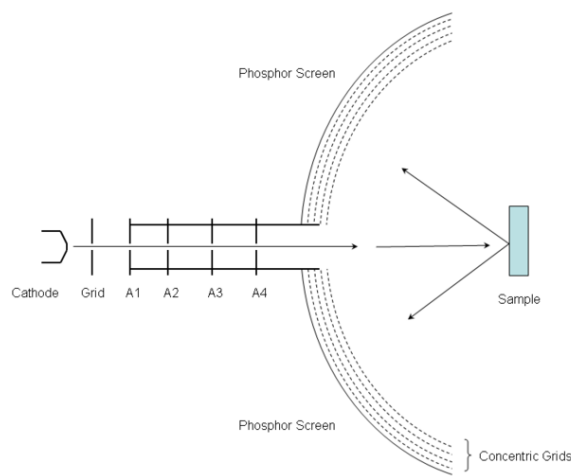


Figure 2.5.: Schematic diagram of an LEED; adapted from [10]

The LEED is composed of the electron gun (Cathode in figure 2.5), the grids and the fluorescent screen. The electron gun produces a beam of collimated low energy electrons whose energies can be varied between 0 - 1000 eV. At the well ordered sample surface these electrons are scattered which is symbolized in figure 2.5 where you can see the scattered electrons propagating to the fluorescent screen. In figure 2.5 it is shown that the screen and the grids are arranged concentrically with the sample position in the center of this arrangement. The de Broglie wavelength of an electron is given by

$$\lambda = \frac{h}{\sqrt{2mE}}, \quad \lambda[\text{\AA}] = \sqrt{\frac{150}{E(\text{eV})}} \quad (2.1)$$

The energy of the electron gun is set in such way that the electrons have a wavelength ( $\approx 0.5 - 2\text{\AA}$ ) where atomic diffraction conditions are ensured.

The configuration of a LEED is shown in more detail in figure 2.6. The electron gun with a diameter of 15 mm consists of the cathode (C) (Thoria coated Iridium), the Wehnelt Cylinder (W), a double anode (A) and 4 lens elements (L1 -L4). The grids are fabricated out of molybdenum which is gold coated to avoid potential changes. The sample as well as the grid G4 are on earth potential so the scattered electrons propagate through a field-free zone towards the grid. To avoid that inelastic scattered electrons hit the screen the grids G3 and G2 are on a potential close to the cathode. To insulate the other grids from the screen, the last grid G1 is on earth potential again.

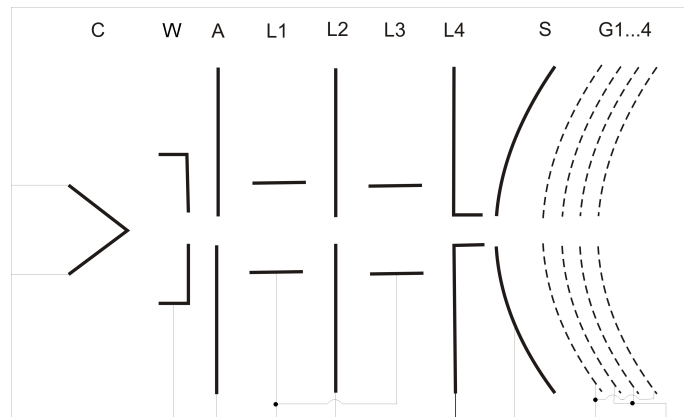


Figure 2.6.: Block diagram of the ErLEED

- C - cathode,
- W - Wehnelt cylinder,
- A - double anode,
- L1,L2,L3 - lens,
- S - Screen,
- G1...4 - grids

The elastic scattered electrons hit the fluorescent screen (S) where they cause a light spot. So a diffraction pattern in the form of the reciprocal lattice of the sample is observed.

Because of the finite space in the used vacuum chamber, it was necessary to use the z-retraction mechanism to extend and withdraw the optics. This component is driven by a UHV rotary drive on the LEED flange. The z-retraction mechanism is shown in figure 2.7 which shows the front side of the LEED. In this figure you can see as well the 12-way feedthrough and the HV feedthrough of the electric control unit. An optional shutter feedthrough which was not in use, is shown too.

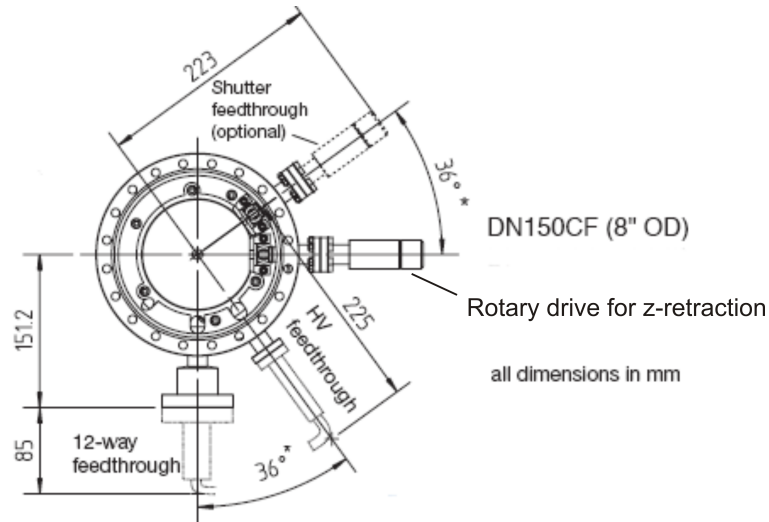


Figure 2.7.: Schematic view of the ErLEED150 optics and the LEED flange; adapted from [11]

### 2.2.2. LEED - theoretical background

The basis for interference of electrons at crystal surfaces is the de Broglie equation 2.2. Constructive interference at a periodic array takes place if the scattered waves from neighbouring lattice points have a path difference of multiples of the wavelength  $\lambda$ .

$$\lambda = \frac{h}{mv} \quad (2.2)$$

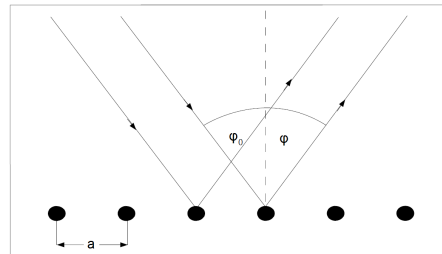


Figure 2.8.: Scattering of a plane wave at a one-dimensional periodic lattice; adapted from [9]

If the incident angle of the primary wave, which strikes the surface, is  $\varphi_0$ , interference of the backscattered waves occurs in direction  $\varphi$  (figure 2.8).  $\varphi$  is given by the condition in equation 2.3.

$$a(\sin\varphi - \sin\varphi_0) = n\lambda \quad (2.3)$$

$n$  is an integer, denoting the order of diffraction,  $a$  is the distance between the periodically arranged scatters, as you can see in figure 2.8.

A two dimensional, periodical array of lattice points may be considered as an ensemble of parallel rows of scatters with directions  $[h' k']$  and mutual distances  $d_{h'k'}$ . Under these terms of conditions, interference maxima are to be expected in directions  $\varphi$  given by equation 2.4.

$$d_{h'k'}(\sin\varphi - \sin\varphi_0) = n\lambda \quad (2.4)$$

Because LEED experiments are performed with normal incidence of the primary electrons ( $\varphi_0 = 0$ ) equation 2.4 simplifies to equation 2.5 :

$$\sin\varphi = \frac{n\lambda}{d_{h'k'}} \approx \frac{n}{d_{h'k'}} \cdot \sqrt{\frac{150}{U}} \quad (2.5)$$

with the electron energy  $U$  in [eV] and the distances  $d_{h'k'}$  in [ $\text{\AA}$ ]. Each atomic row will give rise to a series of diffraction maxima  $nh'$  and  $nk'$  with different order of diffraction  $n$ . Typically  $n$  is included in the Miller indices  $h'$  and  $k'$  which result in the Laue indices  $h = nh'$ ,  $k = nk'$ . So equation 2.5 for interference at normal incidence turns to equation 2.6:

$$\sin\varphi = \frac{n}{d_{hk}} \cdot \sqrt{\frac{150}{U}} \quad (2.6)$$

So a particular reflex  $(hk)$  will appear at an electron energy

$$U = \frac{150}{d_{hk}^2} \quad (2.7)$$

for the first time. The position of the first diffraction maxima depends on the size of the unit cell. The larger the unit cell, the closer the first maxima will be located to the surface normal. With rising electron energy, the diffraction maxima move towards the  $(0,0)$ -reflex, which corresponds to direct reflection. So a complete description of the directions of the interference maxima is given by this simple treatment. The directions can be observed directly in a typical LEED equipment which allows to determine the  $d_{hk}$  and therefore the geometry of the unit cell. Important to say is that the arrangement of the atoms within the unit cell cannot be derived by analyzing the positions of the diffraction maxima on the fluorescence screen. For this an analysis of the information contained in the intensities is necessary [9].

## 2.3. XPS

X-ray photoelectron spectroscopy was mainly used to ensure a clean sample surface but also to analyze the chemical composition of the surface. The experimental arrangement for XPS - measurements is shown schematically in figure 2.9.

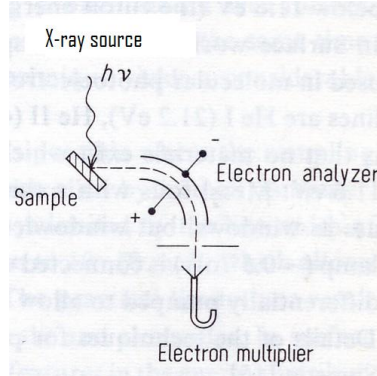


Figure 2.9.: Schematic diagram of the experimental arrangement for photoelectron spectroscopy of solids; adapted from [9]

The essential components are (figure 2.9) the light source (x-ray tube), the electron analyzer and of course the sample. The used x-ray tube has a switchable twin-anode with two different anode materials, aluminum and magnesium, providing characteristic radiation on a bremsstrahlung background. The switchable twin-anode enables the separation of photoemitted electrons whose energy depends on the photon energy. In all experiments the Mg-Anode with  $Mg - K_{\alpha}$  (1253.6 eV) radiation was used. The used detector is based on a concentric hemispherical analyzer together with a retarding lens system which decelerate the incoming electrons in order to improve the resolution. An electron multiplier (channeltron) was used to detect the electrons.

The principle of the XPS-measurement is simple: Bound electrons of the sample are knocked out by X-ray radiation. Knowing the energy of the photons  $h\nu$  and of the work function of the detector  $\phi$  allows to calculate the binding energy  $E_b$  by the kinetic energy  $E_{kin}$  of the free electron as it is shown in the energetic level diagram for X-ray spectroscopy in figure 2.10 [9]. The work function of the analyzer electrode  $\phi$  has to be known because the analyzer selects the electrons with respect to the vacuum level, as illustrated by figure 2.10.

A photon of energy  $h\nu$  is absorbed by an electron at a level  $E_b$  below the Fermi level  $E_F$ . The kinetic energy  $E_{kin}$  is measured which will give the binding energy  $E_b$  of the ejected electron, given by eq. 2.8.

$$E_b = h\nu - E_{kin} - \phi \quad (2.8)$$

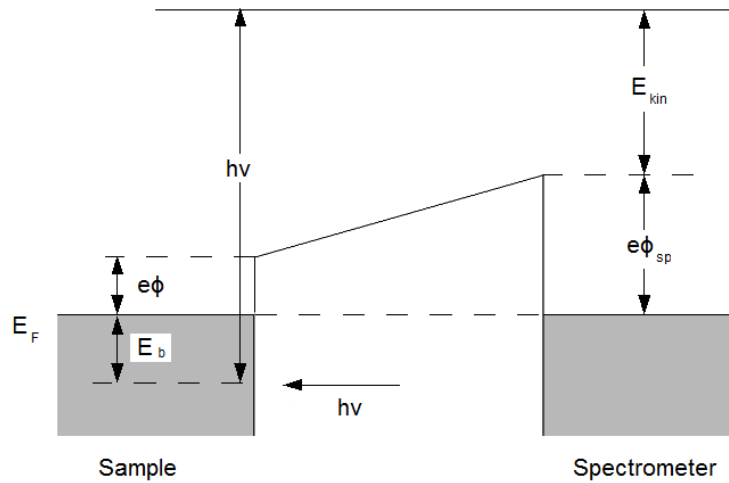


Figure 2.10.: Energy level diagram for XPS; adapted from [9]

In figure 2.11 a XPS-spectrum of the Pd sample is shown with its characteristic peaks ( $Pd4p$ ,  $Pd4s$ ,  $Pd3d_{5/2}$ ,  $Pd3d_{3/2}$ ,  $Pd3p_{3/2}$ ,  $Pd3p_{1/2}$ ,  $Pd3s$  and  $PdM_5VV$ ). 3p means that the electron comes from the 3p-Orbital. The additional denotation 1/2, 3/2 and 5/2 corresponds to the total angular momentum of a particular electron. As it can be seen in figure 2.11 there is some zinc on the sample surface left (zinc peak at 261.2 eV). To check if the sample is clean the measured spectrum can be compared with [12].

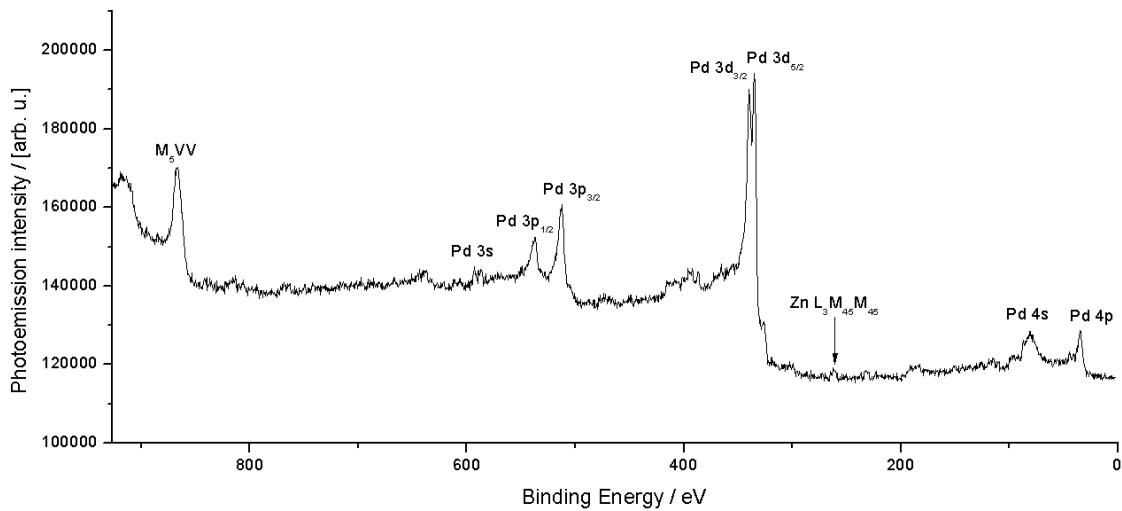


Figure 2.11.: X-ray spectrum of Pd

## 2.4. QMS

A quadrupole mass spectrometer (Pfeiffer QMS 200) was used for residual gas detection (schematic view in figure 2.12 ). Like any other mass spectrometer the QMS consists of 3 parts: the ion source, an analyzer and a detector. The speciality of a QMS consists of the 4 bar-shaped electrodes as seen in figure 2.12. The cross section of these electrodes builds a circle of curvature of a hyperbola. This is why the ambient electric field is nearly hyperbolic. As shown in the picture, a DC and AC voltage is applied to each counterpart electrodes. The applied voltage between the rods of  $U(t) = \pm U + V \cos(\omega t)$  determines the flight path of the ions through the analyzer. So after passing the ion source, only ions with a special mass to charge ratio (equation 2.13), in dependence of the applied voltage can pass the analyzer. One has to keep in mind that the sensitivity of the QMS is not the same for each element due to the different ionization cross sections.

The dimension of the sensor or rather of the separate system is about 15 cm. To get ions from the ion source to the detector the mean free path must be much larger than 15 cm. For an oxygen pressure of  $p = 1 \cdot 10^{-4}$  mbar there is a mean free path of  $\lambda = 60$  cm. This pressure is also known as vacuum minima for mass spectrometer.

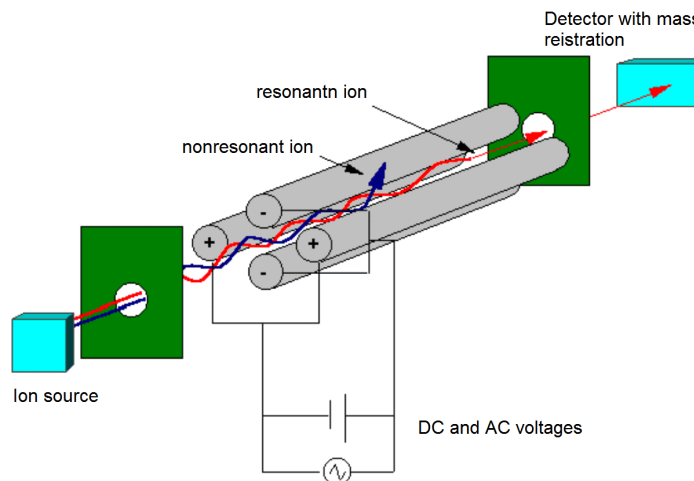


Figure 2.12.: Schematic view of a Quadrupole Mass-Spectrometer; adapted from [13]

### QMS-Ionsource

The ionsource consists of a cathode, an anode and some blinds. The constant emission current leads to an ionisation of the residual gas. By means of the blinds the ions are propagating to the separation system. The cathode consists of an iridium-wire which is coated with thoria-oxide to decrease the electron affinity.

### QMS-separation system

There the ions are separated according to the mass/charge ratio. The electrical field  $\phi$  (is given by equation 2.9) inside the separation system develops as a result of an overlap of the applied DC and AC.

$$\phi = \frac{(U + V \cdot \cos(\omega t)) \cdot (x^2 - y^2)}{r_0^2} \quad (2.9)$$

$r_0$  = radius of the cylinder which could be inscribed into the rod system

The following forces are acting perpendicular to the paraxial velocity of an ion:

$$F_x = -\frac{2e}{r_0^2} \cdot x \cdot \cos(\omega \cdot t) \quad (2.10)$$

$$F_y = -\frac{2e}{r_0^2} \cdot y \cdot \cos(\omega \cdot t) \quad (2.11)$$

$$F_z = 0 \quad (2.12)$$

The equations of motion in equations 2.10, 2.11 and 2.12 lead to the *Mathieu's differential equations*. Solving them leads to equation 2.13. It appears that there are stable and unstable ion-paths. An ion which is on a stable path always has the same  $r_0$  (admission condition). All other ions will collide with the electrodes where they are losing their charge. Therefore, ions on unstable paths do not reach the detector. Equation 2.13 shows the admission condition with  $V$  as high-frequency-amplitude,  $r_0$  the quadrupol-radius and  $f$  the high frequency.

$$\frac{m}{e} \approx M = \frac{V}{14.438 \cdot f^2 \cdot r_0^2} \quad (2.13)$$

### QMS-Detector

Ions on a stable path will reach the detector which is a faraday cage in the simplest way or a channeltron to gain greater sensitivity. The ions will impact the detector whereby electrons are knocked out. The detected ion-current serves as measuring signal. For further descriptions see [14].

## 2.5. FTIR

A possibility to excite vibrations at surfaces is to use infrared radiation. IR spectroscopy has been applied very successfully to study adsorbed species on materials with a high surface to volume ratio. If the adsorbed molecules have a dipole moment perpendicular to the surface, reflection absorption infrared spectra (RAIRS) allows an in situ investigation of these molecules [15].

Infrared spectroscopy was done with a Bruker IFS 66 v/S FT-IR spectrometer which is attached to the UHV-chamber in a RAIRS (reflection absorption infrared spectroscopy) setup which is shown schematically in figure 2.13.

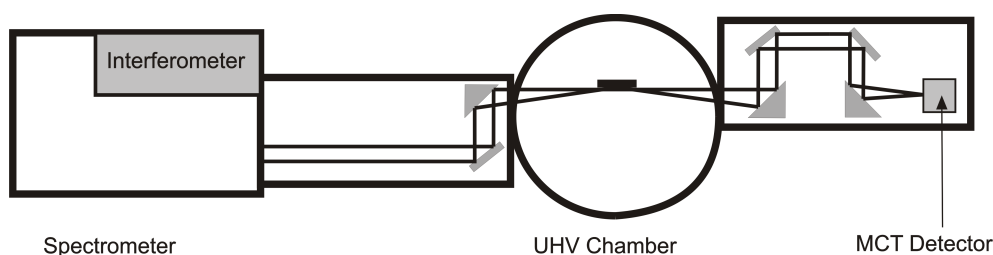


Figure 2.13.: Schematic view of the optical path of the infrared light; adapted from [15]

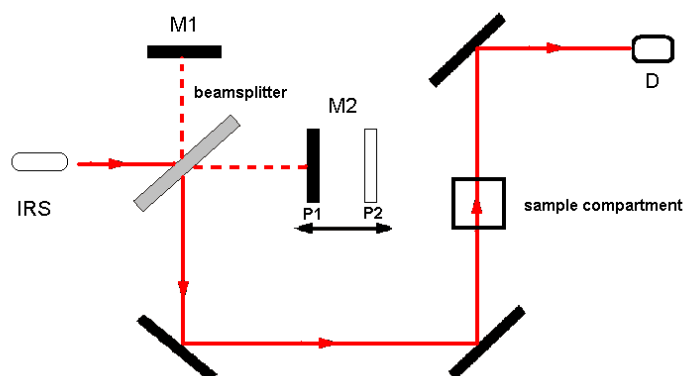


Figure 2.14.: Scheme of a Michelson interferometer

- IRS - Infrared source
- M1 - fixed mirror
- M2 - movable mirror
- P1 - position one
- P2 - position two
- D - detector

The main part of the FT-IR spectrometer is the interferometer, in this case a Michelson interferometer (shown in figure 2.14). The Michelson interferometer consist of two mirrors, a fixed and a movable mirror (M1 and M2 in figure 2.14), and a beam splitter. The whole optical path is evacuated down to a pressure just below 2 mbar to suppress bands from the atmosphere. This is necessary because especially strong water and carbon dioxide absorption bands in air disturb the recording of an IR spectrum. The movable mirror of the Michelson interferometer is nitrogen gas cushioned. That is why only a rough vaccum is achievable. For the measurements a SiC Globar (infrared source, IRS in figure 2.14), a Ge/KBr beam splitter and an external mercury-cadmium-telluride detector (MTC in figure 2.13 and D in figure 2.14) were used. The MCT-detector has to be cooled with liquid nitrogen to reach useable sensitivity. The spectrometer is operated by the *OPUS* software. With it several different measurement parameters can be choosen.

To get an IR-spectrum, first an interferogram is measured. This is then transformed into a single channel signal, using fourier transformation. Finally, the transmission spectrum is obtained by division of the single channel signal by a single channel signal reference spectrum (clean Pd(111) sample). So the transmission  $T$  is obtained by dividing the change of reflectance  $\Delta R$  by the initial value of the reflectance  $R^\circ$  (see equation 2.14).

$$T = \frac{\Delta R}{R^\circ} \quad (2.14)$$

The schematic representation of this operation is shown in figure 2.15. It is important that the reference spectrum and the actual spectrum are measured at the same temperature. If not, shifts of the temperature are seen which make it difficult to see the real peaks.

A detailed overview of the theoretical background as well as the advantages and disadvantages of a FT-IR spectrometer gives [15].

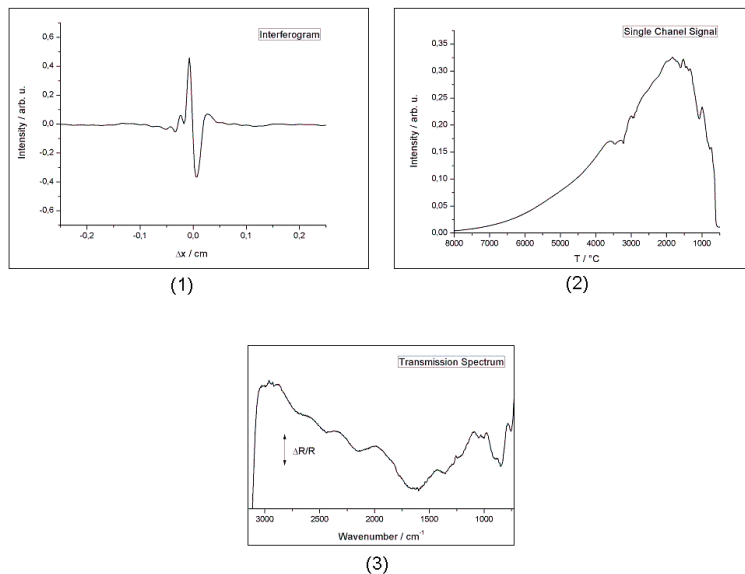


Figure 2.15.: Schematic description how to get an FT-IR spectrum  
 (1) Interferogram, (2) Single channel signal, (3) Transmission spectrum

## 2.6. Thermal Desorption Spectroscopy

Another way to investigate the catalytic reactions on a catalyst surface is thermal desorption spectroscopy (TDS), also called temperature programmed desorption (TPD). (see [16], [17], [18]). This method is one of the most important experimental techniques to study the kinetic parameters for ad molecules desorbing from solid surfaces. Therefore the surface is exposed to molecules at low temperature before it is heated up with a constant heating rate. Meanwhile the desorbing particles are detected with a QMS. In this work this method was used to investigate the decomposition products of methanol on Pd, Pd/Zn and Pd /ZnO.

Theoretically, the desorption process is described by the Polanyi-Wigner-equation:

$$r_d = -\frac{d\theta}{dt} = \nu_n(\theta) \cdot \theta^n \cdot \exp\left(-\frac{E_d(\theta)}{RT}\right) \quad (2.15)$$

In this equation  $r_d$  is the rate of desorption,  $\theta$  the coverage,  $t$  the time,  $n$  the order of desorption,  $T$  the surface temperature,  $R$  the gas constant,  $\nu_n$  the preexponential factor and  $E_d$  the desorption energy. Different desorption orders  $n$  lead to different shapes of the desorption signals as shown in figure 2.16.

In the case of zero-order desorption ( $n = 0$ ) the peak maximum shifts to higher temperatures with increasing coverage  $\theta$  which is characteristic for desorption from the multilayer. The signal is characterized by a common rising edge (see figure 2.16(a)).

In the case of first-order desorption ( $n = 1$ ) the peak in the desorption rate curve does not change in temperature with coverage (see figure 2.16(b)). The spectra show an asymmetric shape. This kind of desorption occurs when single atoms desorb from their adsorption sites without interacting with each other.

In the case of second-order desorption ( $n = 2$ ) the temperature of the peak decreases with increasing coverage  $\theta$ . A symmetric shape of the TDS is characteristic (see figure 2.16(c)). Second-order desorption occurs from the associative desorption of molecules.

An approximation for  $E_d$  is given by Redhead (see [16]) for the case of first-order desorption.

$$E_d = R \cdot T_m \left[ \ln\left(\frac{\nu \cdot T_m}{\beta}\right) - \ln\left(\frac{E_d}{R \cdot T_m}\right) \right] \quad (2.16)$$

In this equation  $T_m$  is the temperature corresponding to the maximum of the desorption spectrum and  $\beta$  is the heating rate. The last term of equation 2.16 can be set as a first approximation to  $\ln\left(\frac{E_d}{R \cdot T_m}\right) \approx 3.64$  and usually  $\nu = 10^{13}$  sec is used.

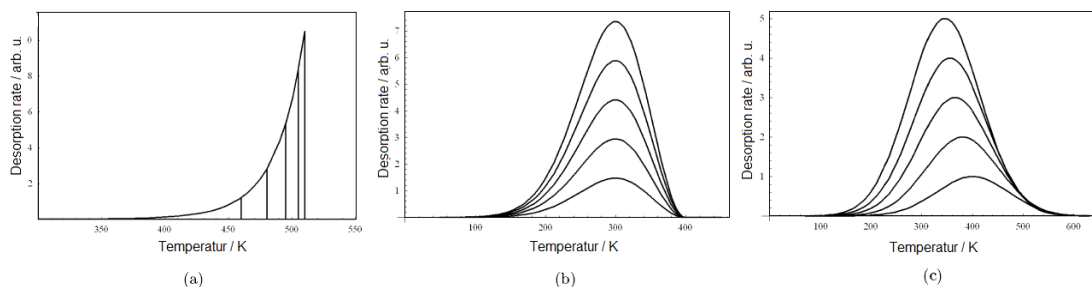


Figure 2.16.: Illustration of the different kinds of desorption spectra: (a) zero-order desorption, (b) first-order desorption and (c) second-order desorption with increasing coverage; adapted from [19]

The area beneath the curve is proportional to the amount of the adsorbate. This fact was used to calculate the Zn-coverage by integrating the desorption spectra of zinc. Knowing that below 1 ML coverage there is only one Zn-peak ( $T = 800$ - $1250$  K) in the TDS (see [20], [19]) offers the opportunity to calculate the Zn-coverage. For this purpose, several zinc layers with different evaporation times were formed, until the second zinc-peak (multilayer-peak at  $T = 450$ - $500$  K) was found for the first time. The last TDS where only one zinc-peak is seen was assumed to show a 1 ML coverage (see [21]). This TDS is shown in figure 2.17. Zinc was evaporated at room temperature which means that the Pd-sample has a temperature of  $25^\circ\text{C}$  during zinc evaporation. The zinc source had a temperature of  $T = 324^\circ\text{C}$  and the evaporation time was 20 seconds.

The area beneath the curve was calculated to  $6.49815 \cdot 10^{-12}$  (see figure 2.17) which conforms to 1 ML. To calculate this area the curve was extended by a lorentz fit until it hits the baseline. This baseline was put inside by hand. This method ensures a keenly calculation of the real amount of desorption. With this knowledge the zinc coverage of all experiments could be calculated by simple division of the particular areas.

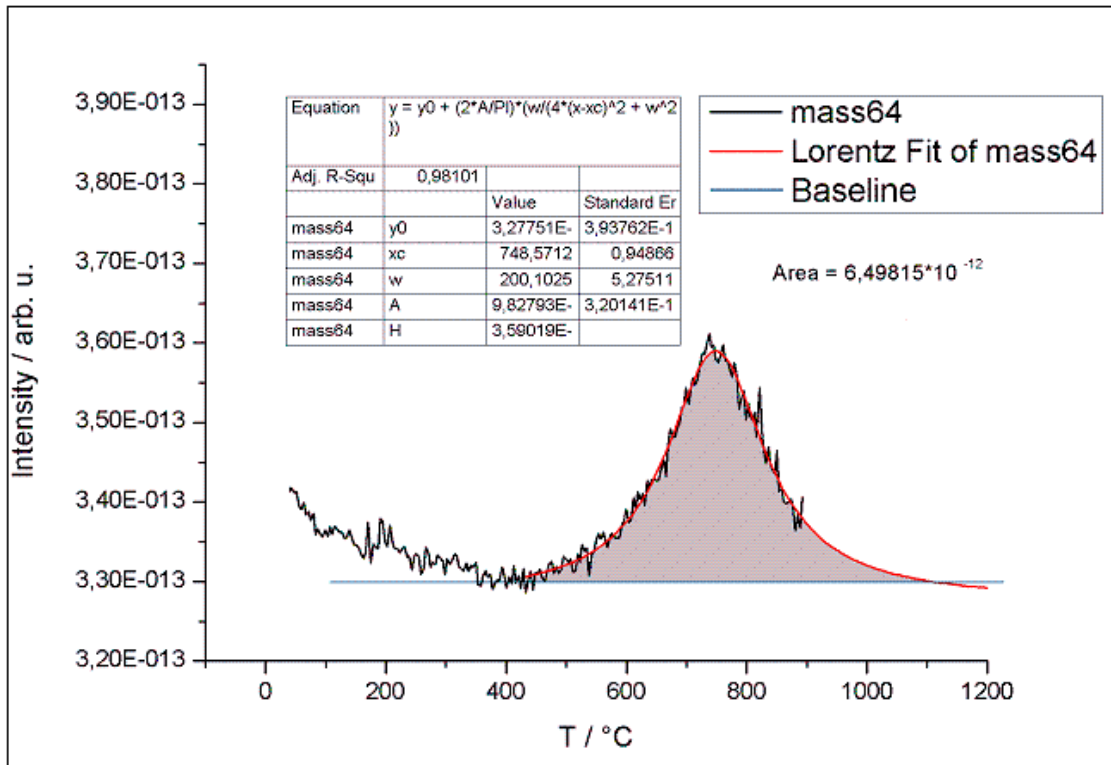


Figure 2.17.: TDS which was used to calculate the area of 1 ML zinc coverage

## 2.7. Sputter gun

Sputtering was used for sample cleaning. The sample is bombarded by noble gas ions, like  $\text{Ar}^+$  to remove surface contaminants. This also leads to the removal of the top layers of the sample itself. The inlet of the Ar-gas was managed by a dosing valve ( $5 \cdot 10^{-5}$  mbar) and the Ar was ionized via electron impact in the ionization chamber of the gun (Purkin Elmer PHI Model 04-161 Sputter Ion Gun). The  $\text{Ar}^+$  ions are accelerated towards the sample-surface (0.5 KV). After sputtering, one has to heat up and anneal (up to  $900^\circ\text{C}$ ) the surface because sputtering leads to a roughening and degradation of the surface. To have a plain surface without adsorbed Ar atoms and to restore the surface structure this heat-treatment is necessary.

## 2.8. Zn Evaporator

For the experiments done in this work, thin Zn and ZnO films were deposited onto the sample surface. Therefore a home built Knudsen cell was used. A short overview is given below (for further descriptions and technical data see [22])

The main part of the evaporator is a simple Knudsen cell consisting of two interleaved molybdenum cylinders. One of them has a tap hole for mounting a Ni/CrNi-thermocouple, the other one has a hole of 1 mm diameter as the Zn outlet. These molybdenum cylinders are surrounded by two concentric ceramic cylinders which include a tantalum coil inbetween for resistive heating. The whole assembly is embedded in a stainless steel tube which is centered in a second stainless steel shroud. To provide a regulation of the deposition time a shutter ( $\varnothing = 8$  mm) at the outlet of the outer shroud is mounted.

The evaporator was filled with high purity Zn pellets (GOODFELLOW, lump size max. 2 mm; purity: 99.98 %). Usually the deposition rate is controlled by the frequency change of a quartz microbalance. A QMB can be used if the sticking coefficient on the sample and the QMB is the same. Generally, this condition is fulfilled for metal vapors. But for zinc this is not the case. Even small amounts of impurities on the sample surface lead to a decrease of the sticking coefficient of zinc (see [23]). The same applies for the metal film on a QMB which can be considered as dirt. So a QMB is inapplicable for the determination of the Zn desorption rate. Therefore the Zn deposition rate was controlled by the Zn cell temperature. To gain a similar deposition rate at each experiment the Knudsen cell was heated up to  $322^\circ\text{C}$  and the deposition time was measured. For an equilibrium temperature of  $322^\circ\text{C}$  a heating current of 0.86 A was needed.

# 3. Adsorption of pyridine on ZnO films on Pd(111)

## 3.1. Sample cleaning

The sample-surface has to be cleaned every time before a ZnO - layer was formed. Therefore every time the same procedure was done:

- 
- sputtering for 30 min (argon-atmosphere of  $5 \cdot 10^{-5}$  mbar, emission current of the sputter gun: 25 mA)
  - annealing: 1000 K for 4 min (last minute under an oxygen-atmosphere of  $5 \cdot 10^{-7}$  mbar)
  - cooling down to room temperature ( 25°C) under oxygen-atmosphere
  - flash to 1000 K without oxygen
- 

To be sure that the sample surface is clean LEED and XPS was used. Figure 2.11 shows a XPS spectrum of the Pd(111) sample surface, in figure 3.1 the LEED pattern of a clean Pd(111) surface is shown. A clean Pd(111) surface is, as seen in figure 3.1, characterized by a (1x1) structure.

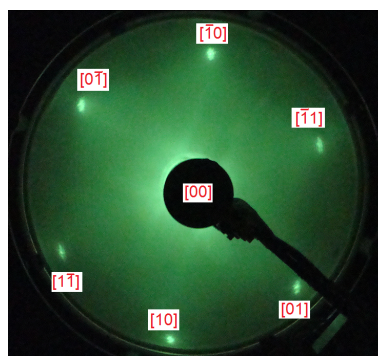


Figure 3.1.: LEED-pattern of a clean Pd(111) surface with corresponding crystallographic directions

### 3.2. ZnO deposition on Pd(111)

There are two ways to form ZnO layers on a Pd(111) surface. The so called post-oxidative and the reactive way.

Post-oxidative ZnO deposition starts with Zn evaporation while the sample is at room temperature (25°C). After evaporating the desired amount of Zn an oxygen pressure of about  $5 \cdot 10^{-7}$  mbar has to be provided. Under this oxygen atmosphere the sample has to be flashed to 550 K.

In contrast to the post-oxidative way, the reactive way starts with rising the oxygen pressure to  $5 \cdot 10^{-7}$  mbar. Under this pressure the Zn evaporation takes place (sample at room temperature again). In the end the sample has to be annealed like in the post-oxidative way.

In the experiments the reactive way was always used because only this way ensures well ordered ZnO islands on the Pd sample as it is shown on the right hand side of figure 3.2. The left side of figure 3.2 shows disordered ZnO - islands which you get, using the post-oxidative way. As figure 3.2 implies, ZnO shows island growth. The growth of ZnO layers is explained in a little more detail below.

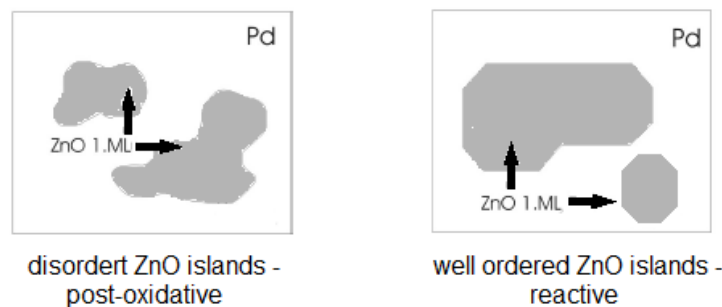


Figure 3.2.: ZnO island formation on Pd(111)

Depending on the amount of Zn and supplied oxygen two different ZnO structures can be found. ZnO forms a (6 x 6) and a (4 x 4) structure below 1 ML coverage as it is shown in figure 3.3 and figure 3.4 [24].

In figure 3.3 and figure 3.4 a STM and a LEED picture of both structures is seen. In these pictures a coverage of 0.7 ML is always given, so both structures (6 x 6) and (4 x 4) can be found. Gunther Weirum who made the STM research of Pd/ZnO discovered that not a uniform ML is built on a surface with 1 ML coverage, but several ZnO islands as it is shown in figure 3.5. So it can be said that ZnO shows island growth on a ZnO layer.

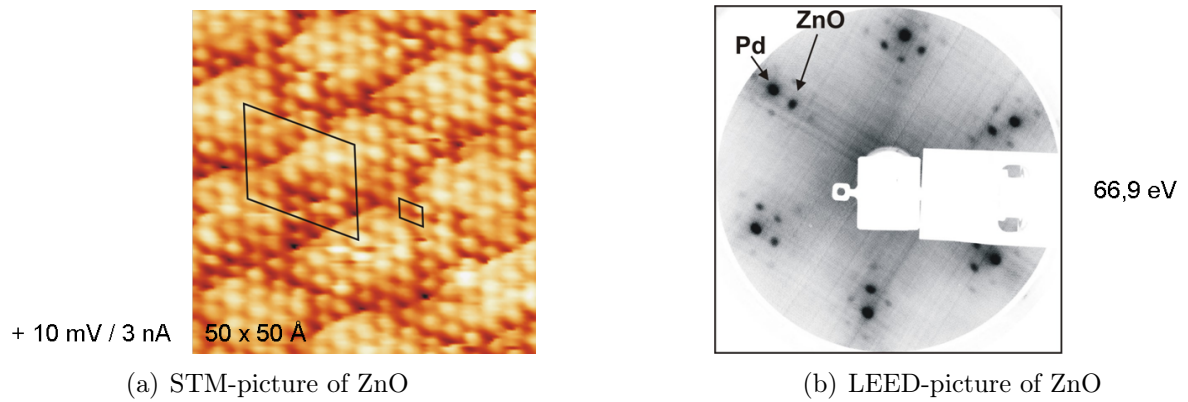


Figure 3.3.: STM- and LEED- picture of the (6x6) structure of ZnO; 0.7 ML coverage; adapted from [24]

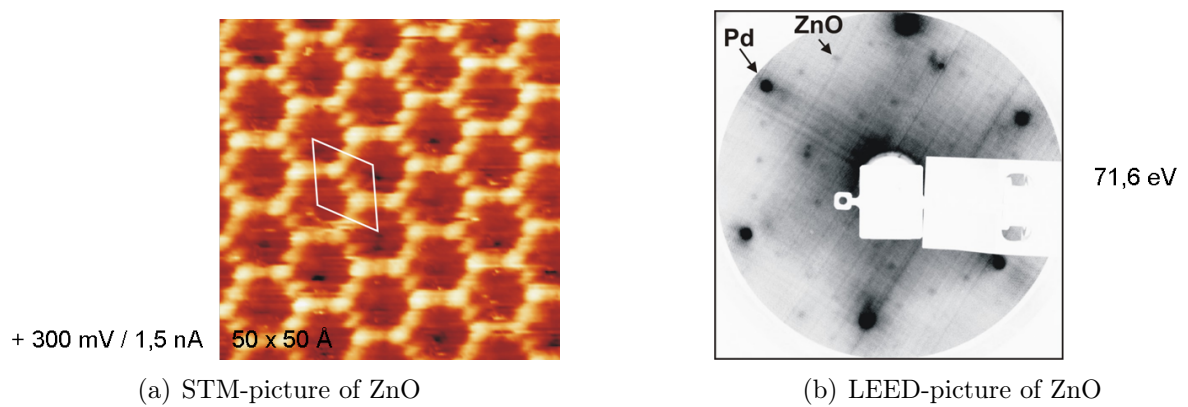


Figure 3.4.: STM- and LEED- picture of the (4x4) structure of ZnO; 0.7 ML coverage; adapted from [24]

Figure 3.3 shows a STM- and a LEED-picture of the (6 x 6) structure. A coverage of 0.7 ML is given. The small parallelogram in figure 3.3(a) shows the unit cell of the Pd structure. The large parallelogram shows the (6 x 6) super structure, the so called *Moire* structure of ZnO. Figure 3.3(b) shows the LEED picture of this structure. The six hexagonal arranged spots are Pd spots (compare with figure 3.1). Around these, the ZnO spots are seen. The (6 x 6) structure is characterised by five ZnO spots between two Pd spots.

In figure 3.4 a STM- and a LEED-picture of the (4 x 4) structure can be seen. Again the parallelogram in figure 3.4(a) symbolizes the unit cell. This structure looks like honeycombs in the STM. The sides of the hexagons consist of three zinc atoms whereas the distance between two of them is approximately 3.5 Å. Figure 3.4(b) shows again the LEED picture of this structure. The (4 x 4) structure is hardly seen in LEED because it is destroyed by the electron beam. It is characterised by three ZnO spots between two Pd spots.

In figure 3.5 a coverage of 1.5 ML ZnO is shown. As one can see, there is a 1 ML coverage over the whole surface (Area A) and several islands of 2 ML (B and D in figure 3.5) and even 3 ML islands (C in figure 3.5). First of all there are two types of ZnO islands which coexist during zinc evaporation: large ones with an open structure and small compact ZnO islands. Between these islands there are worm-like ZnO clusters. These islands are seen in STM at low coverages (e.g. 0.3 ML). If the ZnO coverage approaches 1 ML only the compact islands are seen, which form an almost closed layer with few 2 ML islands on top [25]. At higher coverage several multilayer islands (2ML) develop this first ZnO layer. These islands begin to expand with the amount of the provided Zn. But during this expansion a third ML on the second ML is built. So we have 3 ML island even before the whole surface is covered with a second ML ZnO. Further information of the ZnO growth on Pd(111) are seen in [25].

Islands B and D in figure 3.5 represent 2 ML islands but they have a different height as it can be seen in the linescan in the lower right in figure 3.5. There the apparent height in Å over the island length in Å can be seen. The linescan shows that there is a difference of 0.6 Å between the islands D and B. The question was, how a difference of 0.6 Å can occur.

The assumption was that ZnO built a wurzit - structure (like in a ZnO-single-cristal) on Pd(111) as shown in figure 3.6 and that this structure may show two different terminations of the ZnO islands. With different termination is meant that in one case oxygen is the topmost layer and in the other case Zn as shown in figure 3.7. In order to check if this suggestion is right pyridine was adsorbed on the sample.

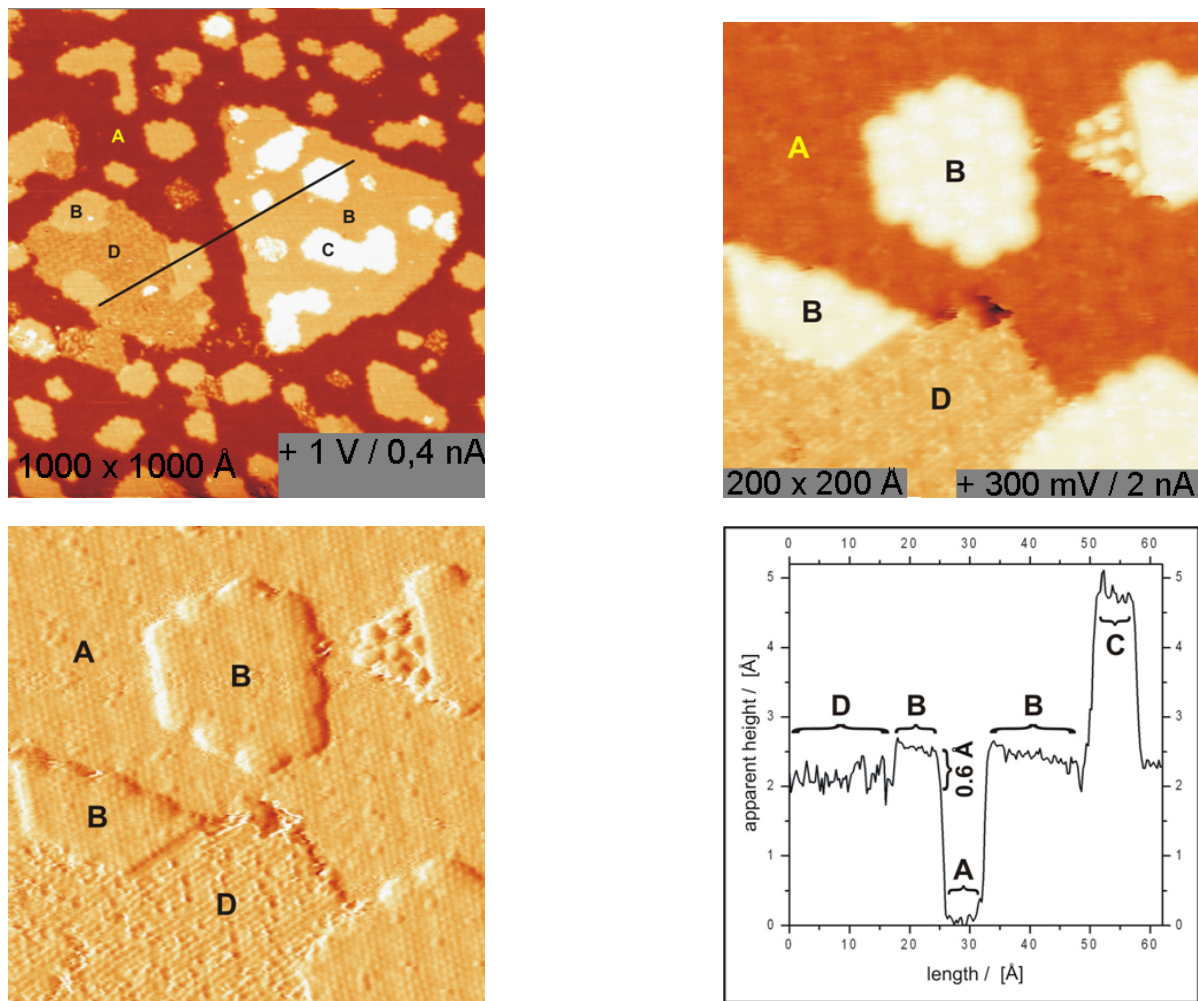


Figure 3.5.: STM picture of ZnO and the apparent height of the islands; 1.5 ML coverage

- A: 1<sup>st</sup> ML
- B: 2<sup>nd</sup> ML
- C: 3<sup>rd</sup> ML
- D: 2<sup>nd</sup> ML; adapted from [24]

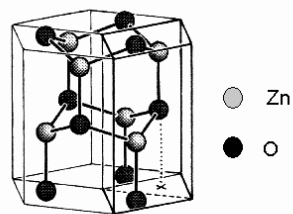


Figure 3.6.: Wurtzite-structure; adapted from [26]

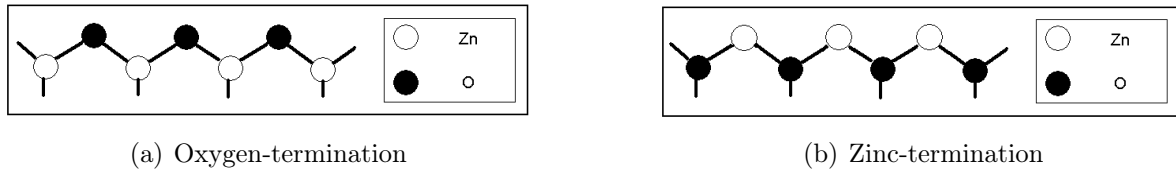


Figure 3.7.: Schematic illustration of the two possible terminations of ZnO in the wurzit-structure

### 3.3. Pyridine adsorption on ZnO

Pyridine was adsorbed on the sample because it forms a physisorption with oxygen and a chemisorption with metal-atoms. This fact is illustrated in figure 3.8 where the Pd-sample with different ZnO-layers is shown. In figure 3.8(a) a ZnO-layer which has a zinc-termination is given. The subsidence of the green pyridine molecule illustrates the chemisorption. Physisorption of pyridine is illustrated in figure 3.8(b) where the pyridine molecule is sitting on the oxygen. The different strength of bond type has to lead to a shift of the peaks in the IR- and TPD-spectra.

Two different ZnO layers were made: one with an oxygen-pressure of  $5 \cdot 10^{-8}$  mbar (0.6 step between island B and D in STM) and another with  $1 \cdot 10^{-5}$  mbar (no step between islands B and D because the whole surface is oxygen covered; illustrated in figure 3.8(b)).

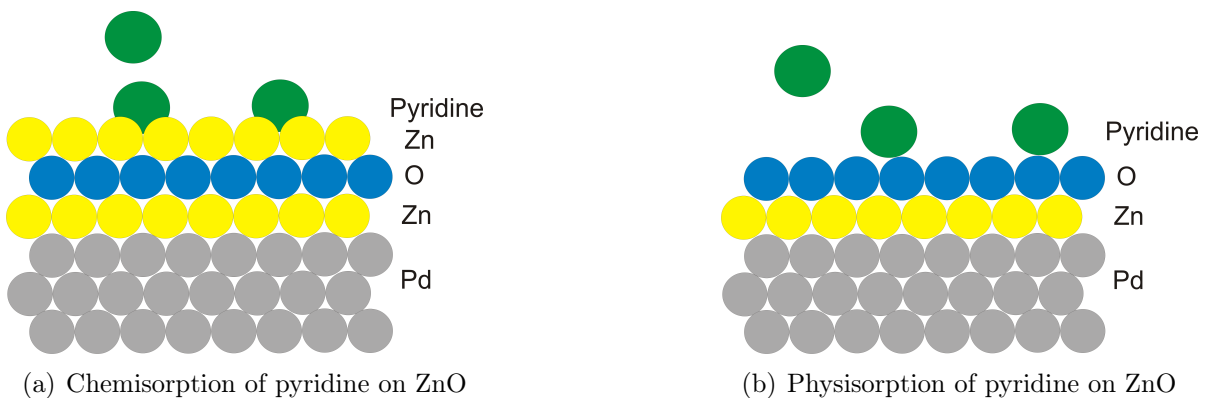


Figure 3.8.: The two possible bond-types of pyridine on ZnO depending on the termination

After that the sample was cooled down to 198 K ( -75 °C) and pyridine was adsorbed on the sample (Exposition: pyridine-pressure:  $1 \cdot 10^{-7}$  Torr for 10 min). The results are shown in figure 3.9. As it is seen in figure 3.9 there is no shift in the IR-spectra. Both pyridine peaks are at  $1442.5 \text{ cm}^{-1}$  (C-N stretch, see [27], [28], [29], [30]) so there is no shift, no matter there is more or less oxygen supplied during the Zn evaporation. There

is a difference in intensity of both peaks. This results from different reflectivity of the sample in each experiment. It is impossible to gain the same surface a second time, so the reflectivity differs every time. The TPD-spectra lead to the same result as the IR-spectra. The curves always show the same shape. That means that there is always the same bond type because it always needs the same amount of energy/heat to desorb pyridine from the surface. It needs to be mentioned, that the high temperature peak in the TPD seems to derive from the sample holder and not from the sample itself. It seems that the sample holder gets warm even if it is nitrogen cooled. Why these high temperature peaks in the TPD can be neglected is explained in detail at chapter 4.1.1. A difference of the intensity of the peaks in the TDS can be seen which arises from different pyridine amounts in each experiment. Because of experimental reasons it was not possible to apply the same amount of pyridine every time.

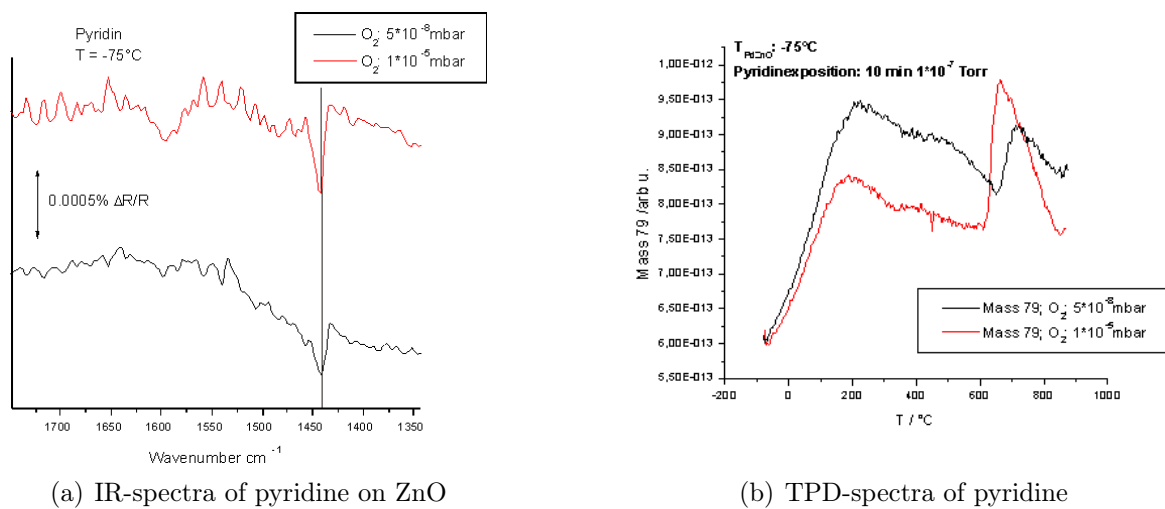


Figure 3.9.: IR- and TPD- spectra of pyridine on ZnO high and low oxidized

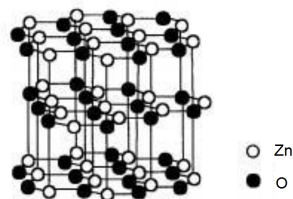


Figure 3.10.: Boron-nitride-structure of ZnO; adapted from [31]

It can be assumed that there is no different termination, the difference in height must have other reasons. The DFT-theory says that ZnO does not form a wurzit - structure as it was assumed but it forms a boron-nitride-structure (figure 3.10) up to 4 ML. This will fit with the results but it does not give an answer why there is a difference in height of the 2 ML islands. This height difference may occur because of electrical interference between STM-tip and sample, or because of OH-groups which are on the sample surface. Newest findings by means of DFT suggest that the height difference occurs because of OH-groups on the sample surface [32].

## 4. TDS - study of methanol desorption from Pd(111), Pd/Zn and Pd/ZnO

To investigate methanol desorption from Pd(111), Pd/Zn and Pd/ZnO several TDS-measurements were done. The principle of a TDS-measurement is explained in chapter 2.6 as well as in [16], [17], [18]. How a TDS was done in this work is explained in detail right below.

### 4.1. TDS - Results

TDS-measurements were always done according to the following description:

1. Sample-cleaning (see 3.1)
2. Depending on the experiment, a Zn or ZnO layer was built after sample-cleaning (In the case of methanol desorption from Pd this step is skipped)
3. Sample cooling down to  $T = -100^{\circ}\text{C}$  ( $\approx 170\text{ K}$ ); *Here is to say that it was not possible to reach the same temperature at each experiment. The reasons for this are unknown.*
4. Methanol exposition: Methanol mass pressure was raised to  $1 \cdot 10^{-7}$  mbar for 10 min to gain a methanol multilayer on the sample (methanol spectrum is shown in figure 4.1)
5. Flash up to  $800^{\circ}\text{C}$  (heating rate  $1\text{ K/s}$ ); During this heat treatment the intensity of the detected masses was measured over temperature.

The same procedure was done for the IR-measurments, but there a heating rate of  $0.1\text{ K/s}$  was given. Table 4.1 shows the detected masses in each experiment with their corresponding species.

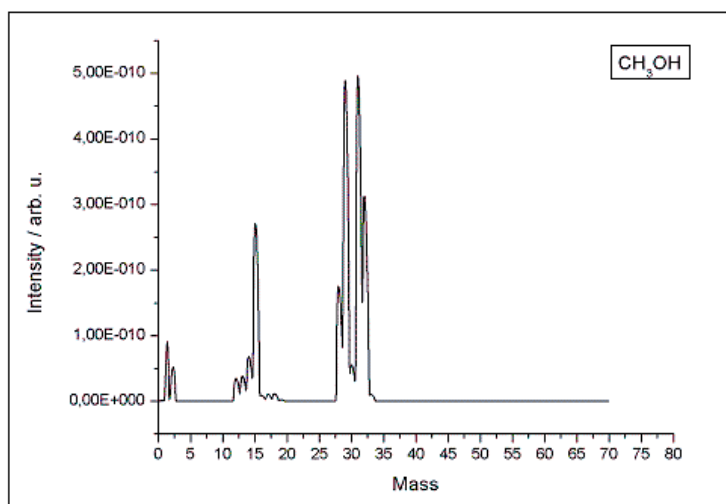


Figure 4.1.: Methanol spectrum during adsorption

| Mass | Formula            | Compound              |
|------|--------------------|-----------------------|
| 2    | H <sub>2</sub>     | Hydrogen              |
| 18   | H <sub>2</sub> O   | Water/Methanol        |
| 29   | CH <sub>2</sub> O  | Formaldehyde/Methanol |
| 31   | CH <sub>3</sub> OH | Methanol              |
| 32   | O <sub>2</sub>     | Oxygen/Methanol       |
| 44   | CO <sub>2</sub>    | Carbon dioxide        |
| 45   | CO <sub>2</sub> H  | Formate               |
| 64   | Zn                 | Zinc                  |

Table 4.1.: Detected mass and corresponding species in each TDS

### 4.1.1. 1<sup>st</sup> Measurement series

#### Methanol desorption from Pd/Zn

First of all Pd/Zn was investigated. A Zn coverage of 0.6 ML was given and the sample was cooled down to  $T = -107.7^\circ\text{C}$  ( $\approx 165\text{ K}$ ) for methanol exposition. Figure 4.2 shows the thermal desorption spectra of methanol desorption from Pd/Zn.

The desorption curves for hydrogen and water are shown in figure 4.2(a). Both curves show the same shape. There is a first large peak for hydrogen at  $T = -24^\circ\text{C}$  and a small one at  $T = 318^\circ\text{C}$ . Nearly the same can be found for water. There a peak at  $T = 22^\circ\text{C}$  and a second one at  $T = 325^\circ\text{C}$  is seen. The peaks around  $800^\circ\text{C}$  originate from the sample holder. Therefore they are not relevant for the measurement.

In figure 4.2(b) desorption curves of mass 29, 31 and 32 are shown. All curves have the same shape and their peaks lie at the same temperature. As one can see there are two peaks for all three species. The first one lies at  $T = -31^\circ\text{C}$  and the second one at  $T = 326^\circ\text{C}$ . From the cracking pattern (figure 4.1) one can calculate the percentage of each mass in the methanol spectrum. Subtracting the calculated amount of each methanol fragment of the detected TDS gives a flat line. So the detected mass 29, 31 and 32 are all methanol species. From this emerges that no formaldehyde and no oxygen is seen. Again, the peaks around  $800^\circ\text{C}$  are neglected.

Figure 4.2(c) shows the carbon dioxide desorption. As it can be seen, there is nearly no  $\text{CO}_2$  desorption. There is a decay of the signal around  $T = 275^\circ\text{C}$ . It seems that this curve only shows the background.

At last the zinc- and formate-desorption curves are shown at figure 4.2(d). There seems to be zinc desorption at the same time when there is formate desorption at low temperatures. Zinc desorption can be seen from  $T = -108^\circ\text{C}$  till  $T = 26^\circ\text{C}$ , formate desorption can be seen from  $T = -102^\circ\text{C}$  till  $T = 36^\circ\text{C}$ . Considering that the temperature-measurement-error is about  $\pm 5^\circ\text{C}$  this can be regarded as the same temperature range. The second zinc peak is where it is expected to be (starting at  $T = 475^\circ\text{C}$  with its maximum at  $T = 759^\circ\text{C}$ , fits with literature [20], [19]).

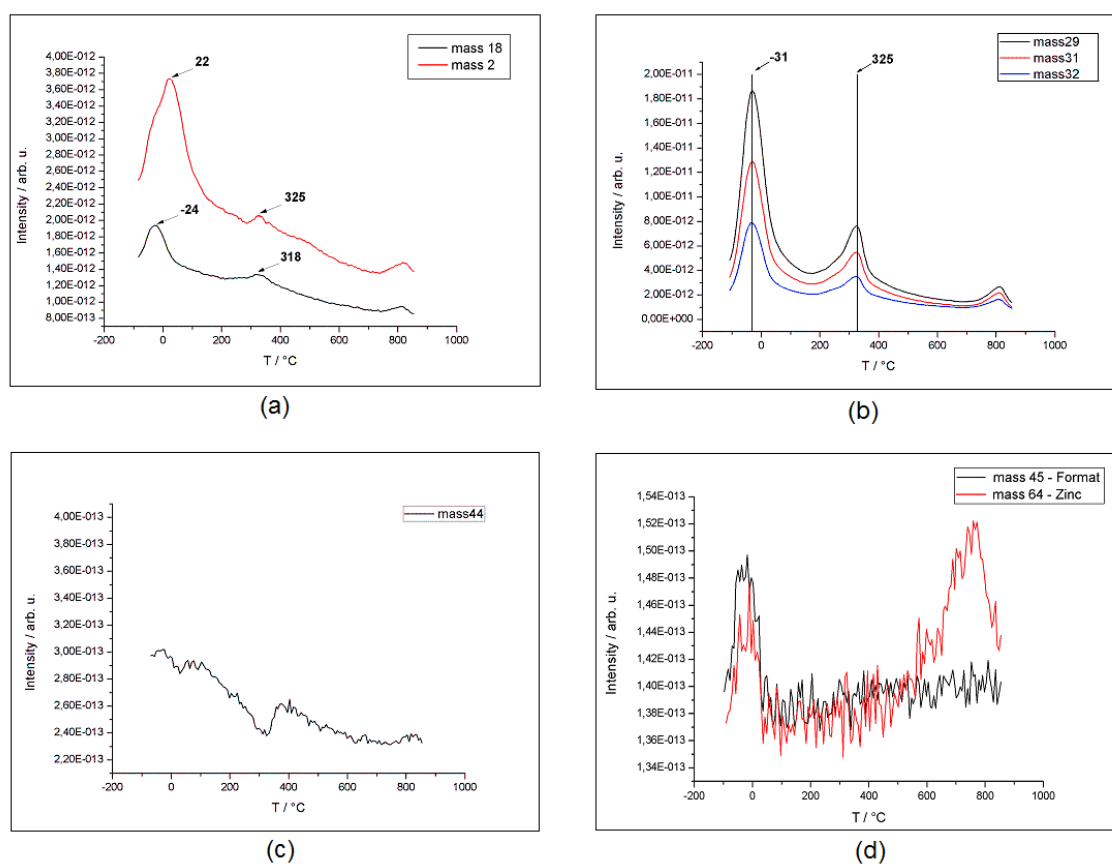


Figure 4.2.: Thermal desorption spectra of methanol desorption from Pd/Zn (Zinc coverage: 0.6 ML); (a) hydrogen- and water-desorption curve, (b) methanol-desorption curves, (c) carbon dioxide-desorption curve, (d) formate- and zinc-desorption curve

### Methanol desorption from Pd/ZnO - high O<sub>2</sub> pressure

Methanol desorption from Pd/ZnO was investigated next. First, methanol desorption from a ZnO-layer which was formed under a high oxygen atmosphere ( $1 \cdot 10^{-5}$  mbar) was studied. The sample had a ZnO coverage of 0.4 ML and was cooled down to  $T = -109.5^\circ\text{C}$  ( $\approx 163.5$  K). Figure 4.3 shows the thermal desorption spectra of this experiment.

The desorption curves of hydrogen and water are shown in figure 4.3(a). The peaks of these curves are seen at different temperatures but the curves have the same shape. For hydrogen the first peak can be found at  $T = -4^\circ\text{C}$ . A second peak is seen at  $T = 217^\circ\text{C}$ . Contrary to Pd/Zn there are a third and fourth peak at  $T = 416^\circ\text{C}$  and  $T = 488^\circ\text{C}$ . The TDS of water also shows four peaks. The first one at  $T = 9^\circ\text{C}$  lies at higher temperatures than the first hydrogen peak. All other water peaks are situated at lower temperatures compared with the hydrogen peaks. Water is seen at  $T = 150^\circ\text{C}$ ,  $263^\circ\text{C}$  and  $409^\circ\text{C}$ . The peaks around  $800^\circ\text{C}$  are neglected again because they originate from the sample holder.

Figure 4.3(b) shows the desorption curves of methanol. Compared with the last experiment they have the same shape. Again, all peaks of all three species lie at the same temperature:  $T = 3^\circ\text{C}$  and  $T = 409^\circ\text{C}$ . The peaks around  $800^\circ\text{C}$  are neglected again. The increase at temperatures above  $800^\circ\text{C}$  originates from desorption from the sample holder.

Desorption of carbon dioxide (figure 4.3(c)) shows two peaks at  $T = -24^\circ\text{C}$  and  $T = 130^\circ\text{C}$ . It seems that there is a background measured, too. The red line symbolizes the background which seems to have an exponential like decay. Because the real background is unknown this line was manually plotted. So after a decay of the CO<sub>2</sub> signal there is carbon dioxide desorbing again from  $T = 409^\circ\text{C}$  till  $T = 700^\circ\text{C}$ .

Once more we have zinc desorption when we have formate desorption (figure 4.3(d)). Zinc is seen from  $T = -68^\circ\text{C}$  till  $T = 76^\circ\text{C}$  for the first time. The second zinc peak starts at  $T = 521^\circ\text{C}$ . Formate can be found from  $T = -58^\circ\text{C}$  until  $T = 70^\circ\text{C}$ .

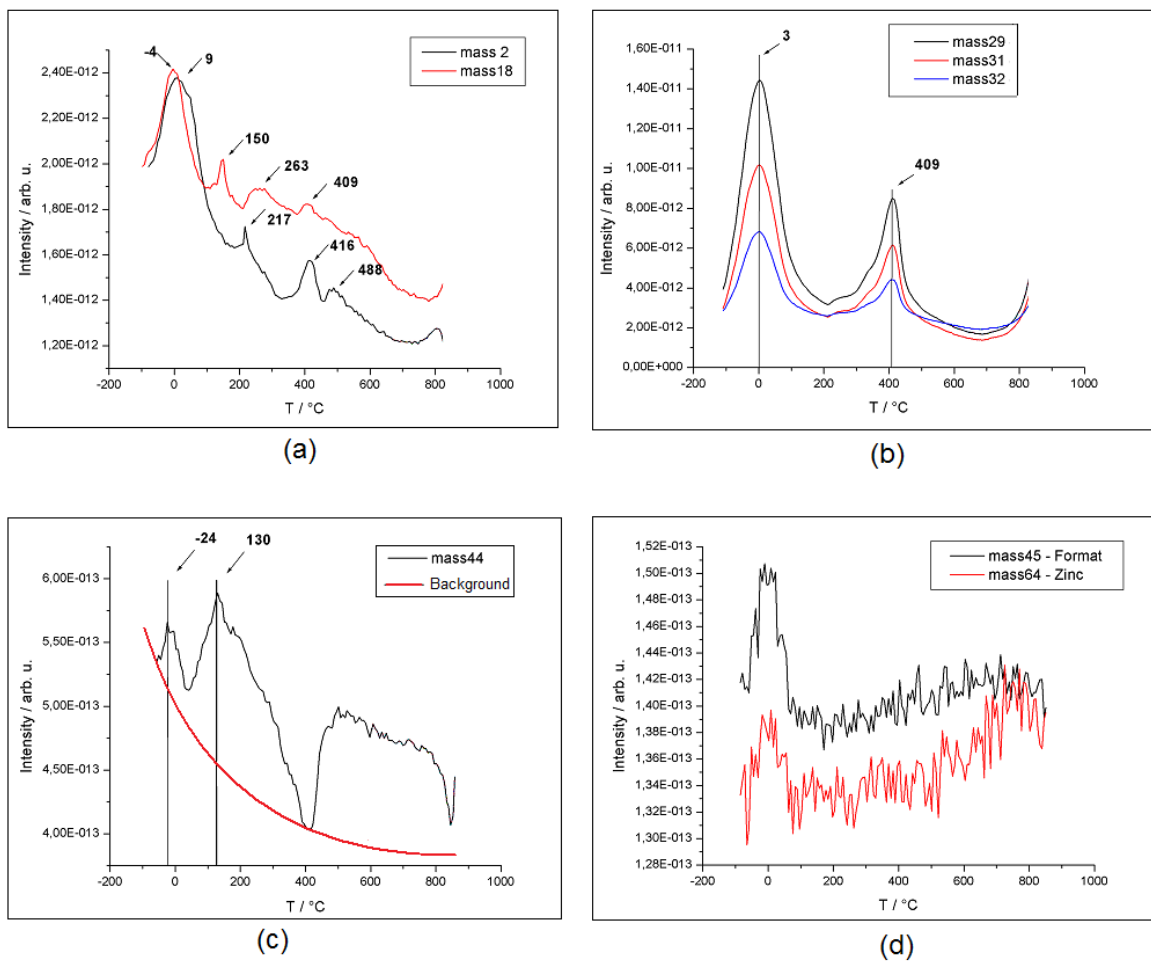


Figure 4.3.: Thermal desorption spectra of methanol desorption from Pd/ZnO (ZnO coverage: 0.4 ML; oxygen pressure during Zn-evaporation:  $1 \cdot 10^{-5}$  mbar); (a) hydrogen- and water-desorption curve, (b) methanol-desorption curves, (c) carbon dioxide-desorption curve, (d) formate- and zinc-desorption curve

### Methanol desorption from Pd/ZnO - low O<sub>2</sub> pressure

The third experiment was done with a ZnO-layer which was formed under a low oxygen atmosphere ( $5 \cdot 10^{-8}$  mbar). A ZnO coverage of 0.6 ML was given and the sample was cooled down to  $T = -108.7^\circ\text{C}$  ( $\approx 164$  K). Figure 4.4 shows the thermal desorption spectra of this experiment.

The water and especially the hydrogen curve seems to bear a resemblance to the corresponding curves for Pd/Zn. Both curves (see figure 4.4(a)) show two peaks again whereof the first hydrogen and the first water peak lie at the same temperature  $T = 36^\circ\text{C}$ . The second water peak can be found at  $T = 150^\circ\text{C}$  and the second hydrogen peak is seen at  $T = 337^\circ\text{C}$ .

Methanol shows the same behavior as in the experiments before (figure 4.4(b)). Peaks can be found at  $T = 29^\circ\text{C}$  and  $T = 331^\circ\text{C}$ . The peak around  $800^\circ\text{C}$  can be neglected again.

The carbon dioxide desorption curve (figure 4.4(c)) looks similar to the CO<sub>2</sub> desorption curve for ZnO formed under high oxygen atmosphere. There is a peak at  $T = 137^\circ\text{C}$ . The red line symbolizes the background signal which was manually plotted again. Thus there is no CO<sub>2</sub> desorbing from the sample at  $T = 324^\circ\text{C}$ . At higher temperature carbon dioxide is desorbing again.

As it is seen in figure 4.4(d) there is again zinc desorption when there is formate desorption. The formate peak can be seen from  $T = -44^\circ\text{C}$  till  $T = 82^\circ\text{C}$ . Zinc is found from  $T = -37^\circ\text{C}$  till  $T = 83^\circ\text{C}$ . The second Zn-peak starts at  $T = 569^\circ\text{C}$ .

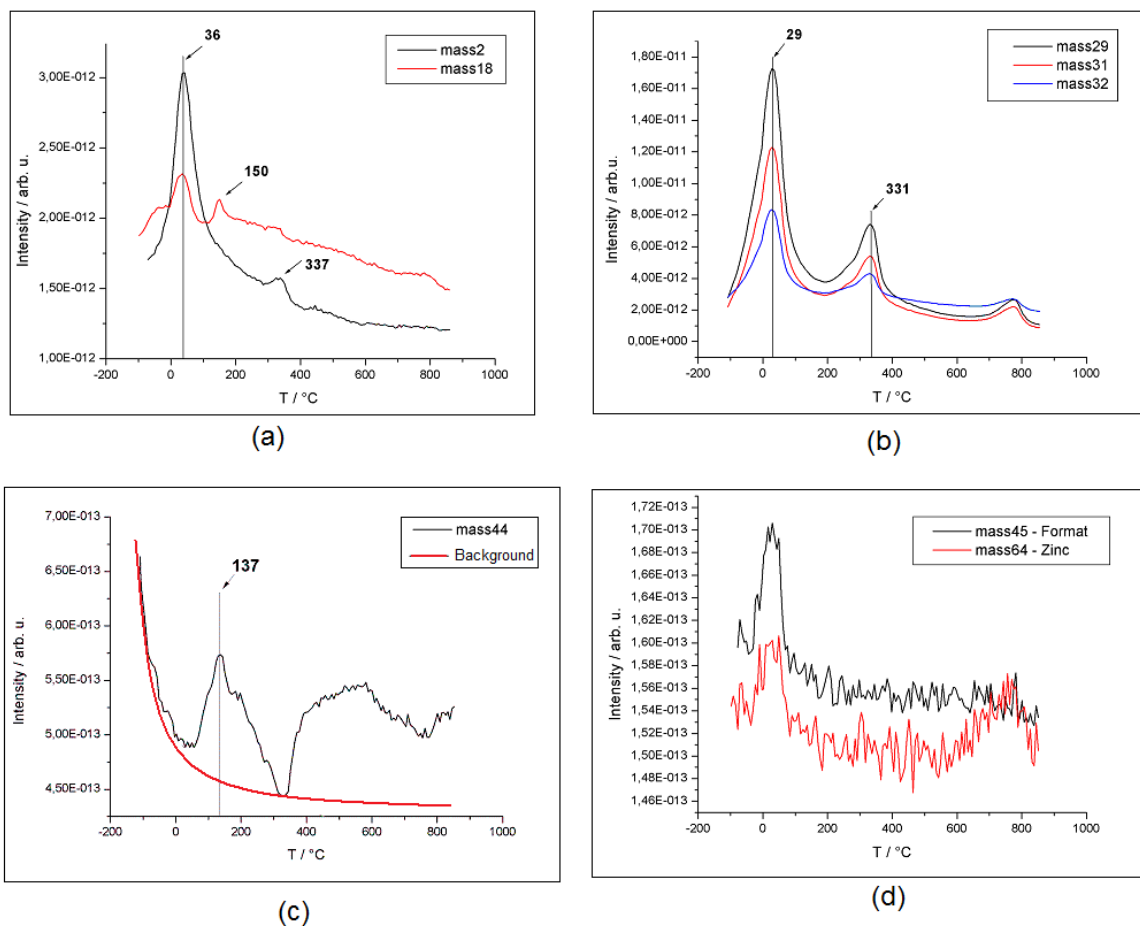


Figure 4.4.: Thermal desorption spectra of methanol desorption from Pd/ZnO (ZnO coverage: 0.6 ML oxygen pressure during Zn-evaporation:  $5 \cdot 10^{-7}$  mbar); (a) hydrogen- and water-desorption curve, (b) methanol-desorption curves, (c) carbon dioxide-desorption curve, (d) formate- and zinc-desorption curve

According to these results it seems that there is always zinc desorption when there is formate desorption. Even at temperatures where there is no zinc desorption from Pd expected. To verify if this is a new, unknown effect methanol desorption from clean Pd(111) was investigated.

### **Methanol desorption from Pd(111) - 1<sup>st</sup> experiment**

The sample was cleaned twice (sample cleaning process see chapter 3.1) before this measurement was done. After that, the sample was cooled down to  $T = -118^{\circ}\text{C}$  ( $\approx 155\text{ K}$ ) for methanol exposition. Then the TDS-measurement was started. Figure 4.5 shows the thermal desorption spectra of this experiment.

Again water and hydrogen show the same behavior, the curves have the same shape. The peaks of each curve nearly lie at the same temperature (within the error of measurement). As it is shown in figure 4.5(a) the first water peak is seen at  $T = 18^{\circ}\text{C}$ , the first hydrogen peak at  $T = 25^{\circ}\text{C}$ . The second water peak can be found at  $T = 404^{\circ}\text{C}$  and the second hydrogen peak lies at  $T = 410^{\circ}\text{C}$ .

In figure 4.5(b) the desorption curves of methanol are shown. As in all experiments before they look like the same and the peaks of all three curves are at the same temperature. So the first peak of all three compounds lies at  $T = 18^{\circ}\text{C}$  and the second one is found at  $T = 404^{\circ}\text{C}$ . They match very well with the water-peaks.

Figure 4.5(c) shows the  $\text{CO}_2$  desorption curve. There is a sharp peak from  $T = -35^{\circ}\text{C}$  till  $T = 58^{\circ}\text{C}$ .

Figure 4.5(d) shows the most surprising result. There is again formate desorption from  $T = -55^{\circ}\text{C}$  till  $T = 98^{\circ}\text{C}$  but there is also zinc desorption. So we have zinc desorption even if there is no zinc exposed to the sample. To verify this results, this measurement was repeated.

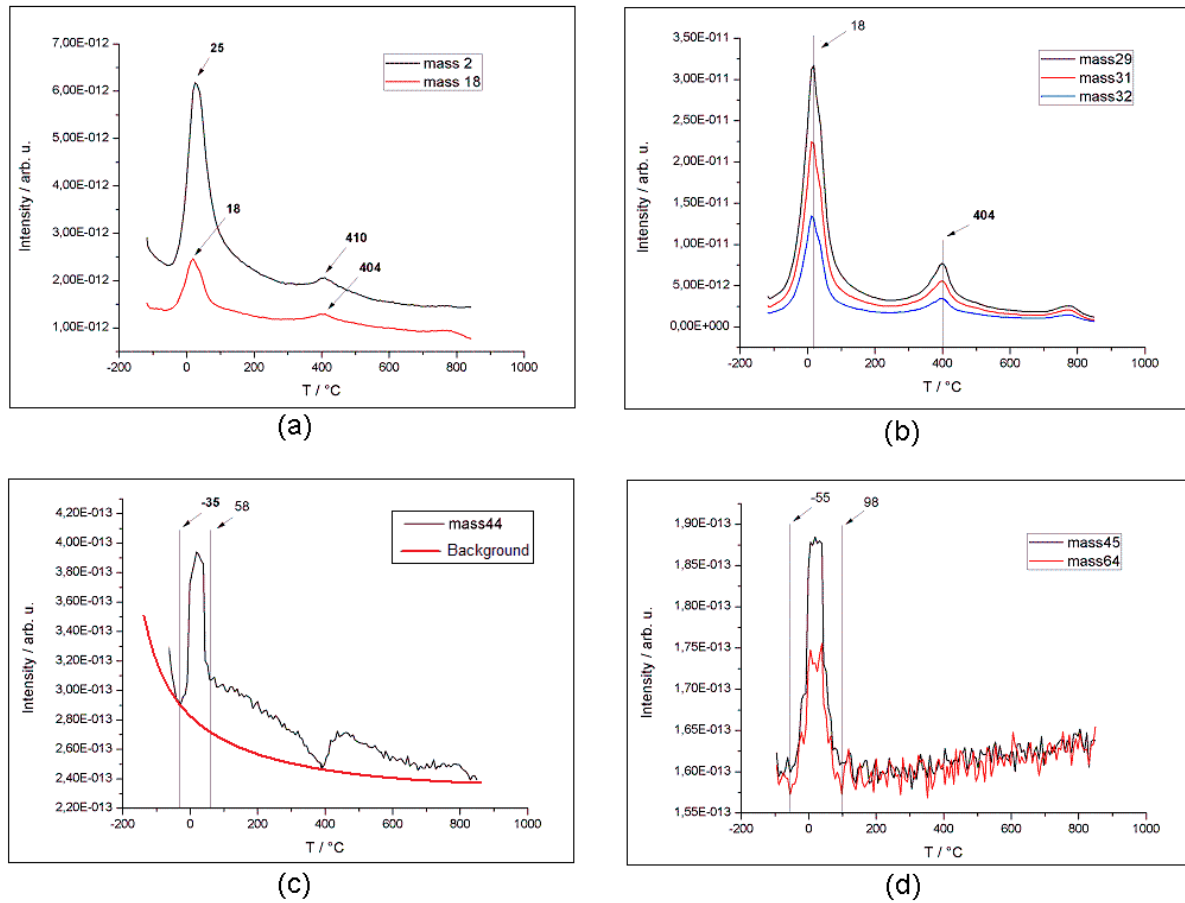


Figure 4.5.: Thermal desorption spectra of methanol desorption from Pd - 1<sup>st</sup> experiment; (a) hydrogen- and water-desorption curve, (b) methanol-desorption curves, (c) carbon dioxide-desorption curve, (d) formate- and zinc-desorption curve

### Methanol desorption from Pd(111) - 2<sup>nd</sup> experiment

The sample was cleaned again before it was cooled down to  $T = -109^{\circ}\text{C}$  ( $\approx 164\text{ K}$ ) for methanol exposition. Afterwards the TDS-measurement was started. Figure 4.6 shows the thermal desorption spectra of this experiment.

The results are similar to the 1<sup>st</sup> Pd-methanol experiment as it is seen in figure 4.6. The water- and hydrogen-desorption curves (figure 4.6(a)) show the same shape and now the peaks are at the same temperature. The first water- and hydrogen-peak can be seen at  $T = 36^{\circ}\text{C}$ , the second one lies at  $T = 416^{\circ}\text{C}$ .

The desorption curves for mass 29, 31 and 32 (methanol-desorption in figure 4.6(b)) are identically (temperatures within the error of measurement) to them in the last experiments. The peaks are at  $T = 30^{\circ}\text{C}$  and  $T = 415^{\circ}\text{C}$ .

Carbon dioxide (figure 4.6(c)) shows the same behavior than in the last experiment. There is a peak from  $T = -4^{\circ}\text{C}$  till  $T = 67^{\circ}\text{C}$ . Again the red line symbolizes the background. After all there seems to be a broad peak from  $T = 428^{\circ}\text{C}$  till the end of the TDS.

Like in the last experiment there is a formate- and zinc-peak from  $T = -23^{\circ}\text{C}$  till  $T = 108^{\circ}\text{C}$  (see figure 4.6(d)). Again there is zinc desorption when there is formate desorption.

Figure 4.7 shows the zinc-desorption-curves of both Pd-methanol-experiments. As it can be seen in figure 4.7(a) there is no decrease of intensity of the peak. There is always the same amount of formate/zinc desorbing from the surface. Both peaks are starting and ending at nearly the same temperature. Figure 4.7(b) and (c) show the whole zinc desorption in both experiments. The blue line symbolizes the background. As it can be seen in figure 4.7(b) a small amount of zinc desorbs from  $T = 430^{\circ}\text{C}$  till  $T = 700^{\circ}\text{C}$ . So in the first experiment there was definitely still zinc on the sample left. In figure 4.7(c) a slight increase of the signal above  $T = 500^{\circ}\text{C}$  is seen, too. So even in the second experiment there was a small amount of zinc on the sample surface left.

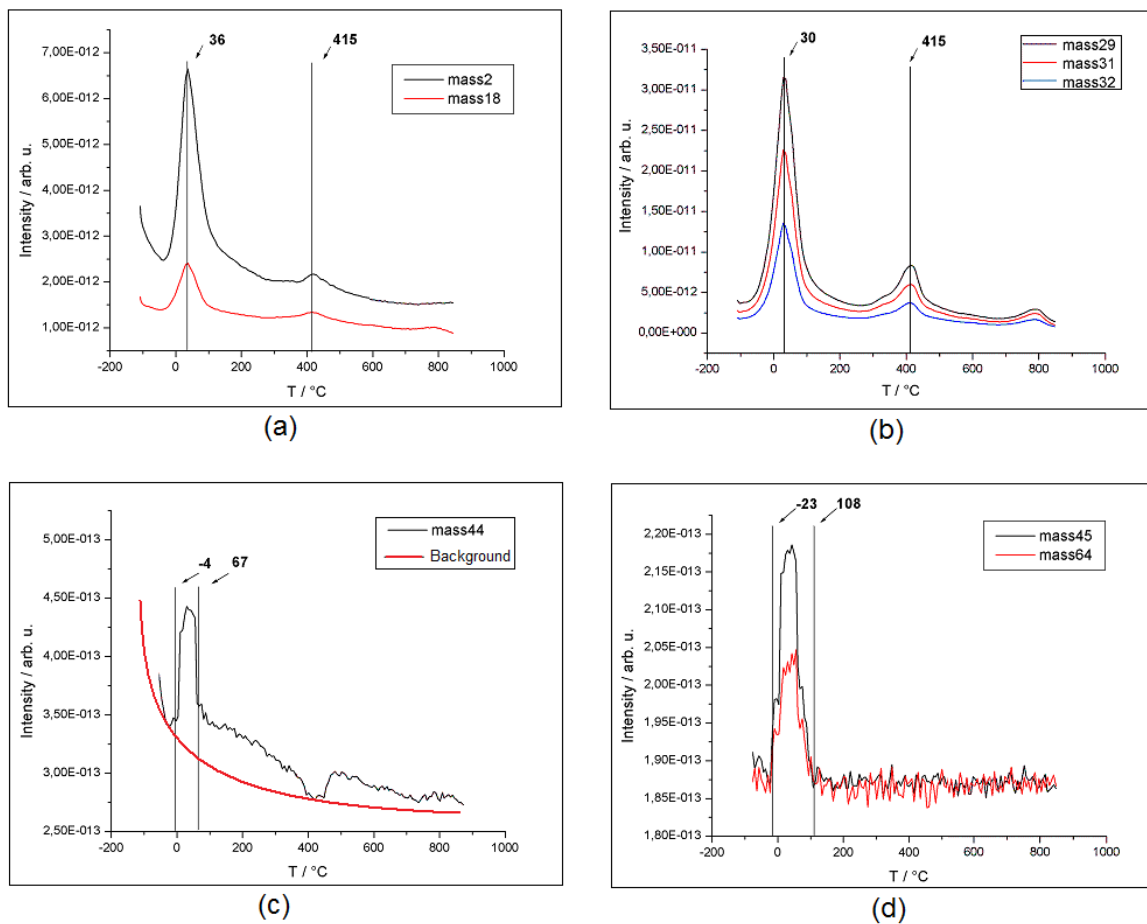


Figure 4.6.: Thermal desorption spectra of methanol desorption from Pd - 2<sup>nd</sup> experiment; (a) hydrogen- and water-desorption curve, (b) methanol-desorption curves, (c) carbon dioxide-desorption curve, (d) formate- and zinc-desorption curve

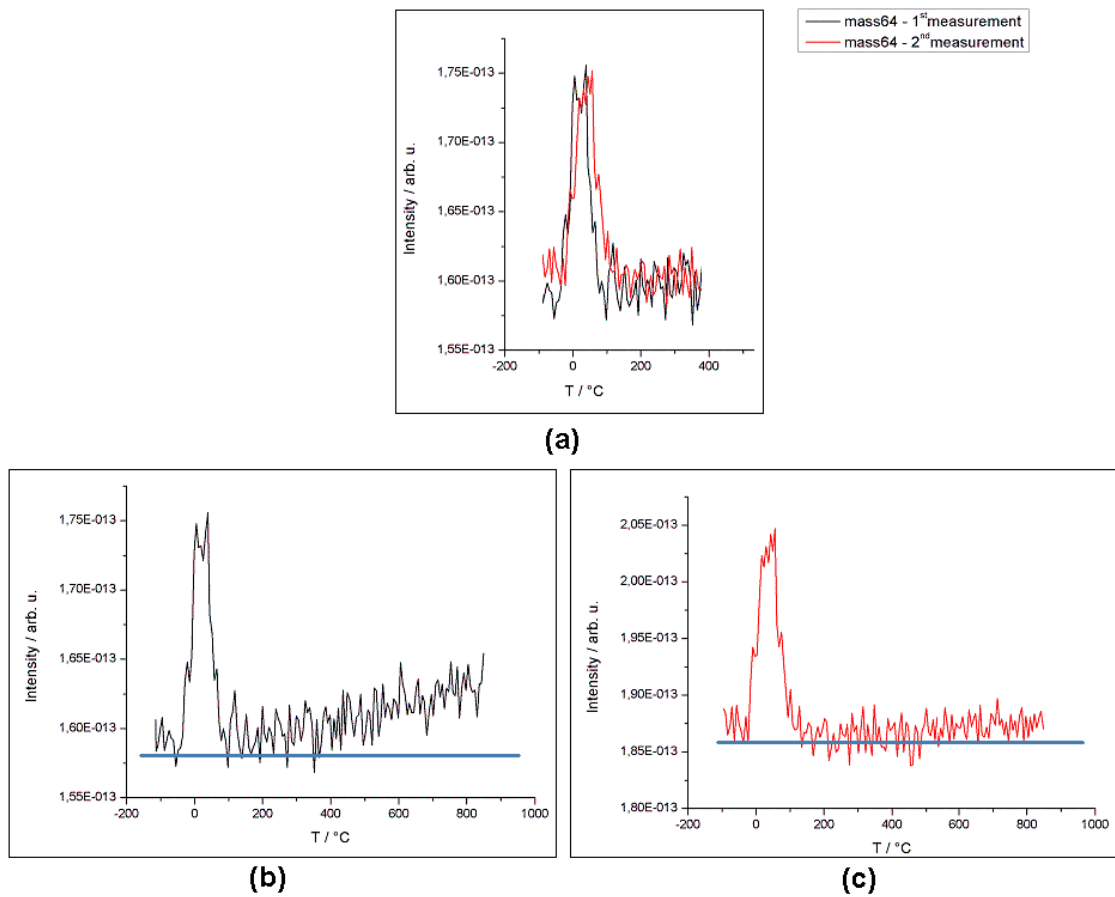


Figure 4.7.: TDS of mass 64 desorption from Pd; Comparison of the two Pd-methanol-TDS-experiments

### Discussion - 1<sup>st</sup> Measurement series

In this 1<sup>st</sup> measurement series methanol desorption from Pd(111), Pd/Zn and Pd/ZnO (with two different ZnO-layers) were investigated. Figure 4.9<sup>1</sup> shows the desorption curves of all detected masses of all experiments (to get a better overview the results of the first methanol/Pd-measurement are not shown in these figures. Besides they are similar to the results in the second methanol/Pd-measurement). In figure 4.9(a) the hydrogen-desorption curves of all measurements in this first series are shown. All curves nearly look the same apart from the desorption from the Pd-sample. There is only a difference in intensity. Highest intensity of the first hydrogen peak is seen for clean Pd. This peak seems to be the smallest if there is a small amount of zinc (0.4 ML) adsorbed to the sample (see red line in figure 4.9(a)). With rising coverage this peak grows again (0.6 ML, see blue and black curve in figure 4.9(a)).

At figure 4.9(b) water desorption of all experiments is shown. As it can be seen, there are four peaks if the sample is covered with high oxidized ZnO. In all other cases there are two peaks. There is a shift between the water peaks desorbing from Pd(111) and Pd/Zn ( Pd:  $T = 36^{\circ}\text{C}$  and  $415^{\circ}\text{C}$ , Pd/Zn:  $T = -24^{\circ}\text{C}$  and  $325^{\circ}\text{C}$ ) but both curves have the same shape. This indicates an electronic influence of the Zn on the Pd, which was found in DFT calculations [21]. So the overall shape is the same which leads to the assumption that the Pd(111) sample was not clean. The first peak for pure Pd lies at the same temperature as the first peak of Pd/ZnO (low oxidized; black curve) at  $T = 36^{\circ}\text{C}$ . The second peak of Pd/ZnO lies at  $T = 150^{\circ}\text{C}$ , independent of the oxidation state.

Figure 4.9(c) shows the desorption curve of methanol. The desorption curves of mass 29, 31 and 32 always look the same. That is why only mass 31 is shown in figure 4.9. Mass 29 and 32 were detected to get an idea of the reactions on the sample. There should be formaldehyde (mass 29) and oxygen (mass 32) in the TDS as a result of methanol dissociation on Pd/ZnO. First, it seemed that there is formaldehyde and oxygen desorbing from the sample. But formaldehyde was also seen during the methanol desorption from clean Pd. To arise from literature (see [33], [34], [35] and [36]), there must not be any formaldehyde desorption from clean Pd because these species rapidly undergo dehydrogenation. So on Pd(111),  $\text{CH}_2\text{O}$  decomposes to CO and  $\text{H}_2$  at temperatures below  $T = -73^{\circ}\text{C}$ .

There are two explanations why there is formaldehyde desorption seen from Pd. The first one is that the sample was not really clean. Maybe there were some Zn-relics on the Pd surface left which were not seen in XPS. Knowing that the Pd(111) crystal was in use for several years, it yields to the assumption that the used crystal is Zn-contaminated

---

<sup>1</sup>In figures 4.9(a)-(d) the TDS is only shown till  $T = 700^{\circ}\text{C}$  because at these high temperatures desorption from the sample holder takes place which affects the spectrum. So the peaks around  $800^{\circ}\text{C}$  are neglected in these figures. In the case of Zn-desorption always the whole TDS is shown to have a look at the whole Zn-peak

so that after several cleaning processes there is still Zn on the surface or in near surface layers left.

The second explanation is that the TDS-measurements are affected by the sample holder. As you can see in figure 4.8 the sample is mounted on a copper holder by two tantalum wires (see chapter 2.1.1). These wires are fixed between two copper blocks (CB1 and CB2 in figure 4.8). Maybe the distance  $d$  between these two copper blocks is too small so that they get warm during a measurement even if they are nitrogen cooled. To avoid this glitch the copper holder has to be redesigned.

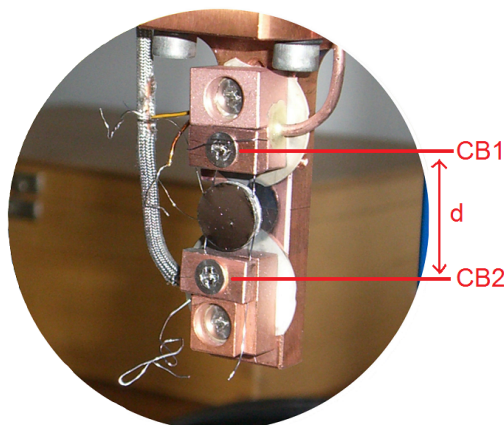


Figure 4.8.: The Pd(111) sample mounted on the copper holder;  
CB1 - copper block 1  
CB2 - copper block 2  
 $d$  - distance between the two copper blocks

In the end the answer was very simple. Subtracting the calculated amount of each methanol fragment of the detected TDS gives a flat line of mass 29, 31 and 32. So the detected mass 29 is no formaldehyde which arises from reaction on the sample. The same applies for oxygen which is not a reaction product. Here only methanol and its fragments are seen which are formed in the QMS. This is an important fact. For each experiment methanol shows the same behavior. As it can be seen in figure 4.9(c), there is only a shift of the peaks between every experiment as well as a difference in intensity. Methanol is desorbing from Pd/Zn at lowest temperatures ( $T = -31^{\circ}\text{C}$ ). For Pd/ZnO this peak shifts up to  $T = 3^{\circ}\text{C}$  (high oxidated) and  $T = 29^{\circ}\text{C}$  (low oxidized). Desorbing from pure Pd this peak appears at  $T = 30^{\circ}\text{C}$  with highest intensity. The second peak can be found at  $T = 326^{\circ}\text{C}$  for Pd/Zn (0.6 ML Zn) and at  $T = 331^{\circ}\text{C}$  for Pd/ZnO (0.6 ML ZnO; low oxidized). If the sample is clean (Pd:  $T = 415^{\circ}\text{C}$ ) or has a coverage of 0.4 ML ZnO (Pd/ZnO:  $T = 409^{\circ}\text{C}$ ) this peak lies almost at the same temperature. So the second peak correlates with the amount of Zn or rather ZnO. This correlation cannot be found for the first peak.

In figure 4.9(d) the desorption curves for CO<sub>2</sub> are shown. As it is seen, they always look different. There is some similarity between the curves if CO<sub>2</sub> desorbs from Pd/ZnO but even there is a difference. Assuming that the baseline is not a horizontal but falls with rising temperature, leads to the following results. First of all there is nearly no CO<sub>2</sub> desorbing from Pd/Zn. A very small amount desorbs at low temperature. No CO<sub>2</sub> is seen at T = 325°C. At higher temperatures there is a small amount seen again. Nearly the same applies for clean Pd with the exception that a large peak is seen from T = -4°C till T = 67°C. No CO<sub>2</sub> is seen from T = 375°C until T = 428°C. At higher temperatures (above T = 300°C) a small amount of CO<sub>2</sub> is seen again. This leads to the assumption again that the sample was not really clean. As well, this CO<sub>2</sub> amount may origin from the sample holder. The similarity of the CO<sub>2</sub> desorption curves of Pd/ZnO was already mentioned. Both curves have the same shape. There is a shift of the peaks between these curves which may arise from different ZnO coverage. Hence the first peak of the high oxidized ZnO layer is only seen partial for low oxidized ZnO.

In figure 4.9(e) and (f) the desorption curves of formate and zinc are shown. Table 4.2 shows the temperatures where these peaks are seen. In the left hand side of table 4.2 the temperatures of the formate peaks are shown for each sample. On the right hand side they are shown for zinc. The temperatures where the second zinc peaks start to grow are displayed in the rightmost column. As one can see, there is always a zinc peak if there is a formate peak. Depending on the substrate these peaks appear at different temperatures. Nevertheless, they always appear together. In all experiments methanol exposition took place under nearly the same temperature (around T = -108°C) so there is no correlation between the peaks and the adsorption temperature seen. As well there seems to be no correlation between Zn coverage and desorption temperature. First, this seemed to be a new effect, so that formate desorption at low temperature leads to a zinc desorption where normally no zinc desorption is expected. But this zinc peak is also seen for methanol desorption from clean Pd. Again the reason for this behavior could be an influence by the sample holder. Another reason could be that the sample was not clean.

| Mass 45                      | Start  | End   | Mass 64                      | Start  | End   | 2.Peak start |
|------------------------------|--------|-------|------------------------------|--------|-------|--------------|
| Pd                           | -23°C  | 108°C | Pd                           | -23°C  | 108°C | —            |
| Pd/Zn                        | -102°C | 36°C  | Pd/Zn                        | -108°C | 26°C  | 475°C        |
| Pd/ZnO - low O <sub>2</sub>  | -44°C  | 82°C  | Pd/ZnO - low O <sub>2</sub>  | -37°C  | 83°C  | 475°C        |
| Pd/ZnO - high O <sub>2</sub> | -58°C  | 70°C  | Pd/ZnO - high O <sub>2</sub> | -65°C  | 76°C  | 521°C        |

Table 4.2.: Start- and end-temperature of the formate and the zinc peak in the first series of measurements

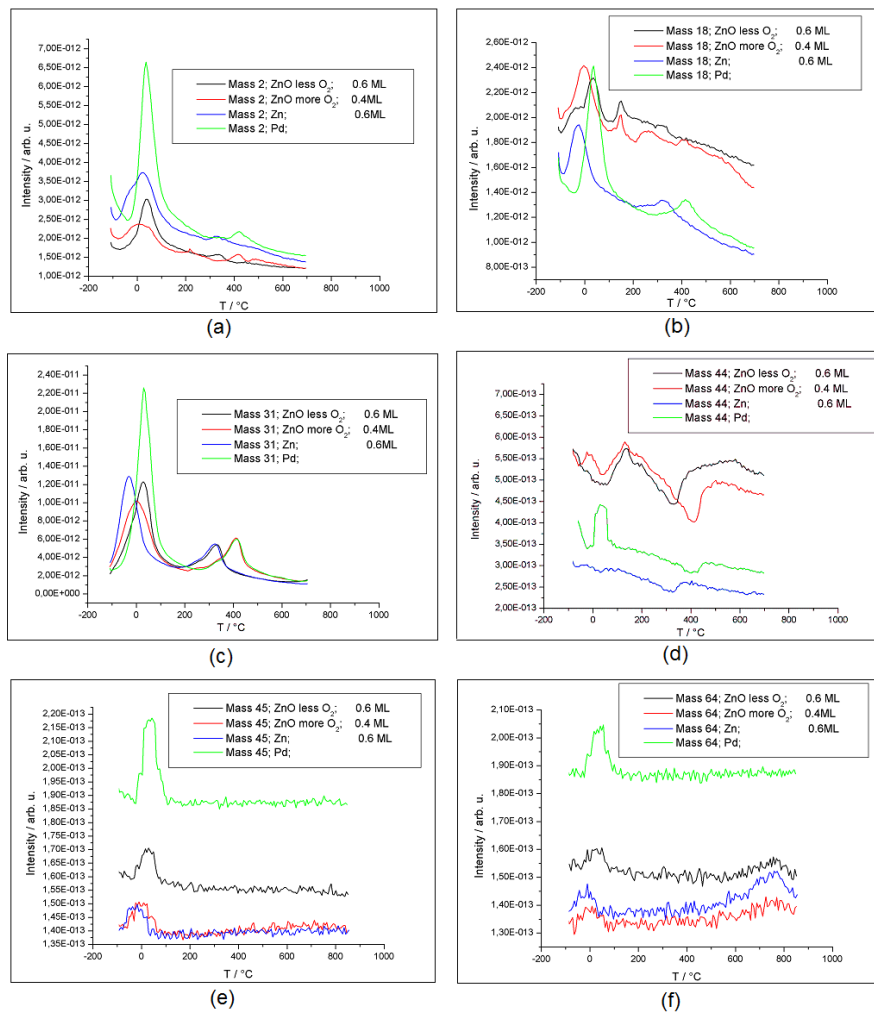


Figure 4.9.: TDS of the 1<sup>st</sup> Measurement series; (a) hydrogen-desorption, (b) water-desorption, (c) methanol-desorption, (d) carbon dioxide-desorption, (e) formate-desorption, (f) zinc-desorption, of all experiments

### 4.1.2. 2<sup>nd</sup> Measurement series

Until now, a coverage below 1 ML was always investigated. Now a ZnO-multilayer was formed. Therefore, two measurements with high oxidized ZnO were done.

#### Methanol desorption from Pd/ZnO - high O<sub>2</sub> pressure - 1<sup>st</sup> measurement

After the cleaning process Zn was evaporated under a high oxygen atmosphere ( $1 \cdot 10^{-5}$  mbar) for 50 seconds (instead of 10 seconds in the last series) to gain a ZnO multilayer. The results show that only 0.8 ML of ZnO were given. That is why two experiments were done. The sample was cooled down to  $T = -64^\circ\text{C}$  ( $\approx 209$  K) for methanol exposition. Figure 4.10 shows the thermal desorption spectra of this experiment. As one can see, the results are completely different to the ones from the first series.

Figure 4.10(a) shows the hydrogen- and water-desorption curves. Water-peaks are seen at  $T = -19^\circ\text{C}$ ,  $410^\circ\text{C}$ ,  $529^\circ\text{C}$  and  $606^\circ\text{C}$ . At  $T = 21^\circ\text{C}$  there could be a very small water peak. Another small water peaks is seen at  $T = 600^\circ$  and around  $T = 708^\circ\text{C}$ . Hydrogen has one peak at  $T = 529^\circ\text{C}$ .

Figure 4.10(b) shows a totally different behavior of the methanol compounds compared to the last experiments. All of them have two peaks at  $T = 516^\circ\text{C}$  and  $T = 600^\circ\text{C}$ . Additionally there is a third mass 32 peak at  $T = 709^\circ\text{C}$  which is a real oxygen peak. This one originates from ZnO desorption (Zn desorbs at nearly the same temperature  $T = 715^\circ\text{C}$ ). The first peak from the 1<sup>st</sup> measurement series is seen partial around  $T = -50^\circ\text{C}$ .

The first CO<sub>2</sub> peak (figure 4.10(c)) lies at the same temperature as water ( $T = -19^\circ\text{C}$ ). There is a second peak from  $T = 483^\circ\text{C}$  till  $T = 747^\circ\text{C}$ .

The greatest difference between this experiment and all previous measurements is seen at figure 4.10(d). There the desorption curves of zinc and formate are shown. No formate is detected, and there is only a high temperature zinc peak at  $T = 715^\circ\text{C}$  which looks like a Pd/Zn-alloy peak (see [19]).

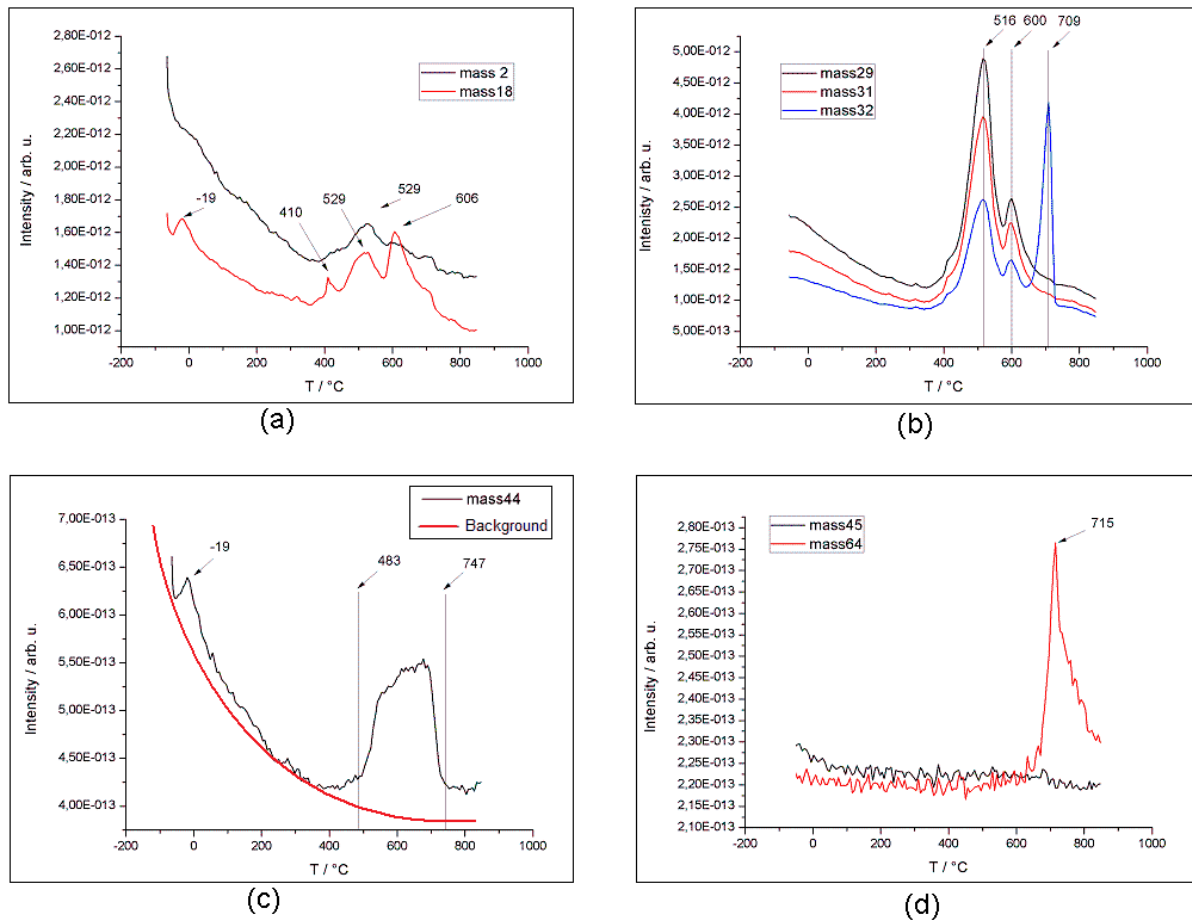


Figure 4.10.: Thermal desorption spectra of methanol desorption from Pd/ZnO (ZnO coverage: 0.8 ML; oxygen pressure during Zn-evaporation:  $1 \cdot 10^{-5}$  mbar); (a) hydrogen- and water-desorption curve, (b) methanol-desorption curves, (c) carbon dioxide-desorption curve, (d) formate- and zinc-desorption curve

### Methanol desorption from Pd/ZnO - high O<sub>2</sub> pressure - 2<sup>nd</sup> measurement

In the last experiment of this series a coverage of 0.8 ML ZnO was given. The aim was to get a multilayer, so the experiment was repeated. In this experiment Zn was evaporated under a high oxygen atmosphere for 90 seconds. The results show that a coverage of 2.2 ML was given. The sample was cooled down to  $T = -69^{\circ}\text{C}$  ( $\approx 204\text{ K}$ ). Figure 4.11 shows the thermal desorption spectra of this experiment. Again the results differ from previous experiments.

Figure 4.11(a) shows the water- and hydrogen-desorption curves. Hydrogen-peaks are seen at  $T = 18^{\circ}\text{C}$ ,  $145^{\circ}\text{C}$ ,  $551^{\circ}\text{C}$  and  $744^{\circ}\text{C}$ . The peak at  $T = 145^{\circ}\text{C}$  seems to be an artefact due to the unusual peak shape. The first water peak is seen at  $T = -22^{\circ}\text{C}$ . A broad water peak can be found from  $T = 498^{\circ}\text{C}$  till  $T = 531^{\circ}\text{C}$  which seems to consist of two peaks. A last water-peak can be seen at the same temperature than the last hydrogen-peak at  $T = 744^{\circ}\text{C}$ .

Mass 29, 31 and 32 (figure 4.11(b)) show a completely different behavior than in the previous experiments. All three species show again the same behavior (apart from the last oxygen-peak at  $T = 738^{\circ}\text{C}$ ) but compared to the last experiments the peaks are at different temperatures. Also the number of peaks is different to the last experiments. All three compounds have peaks at  $T = 4^{\circ}\text{C}$ ,  $159^{\circ}\text{C}$ ,  $206^{\circ}\text{C}$ ,  $233^{\circ}\text{C}$  and  $531^{\circ}\text{C}$ . Oxygen has a sixth peak at  $T = 738^{\circ}\text{C}$  which again arises from ZnO desorption.

The desorption curve of CO<sub>2</sub> (figure 4.11(c)) looks similar to the last experiment. There are two broad peaks, the first one from  $T = -50^{\circ}\text{C}$  till  $T = 11^{\circ}\text{C}$  and the second one from  $T = 518^{\circ}\text{C}$  until  $T = 763^{\circ}\text{C}$ .

Again there is no formate detected (black line in figure 4.11(d)). The zinc desorption curve shows the same shape than in the last experiment. There is a sharp peak at  $T = 744^{\circ}\text{C}$ .

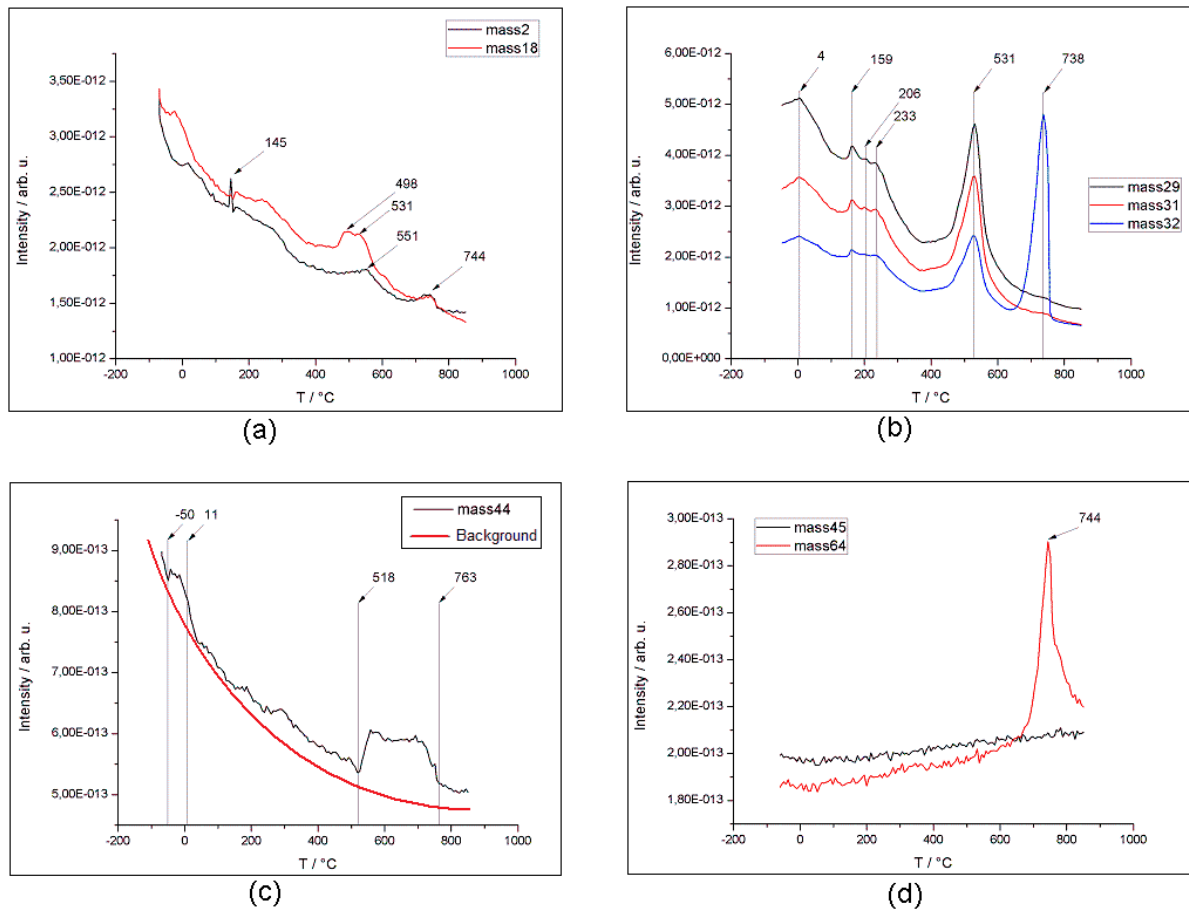


Figure 4.11.: Thermal desorption spectra of methanol desorption from Pd/ZnO (ZnO coverage: 2.2 ML; oxygen pressure during Zn-evaporation:  $1 \cdot 10^{-5}$  mbar); (a) hydrogen- and water-desorption curve, (b) methanol-desorption curves, (c) carbon dioxide-desorption curve, (d) formate- and zinc-desorption curve

## Discussion - 2<sup>nd</sup> Measurement series

Methanol desorption from Pd/ZnO was investigated in this series of measurements. The aim was to investigate methanol desorption from a ZnO-multilayer. In the first experiment a coverage of 0.8 ML is given. Because of this, a second experiment was done. There a coverage of 2.2 ML is given. Figure 4.12 shows the desorption curves of all detected masses of this series (except mass 29; mass 29 looks like mass 31 so it is not shown in this figure). There one can see the differences of a sub-monolayer and a multilayer coverage. Figure 4.12(a) shows the desorption curves of hydrogen. The black curve shows the hydrogen desorption of the ZnO-sub-monolayer (0.8 ML). There are peaks at  $T = -19^{\circ}\text{C}$ ,  $410^{\circ}\text{C}$ ,  $529^{\circ}\text{C}$  and  $606^{\circ}\text{C}$ . The red line (2.2 ML ZnO-coverage) shows three peaks at  $T = 18^{\circ}\text{C}$ ,  $551^{\circ}\text{C}$  and  $744^{\circ}\text{C}$ . At  $T = 145^{\circ}\text{C}$  an artefact is seen. Except for the first peak both curves nearly look the same. It seems that the last two peaks shift to higher temperatures with higher coverage.

The water desorption also looks different depending on the ZnO coverage. There are four peaks ( $T = -19^{\circ}\text{C}$ ,  $410^{\circ}\text{C}$ ,  $521^{\circ}\text{C}$  and  $606^{\circ}\text{C}$ ) for the sub-monolayer and only three ( $T = 498^{\circ}\text{C}$ ,  $531^{\circ}\text{C}$ ,  $744^{\circ}\text{C}$ ) if there is a coverage of 2.2 ML.

Methanol desorption is shown in figure 4.12(c). For a coverage of 0.8 ML there are two peaks ( $T = 516^{\circ}\text{C}$  and  $T = 600^{\circ}\text{C}$ ) for 2.2 ML ZnO there are five peaks seen ( $T = 4^{\circ}\text{C}$ ,  $159^{\circ}\text{C}$ ,  $206^{\circ}\text{C}$ ,  $233^{\circ}\text{C}$  and  $531^{\circ}\text{C}$ ). The oxygen-desorption curve looks identical to the corresponding methanol-curve but has always one more peak at higher temperature. So there is an additional peak at  $T = 709^{\circ}\text{C}$  at 0.8 ML coverage. At a ZnO coverage of 2.2 ML there is an additional oxygen-peak (figure 4.12(d)) at  $T = 738^{\circ}\text{C}$ . These peaks seem to be real oxygen peaks which arise from ZnO desorption.

The  $\text{CO}_2$ -desorption curves always have the same shape (figure 4.12(e)). There are peaks below zero degrees, at  $T = -19^{\circ}\text{C}$  for 0.8 ML as well as at  $T = -50^{\circ}\text{C}$  and  $11^{\circ}\text{C}$  for 2.2 ML. At higher temperatures there is a broad peak from  $T = 483^{\circ}\text{C}$  till  $T = 747^{\circ}\text{C}$  for 0.8 ML ZnO coverage which shifts to higher temperatures (from  $T = 518^{\circ}\text{C}$  till  $T = 763^{\circ}\text{C}$ ) for a coverage of 2.2 ML.

No formate peak is seen in this series of measurements (see figure 4.12(f)). The Zn-desorption looks different compared with the last series. No matter if there is a sub-monolayer or a multilayer of ZnO there is always a sharp peak around  $T = 730^{\circ}\text{C}$ . In combination with the absence of the formate-peak it seems that the reaction path depends on the amount of supplied ZnO. At a coverage  $< 1$  ML the surface is covered with several ZnO islands which results in many Pd/ZnO-interfaces. At a coverage  $> 1$  ML the whole surface is covered with ZnO, so there are no interfaces left. In the first experiment of this series a ZnO coverage of 0.8 ML was calculated. So almost the whole surface is covered with ZnO. Hence there are less Pd/ZnO-interfaces than in the 1<sup>st</sup> measurement series. The calculation of the ZnO coverage has an approximative measurement error of  $\pm 0.2$  ML. So it could be that there is already 1 ML coverage. In the second experiment

of this measurement series a ZnO coverage of 2.2 ML is given. No Pd/ZnO-interfaces are present anymore. So in this measurement series the Pd surface is covered with much more ZnO than in the last series of measurement where a coverage around 0.5 ML was given. For this reason there are no Pd/ZnO-interfaces on the surface left. The comparison of the results of the 1<sup>st</sup> (< 1 ML ZnO) and the 2<sup>nd</sup> measurement series (> 1 ML ZnO) leads to the conclusion that the dissociation of methanol occurs at the Pd/Zn or rather Pd/ZnO interfaces. This would explain the differences in the desorption curves of mass 31 and mass 32 between these measurements series.

Of course another explanation is that only  $T = -64^{\circ}\text{C}$  in the first and  $T = -69^{\circ}\text{C}$  in the second experiment were reached (compared with  $T = -108^{\circ}\text{C}$  in the 1<sup>st</sup> series). So methanol desorption took place even before the TDS was started. This also may be a reason why no formate desorption is seen.

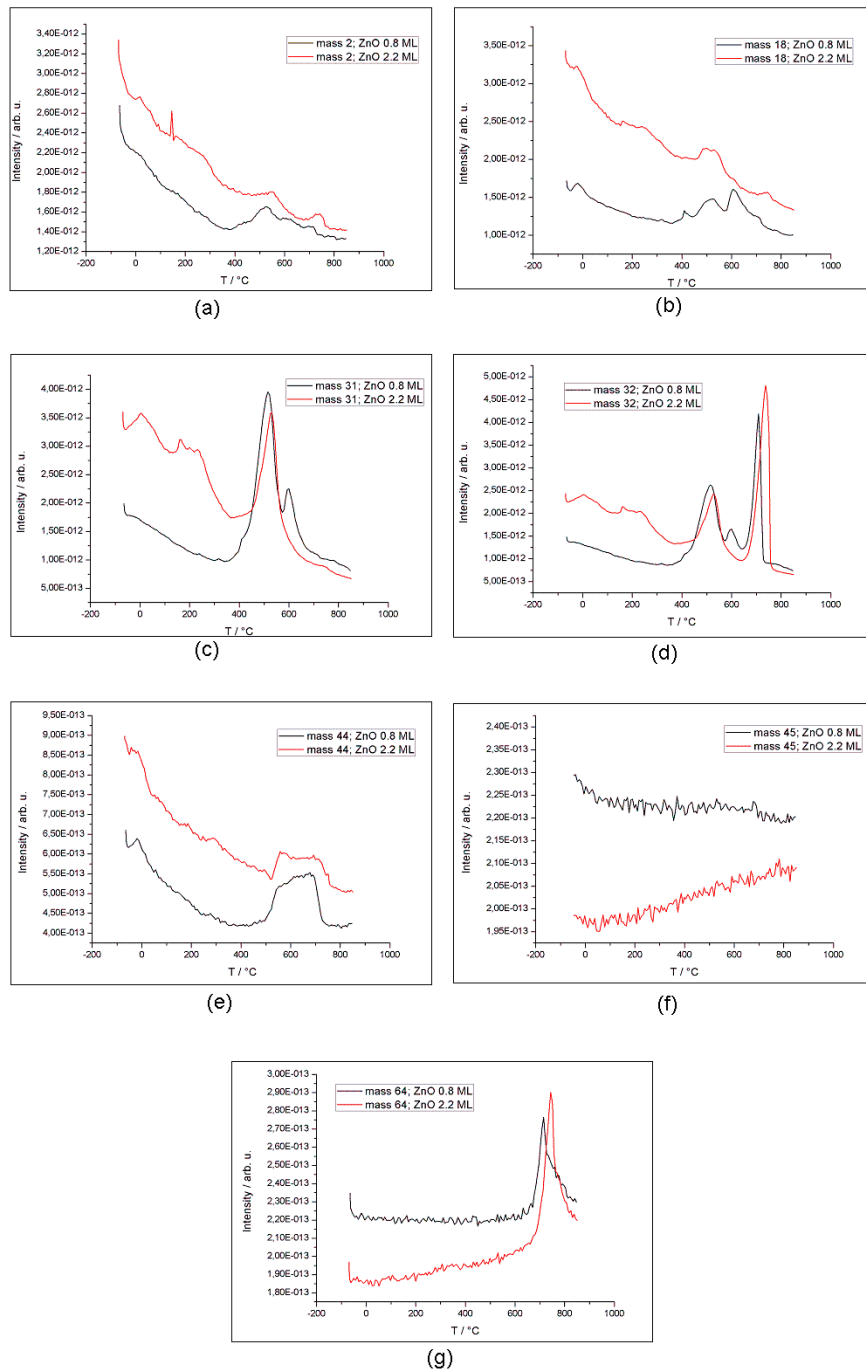


Figure 4.12.: TDS of the 2<sup>st</sup> Measurement series; (a) hydrogen-desorption, (b) water-desorption, (c) methanol-desorption, (d) oxygen-desorption, (e) carbon dioxide-desorption, (f) formate-desorption, (g) zinc-desorption, of all experiments

### 4.1.3. 3<sup>rd</sup> Measurement series

Again methanol desorption from Pd/ZnO (submonolayer) and clean Pd were investigated. This series was done to check if the zinc-formate peak which was seen in the first series will appear again.

#### Methanol desorption from Pd(111) - 3<sup>rd</sup> Series of Measurement

In the first experiment of this series methanol desorption from the clean Pd sample was investigated. After the cleaning process the sample was cooled down to  $T = -89^{\circ}\text{C}$  ( $\approx 184\text{ K}$ ) for methanol exposition. Figure 4.13 shows the thermal desorption spectra of this experiment.

Figure 4.13(a) shows the thermal desorption spectra of hydrogen and water. With the exception of the first hydrogen-peak ( $T = 26^{\circ}\text{C}$ ) both curves look the same. There are peaks at  $T = 274^{\circ}\text{C}$  and  $T = 674^{\circ}\text{C}$ .

Again the desorption spectra of mass 29, 31 and 32 look the same. Compared to the last series of measurement mass 32 has now the same behavior than mass 31 and mass 29. So there is no individual oxygen peak at high temperature. There are peaks at  $T = -15^{\circ}\text{C}$ ,  $214^{\circ}\text{C}$ ,  $268^{\circ}\text{C}$  and  $668^{\circ}\text{C}$ . Like in the 1<sup>st</sup> measurement series it seems that only methanol is seen, referring to the background.

$\text{CO}_2$  desorption is seen in figure 4.13(c). Again there is a falling baseline. So there is little amount of  $\text{CO}_2$  desorbing at low temperatures. At  $T = 247^{\circ}\text{C}$  no  $\text{CO}_2$  is seen. Carbon dioxide desorbs again from  $T = 307^{\circ}\text{C}$  till  $T = 713^{\circ}\text{C}$ .

As it can be seen at figure 4.13(d) there is no formate and no zinc desorption.

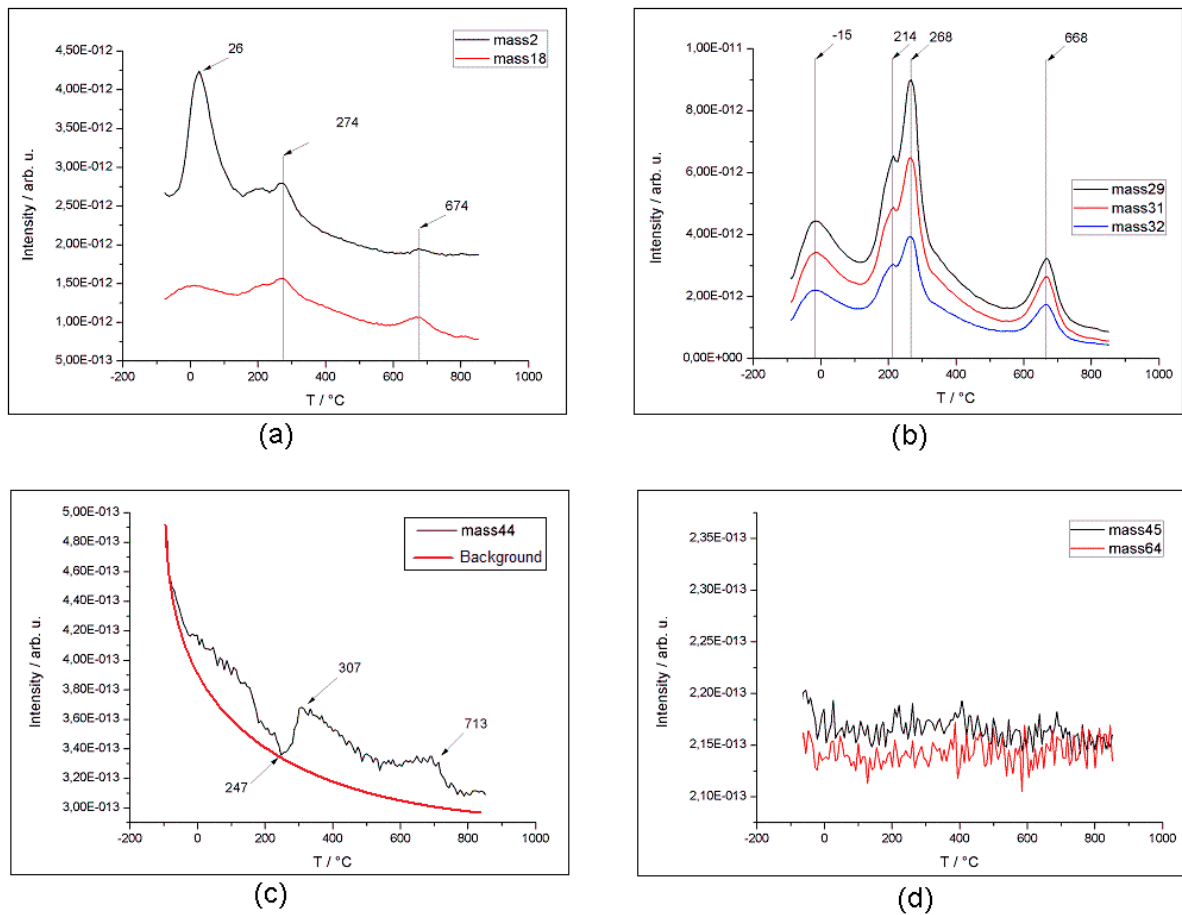


Figure 4.13.: Thermal desorption spectra of methanol desorption from Pd - 3<sup>rd</sup> Measurement series;

(a) hydrogen- and water-desorption curve, (b) methanol-desorption curves, (c) carbon dioxide-desorption curve, (d) formate- and zinc-desorption curve

### Methanol desorption from Pd/ZnO - high O<sub>2</sub> pressure - 3<sup>rd</sup> measurement

At last methanol desorption from Pd/ZnO was investigated again. A ZnO coverage of 0.3 ML was given. The Zn evaporation took place under a high oxygen atmosphere ( $1 \cdot 10^{-5}$  mbar). The sample was cooled down to  $T = -86^\circ\text{C}$  ( $\approx 187$  K) for methanol exposition. Figure 4.14 shows the thermal desorption spectra of this experiment.

Figure 4.14(a) shows the thermal desorption spectra of hydrogen and water. With the exception of the first water-peak ( $T = -18^\circ\text{C}$ ) both curves look the same. There are peaks at  $T = 178^\circ\text{C}$  and  $T = 712^\circ\text{C}$ . A very small hydrogen-peak can be found at  $T = 43^\circ\text{C}$ .

Figure 4.14(b) shows the desorption curves of methanol. It can be seen that all three curves look the same except that there is an additional oxygen-peak at  $T = 648^\circ\text{C}$ . This peak seems to be an artefact. Apart from that all three species have peaks at the same temperatures ( $T = 171^\circ\text{C}$  and  $T = 699^\circ\text{C}$ ). A small peak is also seen around  $T = -38^\circ\text{C}$ .

The CO<sub>2</sub> desorption curve (figure 4.14(c)) looks similar to the CO<sub>2</sub> desorption curve from clean Pd. The differences are as follows: There are two peaks at low temperature ( $T = -65^\circ\text{C}$  and  $T = -18^\circ\text{C}$ ). No CO<sub>2</sub> is seen at  $T = 158^\circ\text{C}$  (assumption that the baseline falls). The two high temperature peaks are at  $T = 224^\circ\text{C}$  and  $T = 629^\circ\text{C}$ .

Again there is a small Zn and formate peak at  $T = 178^\circ\text{C}$  (see figure 4.14(d)). A second Zn-peak starts at  $T = 578^\circ\text{C}$ . So there is a formate/zinc-peak like in the first series again. In contrast to the first series they lie at a higher temperature.

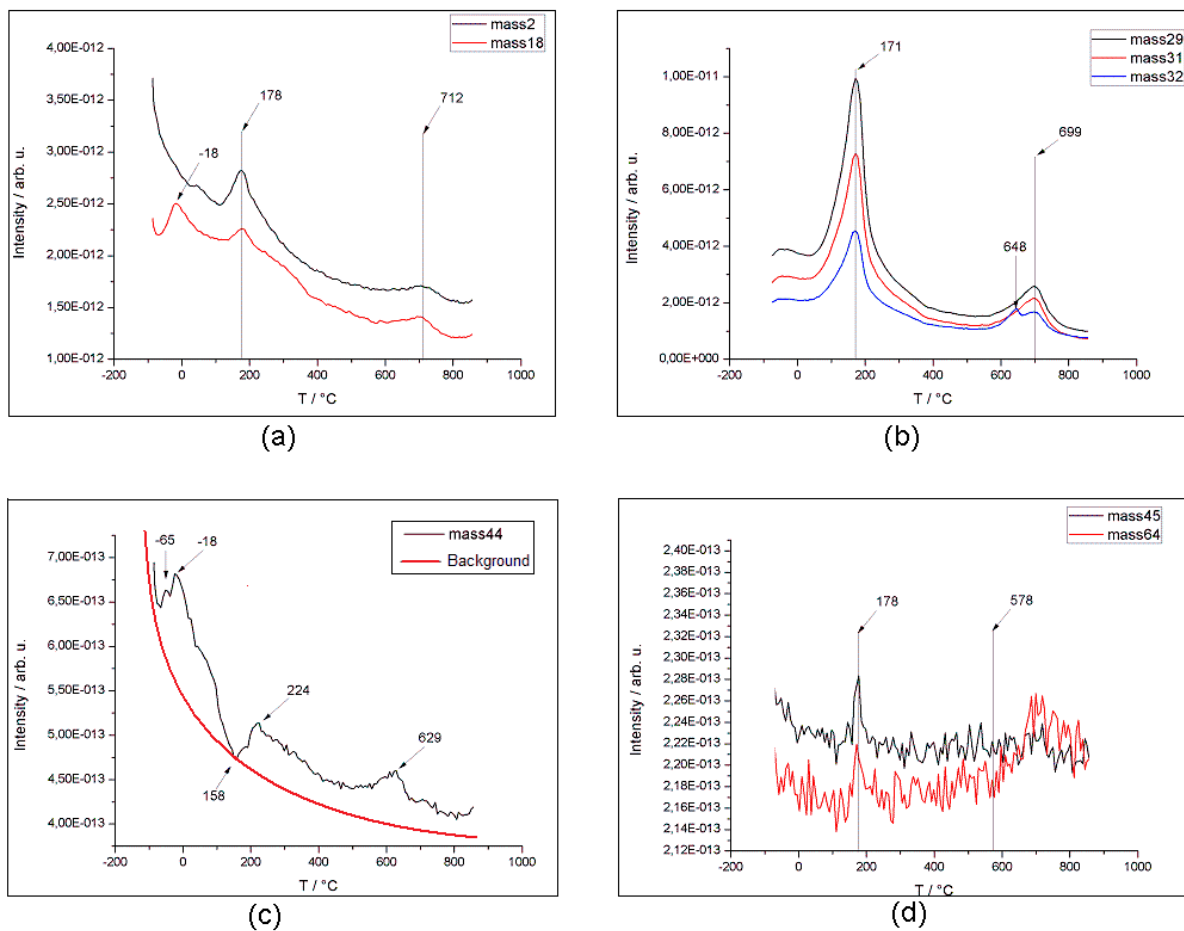


Figure 4.14.: Thermal desorption spectra of methanol desorption from Pd/ZnO (ZnO coverage: 0.3 ML; oxygen pressure during Zn-evaporation:  $1 \cdot 10^{-5}$  mbar); (a) hydrogen- and water-desorption curve, (b) methanol-desorption curves, (c) carbon dioxide-desorption curve, (d) formate- and zinc-desorption curve

### Discussion - 3<sup>rd</sup> Measurement series

In this measurement series methanol desorption from Pd and Pd/ZnO was investigated. Figure 4.15 shows the desorption curves of all detected masses of all experiments in this series. The spectra are similar to the spectra of the first series although there are some differences. At figure 4.15(a) the hydrogen-desorption spectra is shown. As one can see, there is a great difference depending if the sample is clean or ZnO covered. For the clean sample there are peaks at  $T = 26^{\circ}\text{C}$ ,  $274^{\circ}\text{C}$  and  $674^{\circ}\text{C}$ . Otherwise there are peaks at  $T = 178^{\circ}\text{C}$  and  $T = 712^{\circ}\text{C}$ .

The water desorption spectra (figure 4.15(b)) look similar. It seems that there is a shift of the high temperature peaks to lower temperatures if the sample is ZnO covered. An additional water-peak at  $T = -18^{\circ}\text{C}$  can be found for Pd/ZnO.

As every time mass 29, 31 (figure 4.15(c)) and 32 show the same behavior. Again, only methanol and its fragments are seen which are formed in the QMS. But there are differences depending on the substrate surface. If the substrate is clean Pd there are four methanol peaks seen. At a ZnO coverage of 0.3 ML they are reduced to two peaks. Again there is an additional oxygen-peak if the sample is covered with ZnO. This peak can be found at  $T = 648^{\circ}\text{C}$  and it seems to be an artefact.

Figure 4.15(d) shows the  $\text{CO}_2$  desorption spectra. Like the water spectra they nearly look the same. As well as water desorption,  $\text{CO}_2$  desorption shows a shift of the high temperature peaks to lower temperatures if the sample is covered with ZnO. In both cases (Pd, Pd/ZnO) there is a decay of the  $\text{CO}_2$  signal seen around  $T = 230^{\circ}\text{C}$ .

No formate desorption is seen for pure Pd (black line in figure 4.15(e)). This is the largest difference to the results of the first series. Maybe the sample was not clean in the first series and now it was. But there is a formate peak at  $T = 178^{\circ}\text{C}$  if the sample is ZnO covered. As it was seen in the first series of measurement, there is zinc desorption if there is formate desorption. So there is a small Zn peak seen at  $T = 178^{\circ}\text{C}$ . These peaks are much smaller and at higher temperature than in chapter 4.1.1. This differences may occur because of the low ZnO coverage (0.3 ML) which is the lowest ZnO coverage of all experiments. However there is a low temperature Zn-peak again. Maybe this peak arises from interference of the sample holder again. But these peaks are only seen if there is a ZnO-coverage below one monolayer. So it could be that these reactions occur at the Pd-ZnO-interface. Finally, the second Zn-peak at high temperature starts at  $T = 578^{\circ}\text{C}$ , where it is expected to be seen ([20], [19], [21]).

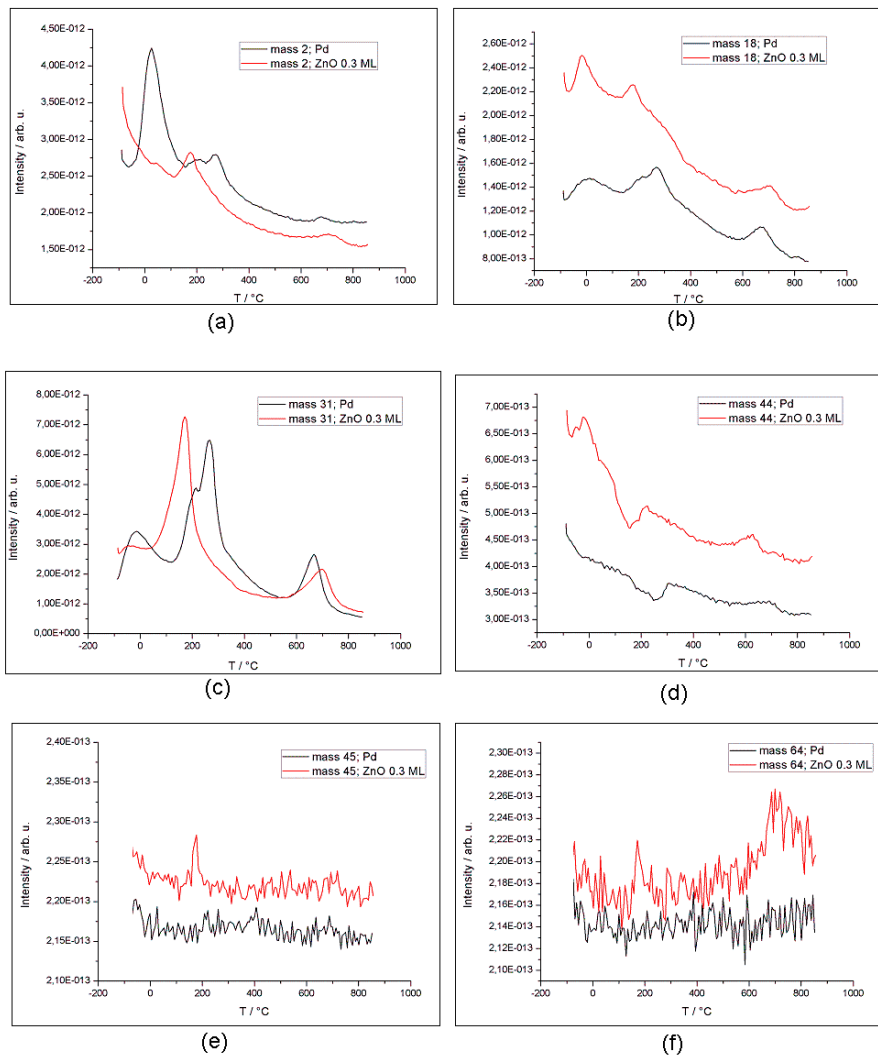


Figure 4.15.: TDS of the 3<sup>rd</sup> Measurement series; (a) hydrogen-desorption, (b) water-desorption, (c) methanol-desorption, (d) carbon dioxide-desorption, (e) formate-desorption, (f) zinc-desorption, of all experiments

## 4.2. TDS - Summary

Methanol desorption from Pd(111), Pd/Zn and Pd/ZnO was investigated. For this purpose several TDS-measurements with different Zn and ZnO coverages were done. It turned out that depending on the coverage different reactions occur. Below 1 ML Zn coverage formate desorption was seen at low temperature (in the last experiment at higher temperature  $T = 178^{\circ}\text{C}$ ). If there was formate desorption there always was Zn desorption, too. So formate desorption leads to Zn desorption. This effect was not seen if there was more than 1 ML Zn coverage. So it seems that this reaction occurs at the Pd/Zn or rather Pd/ZnO interfaces.

An effect which was only seen above 1 ML ZnO coverage was oxygen desorption at  $T = 738^{\circ}\text{C}$ . At this temperature oxygen desorption is expected because of the dissociation of ZnO. This effect was only seen above 1 ML ZnO coverage because only there enough oxygen was given. Below 1 ML, all oxygen of the ZnO dissociation is used to form  $\text{CO}_2$ .

In the first experiments with Pd(111) it seems that the sample was not clean because Zn desorption was seen. First it seemed that the results were affected by the sample holder. But a small amount of zinc was found (peak at  $T = 430^{\circ}\text{C}$  till  $T = 700^{\circ}\text{C}$  in figure 4.7(b)). So in this experiment there was definitely still zinc on the sample left.

# 5. IR - study of methanol desorption from Pd(111), Pd/Zn and Pd/ZnO

IR-spectroscopy was done to investigate methanol desorption in situ. The principle of a IR-measurement is explained in chapter 2.5. How an IR-measurement was done in this work is explained in detail right below.

## 5.1. IR - Results

First of all, the sample was cleaned (cleaning process see chapter 3.1). After that, depending on the experiment, a Zn or ZnO layer was formed on the Pd-sample. Then the whole sample was cooled down as cold as possible before methanol was exposed to the chamber. So far, this is the same process which was done for the TDS-study (see 4.1). But contrary to the TDS-study the sample was now heated with a heating rate of 0.1 K/s. The mirror velocity (movable mirror of the michelson interferometer; see figure 2.14) was set to 60 kHz and a 9 mm aperture was used. The measuring time for one spectrum was set to one minute (= 396 scans). Between each spectrum there was a waiting time of 10 seconds so every 70 seconds (= 7 Kelvin) one spectrum was measured. Between 75 and 80 spectra were done, depending on the temperature, which was reached during the sample cooling, to make sure that always nearly the same end temperature was reached. So the sample was heated up to around 500 °C, depending on the starting temperature.

The wavenumbers of the detected peaks were allocated according to [37] for the methanol species and via [38] for all other compounds.

### 5.1.1. Methanol desorption from Pd(111)

At first methanol desorption from pure Pd was investigated. The sample had a temperature of  $T = -97^{\circ}\text{C}$  ( $\approx 176\text{ K}$ ) during the methanol exposition. Table 5.1 shows the wavenumbers of the detected peaks with their corresponding compounds on the sample. Figure 5.1 gives an overview at which temperature each peak was detected.

As it is shown in figure 5.1 peaks at  $2960\text{ cm}^{-1}$  - formate or OH,  $2920\text{ cm}^{-1}$  and  $2850\text{ cm}^{-1}$  for methanol are found over the whole temperature region. The same results are

found for the formaldehyde peaks at  $1260\text{ cm}^{-1}$ ,  $1100\text{ cm}^{-1}$ , and  $900\text{ cm}^{-1}$ . Carbon dioxide ( $1830\text{ cm}^{-1}$ ) can be found at a temperature  $T = -13^\circ\text{C}$  until  $T = 176^\circ\text{C}$ . A very last  $\text{CO}_2$  peak is found at  $T = 239^\circ\text{C}$ . For water there are peaks found at  $1570\text{ cm}^{-1}$  at low temperature ( $T = -90^\circ\text{C}$  till  $T = -48^\circ\text{C}$ ) as well as at mean temperature ( $T = 57^\circ\text{C}$  till  $T = 260^\circ\text{C}$ ). As it can be seen in figure 5.1 the peak is only seen fractional. The same applies for the other water peaks  $1590\text{ cm}^{-1}$  and  $1580\text{ cm}^{-1}$ .

The sample seems not to be perfectly clean because there are also ZnO peaks at  $800\text{ cm}^{-1}$  and  $700\text{ cm}^{-1}$ . Figure 5.2 shows the first spectrum at  $T = -97^\circ\text{C}$  with peaks at  $2960\text{ cm}^{-1}$ ,  $2850\text{ cm}^{-1}$ ,  $1620\text{ cm}^{-1}$ , and  $900\text{ cm}^{-1}$ .

| Wavenumber | Vibration              | Compound                               |
|------------|------------------------|--|
| 2960       | CH-stretch             | $\text{CO}_2\text{H}$                  |
| 2920       | $\text{CH}_3$ -stretch | $\text{CH}_3\text{OH}$                 |
| 2850       | CH-stretch             | $\text{CH}_3\text{OH}$                 |
| 1830       | asym. stretch          | $\text{CO}_2$                          |
| 1620       | asym. stretch          | $\text{CO ?}$                          |
| 1590       | bend                   | $\text{H}_2\text{O}$                   |
| 1580       | bend                   | $\text{H}_2\text{O}$                   |
| 1570       | bend                   | $\text{H}_2\text{O}$                   |
| 1260       | rocking vibration      | $\text{CO}_2$ or $\text{CH}_2\text{O}$ |
| 1100       | rocking vibration      | $\text{CH}_2\text{O}$                  |
| 1020       | CO-stretch             | $\text{CH}_3\text{OH}$                 |
| 900        | $\text{CH}_2$ -wagging | $\text{CH}_2\text{O}$                  |
| 800        | -                      | ZnO                                    |
| 700        | asym. stretch          | ZnO                                    |

Table 5.1.: Detected wavenumbers and possible compounds during the methanol desorption from Pd

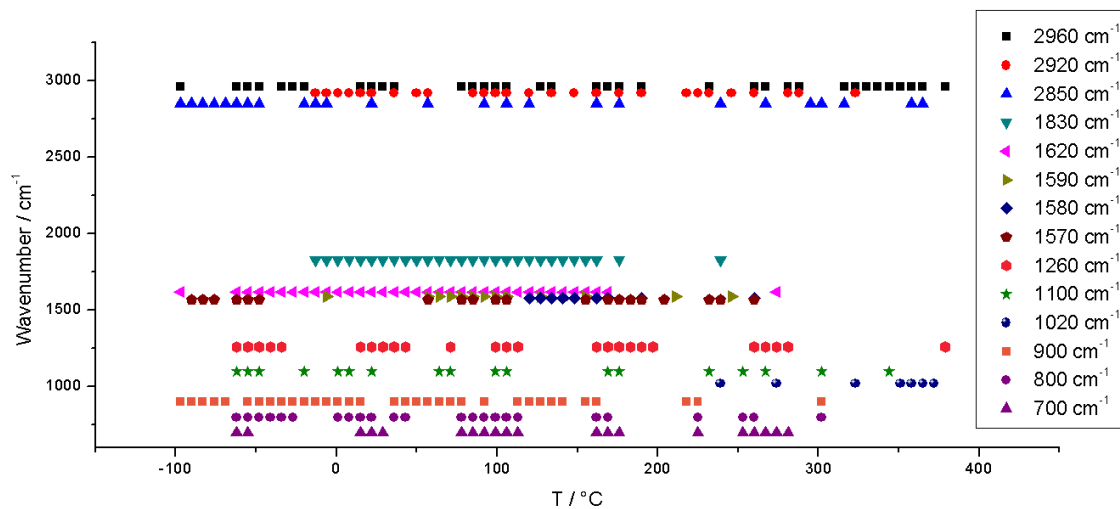


Figure 5.1.: Detected wavenumbers over temperature during methanol desorption from Pd

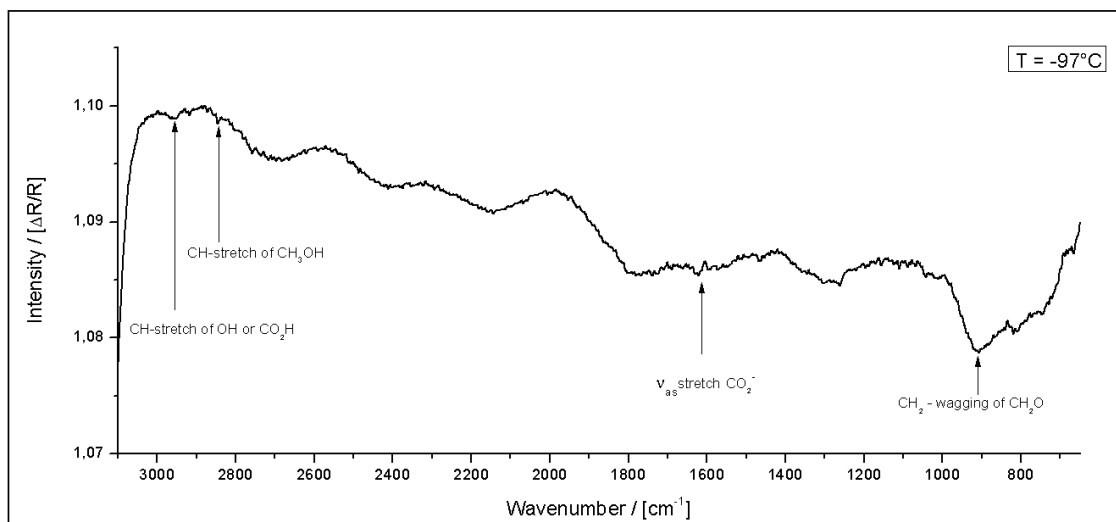


Figure 5.2.: First IR-spectrum of methanol adsorbed on Pd at  $T = -97^\circ\text{C}$

### 5.1.2. Methanol desorption from Pd/Zn

After the clean Pd sample Pd/Zn was investigated. Four experiments were done with different Zn-coverages and at different temperatures.

#### 1<sup>st</sup> experiment

In this experiment the sample was cooled down till  $T = -87^{\circ}\text{C}$  ( $\approx 186\text{ K}$ ). A Zn-layer-thickness of 0.7 ML was given. Table 5.2 shows the wavenumbers of the detected peaks with their corresponding compounds on the sample. Figure 5.3 gives an overview at which temperature each peak was detected.

At  $1840\text{ cm}^{-1}$  a peak of  $\text{CO}_2$  is found at low temperature ( $T = -87^{\circ}\text{C}$ ) which shifts at  $T = -10^{\circ}\text{C}$  to a higher wavenumber ( $1850\text{ cm}^{-1}$ ). At  $T = 130^{\circ}\text{C}$  this peak shifts back to  $1840\text{ cm}^{-1}$  before it disappears at  $T = 151^{\circ}\text{C}$ . There are only two peaks representing formaldehyde:  $1260\text{ cm}^{-1}$  and  $900\text{ cm}^{-1}$ . Both are seen fractional up to  $T = 354^{\circ}\text{C}$ .

$880\text{ cm}^{-1}$ ,  $800\text{ cm}^{-1}$ ,  $750\text{ cm}^{-1}$ ,  $740\text{ cm}^{-1}$ ,  $730\text{ cm}^{-1}$  and  $720\text{ cm}^{-1}$  are ZnO - peaks. Therefrom  $750\text{ cm}^{-1}$  and  $740\text{ cm}^{-1}$  are seen up to high temperature ( $750\text{ cm}^{-1}$  till  $T = 361^{\circ}\text{C}$ ;  $740\text{ cm}^{-1}$  till  $T = 375^{\circ}\text{C}$ ). No methanol peaks were found. Figure 5.4 shows the first spectrum at  $T = -87^{\circ}\text{C}$  with peaks at  $1840\text{ cm}^{-1}$ ,  $1260\text{ cm}^{-1}$ ,  $900\text{ cm}^{-1}$ ,  $880\text{ cm}^{-1}$ ,  $800\text{ cm}^{-1}$ ,  $720\text{ cm}^{-1}$ .

| Wavenumber | Vibration              | Compound                               |
|------------|------------------------|--|
| 1850       | $\text{CO}_2$ -stretch | $\text{CO}_2$                          |
| 1840       | $\text{CO}_2$ -stretch | $\text{CO}_2$                          |
| 1620       | -                      | ?                                      |
| 1600       | -                      | ?                                      |
| 1260       | rocking vibration      | $\text{CO}_2$ or $\text{CH}_2\text{O}$ |
| 900        | $\text{CH}_2$ -wagging | $\text{CH}_2\text{O}$                  |
| 880        | -                      | ZnO                                    |
| 800        | -                      | ZnO                                    |
| 750        | asym.-stretch          | ZnO                                    |
| 740        | asym.-stretch          | ZnO                                    |
| 730        | asym.-stretch          | ZnO                                    |
| 720        | asym.-stretch          | ZnO                                    |

Table 5.2.: Detected wavenumbers and possible compounds during the methanol desorption from Pd/Zn; 1<sup>st</sup> experiment

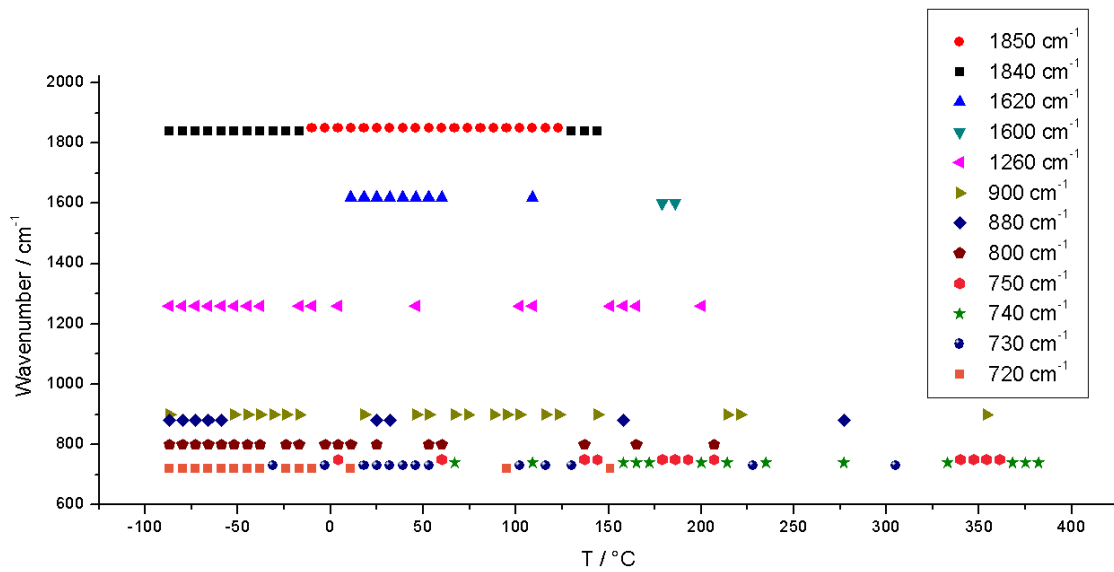


Figure 5.3.: Detected wavenumbers over temperature during methanol desorption from Pd/Zn; 1<sup>st</sup> experiment

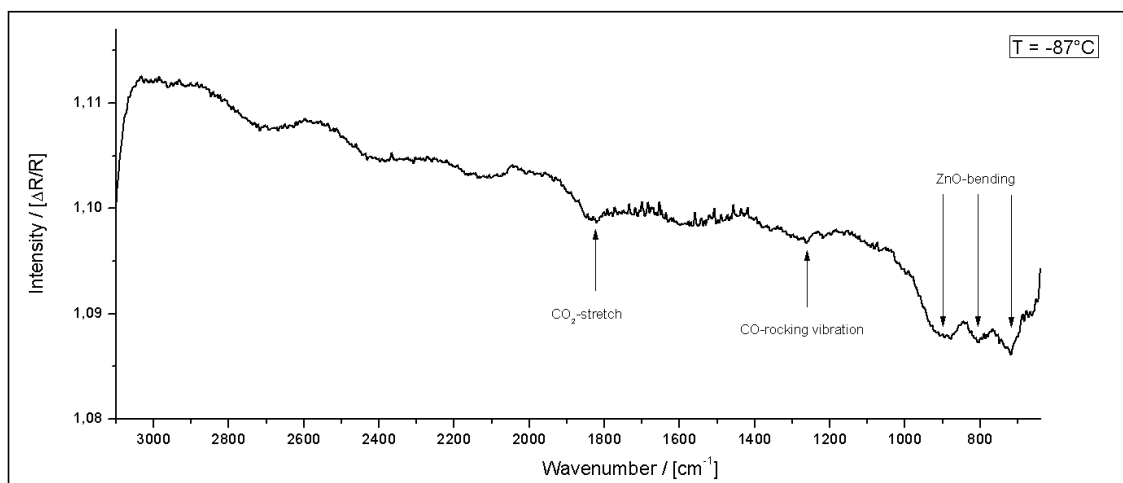


Figure 5.4.: First IR-spectrum of methanol adsorbed on Pd/Zn; 0.7 ML Zn-coverage at  $T = -87^{\circ}\text{C}$

## 2<sup>nd</sup> experiment

In this experiment the sample was cooled down to  $T = -100^{\circ}\text{C}$  ( $\approx 173\text{ K}$ ) and 0.4 ML of Zn were deposited on the Pd sample. Table 5.3 shows the wavenumbers of the detected peaks with their corresponding compounds on the sample. Figure 5.5 gives an overview at which temperature each peak was detected.

In figure 5.5 the methanol peak at  $2920\text{ cm}^{-1}$  is seen fractional in the temperature range between  $T = -100^{\circ}\text{C}$  and  $T = 138^{\circ}\text{C}$ . There are also two peaks at  $T = 292^{\circ}\text{C}$  and  $T = 299^{\circ}\text{C}$ . A second methanol peak is found at  $1045\text{ cm}^{-1}$  which appears over the whole temperature range as well as  $910\text{ cm}^{-1}$  - formaldehyde. At  $900\text{ cm}^{-1}$  there is always a peak when there is no  $910\text{ cm}^{-1}$  peak. So this could be a shift of the  $910\text{ cm}^{-1}$  formaldehyde peak. There are three peaks corresponding to  $\text{CO}_2$ :

- $1870\text{ cm}^{-1}$  (  $T = -9^{\circ}\text{C}$  up to  $T = 12^{\circ}\text{C}$ , one peak at  $T = 82^{\circ}\text{C}$  and constant from  $T = 152^{\circ}\text{C}$  to  $T = 208^{\circ}\text{C}$  as well as from  $T = 229$  up to  $T = 278^{\circ}\text{C}$  )
- $1840\text{ cm}^{-1}$  ( peaks at  $T = -9^{\circ}\text{C}$  and  $T = 12$ , from  $T = 82^{\circ}\text{C}$  up to  $T = 271^{\circ}\text{C}$  )
- $1350\text{ cm}^{-1}$  ( four peaks at  $T = -44^{\circ}\text{C}$ ,  $-30^{\circ}\text{C}$ ,  $68^{\circ}\text{C}$  and  $124^{\circ}\text{C}$  )

A peak at  $660\text{ cm}^{-1}$  is found between  $T = -100^{\circ}\text{C}$  and  $T = 110^{\circ}\text{C}$ . A last peak is found at  $T = 201^{\circ}\text{C}$ . Figure 5.6(a) shows the first spectrum at  $T = -100^{\circ}\text{C}$  with peaks at  $2920\text{ cm}^{-1}$ ,  $2020\text{ cm}^{-1}$ ,  $1045\text{ cm}^{-1}$ ,  $910\text{ cm}^{-1}$ ,  $660\text{ cm}^{-1}$ . Figure 5.6(b) shows the area between wavenumber  $3100\text{ cm}^{-1}$  and  $1400\text{ cm}^{-1}$  for a better view of the first two peaks.

| Wavenumber | Vibration                | Compound                 |
|------------|--------------------------|--------------------------|
| 2920       | CH <sub>3</sub> -stretch | CH <sub>3</sub> OH       |
| 2020       | -                        | ?                        |
| 1870       | CO <sub>2</sub> -stretch | CO <sub>2</sub>          |
| 1840       | CO <sub>2</sub> -stretch | CO <sub>2</sub>          |
| 1350       | CO <sub>2</sub> -stretch | CO <sub>2</sub>          |
| 1045       | CO-stretch               | CH <sub>3</sub> OH       |
| 910        | CH <sub>2</sub> -wagging | CH <sub>2</sub> O        |
| 900        | CH <sub>2</sub> -wagging | CH <sub>2</sub> O or ZnO |
| 660        | -                        | ?                        |

Table 5.3.: Detected wavenumbers and possible compounds during the methanol desorption from Pd/Zn; 2<sup>nd</sup> experiment

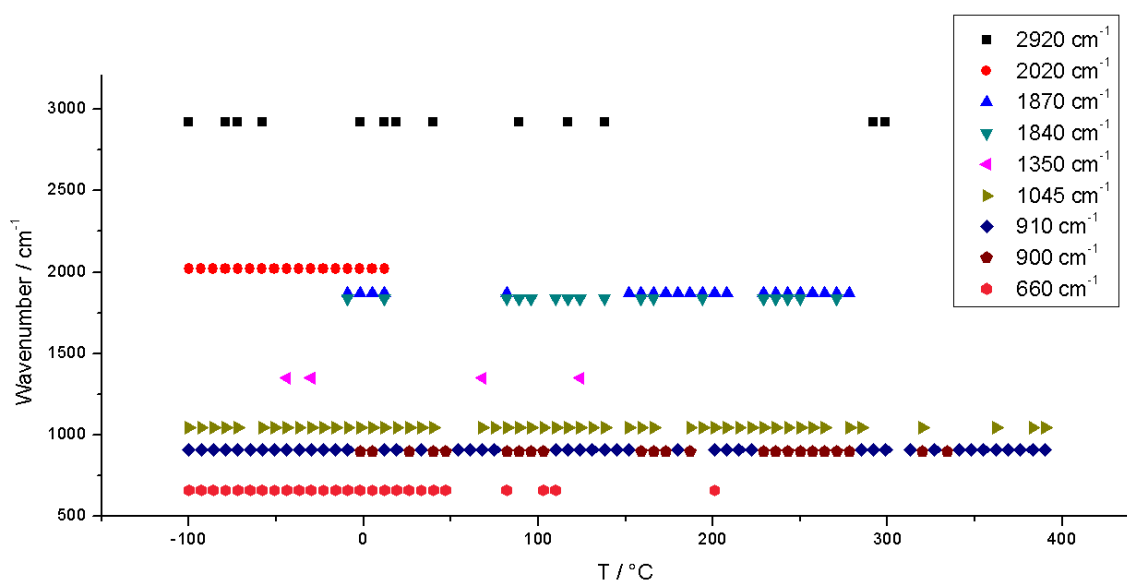


Figure 5.5.: Detected wavenumbers over temperature during methanol desorption from Pd/Zn; 2<sup>nd</sup> experiment

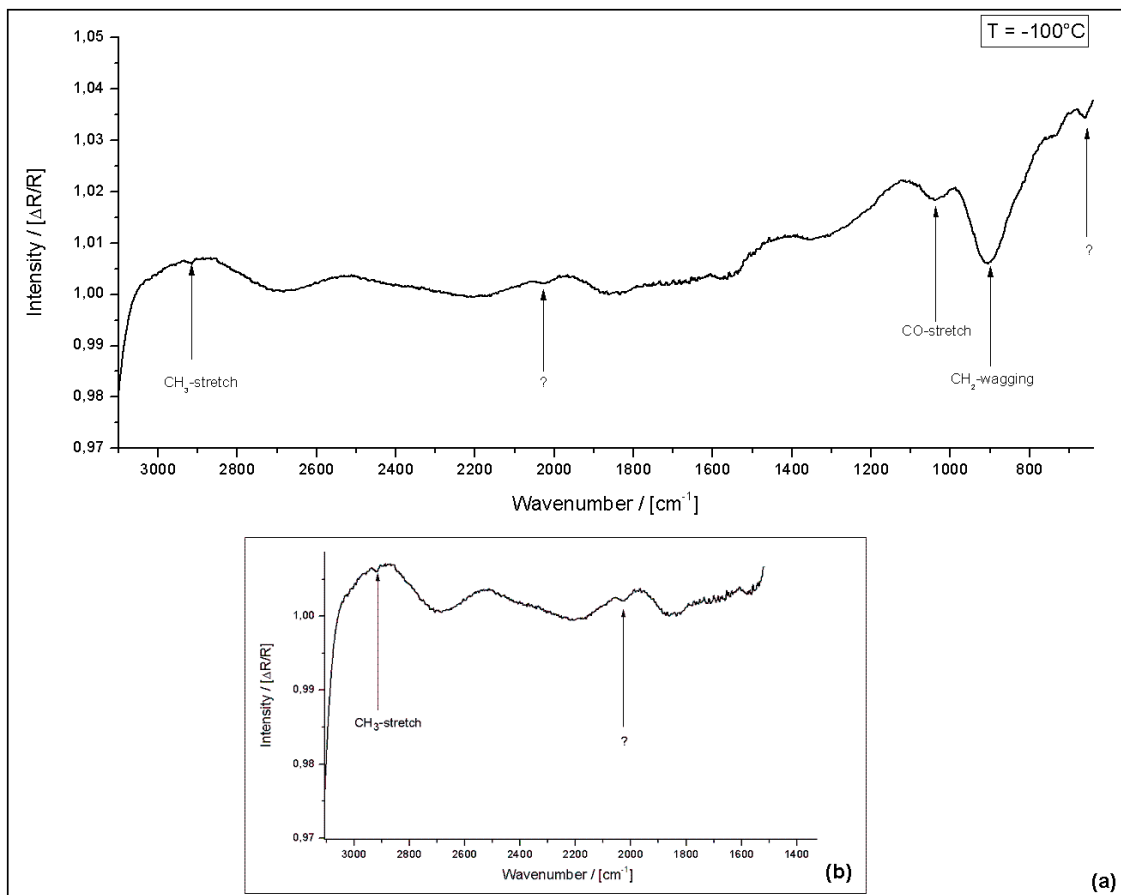


Figure 5.6.: First IR-spectrum of methanol adsorbed on Pd/Zn; 0.4 ML Zn-coverage at  $T = -100^\circ\text{C}$

### 3<sup>rd</sup> experiment

In the third experiment the sample was cooled down to  $T = -84.5^{\circ}\text{C}$  ( $\approx 189\text{ K}$ ) before methanol was exposed to the sample. A Zn coverage of 0.8 ML was given. Table 5.4 shows the wavenumbers of the detected peaks with their corresponding compounds on the sample. Figure 5.7 gives an overview at which temperature each peak was detected.

In this experiment a formate peak is seen which also can be an OH-peak at  $2960\text{ cm}^{-1}$  over the whole temperature range up to  $T = 482.5^{\circ}\text{C}$  as well as a methanol peak at  $2850\text{ cm}^{-1}$ . There is a methanol peak  $2920\text{ cm}^{-1}$  found at  $T = -84.5^{\circ}\text{C}$  up to  $T = 307.5^{\circ}\text{C}$  where it disappears. At  $T = 342.5^{\circ}\text{C}$ ,  $363.5^{\circ}\text{C}$  and  $440.5^{\circ}\text{C}$  it is seen again.

Four  $\text{CO}_2$  peaks are seen. The first one at  $1870\text{ cm}^{-1}$  starts at  $T = 125.5^{\circ}\text{C}$  and is seen up to  $T = 265.5^{\circ}\text{C}$  before it shifts to  $1860\text{ cm}^{-1}$ . There it is seen between  $T = 300.5^{\circ}\text{C}$  and  $T = 335.5^{\circ}\text{C}$  before it shifts back to  $1870\text{ cm}^{-1}$ . There the peak is seen till  $T = 370.5^{\circ}\text{C}$ . The last two  $\text{CO}_2$  peaks are at  $1840\text{ cm}^{-1}$  and  $1830\text{ cm}^{-1}$ . Both are seen at  $T = 279.5^{\circ}\text{C}$  for the first time. Then they are seen alternately till  $T = 363.5^{\circ}\text{C}$  where the peak at  $1830\text{ cm}^{-1}$  disappears and only the peak at  $1840\text{ cm}^{-1}$  remains. This one is seen till  $T = 447.5^{\circ}\text{C}$ . At  $1260\text{ cm}^{-1}$  a peak for  $\text{CO}_2$  or  $\text{CH}_2\text{O}$  can be found over the whole temperature range. Another formaldehyde peak is found between  $T = -84.5^{\circ}\text{C}$  and  $T = 426.5^{\circ}\text{C}$  which alternates between  $910\text{ cm}^{-1}$  and  $900\text{ cm}^{-1}$ . The last peak at  $910\text{ cm}^{-1}$  is found at  $T = 167.5^{\circ}\text{C}$  whereas the last peak at  $900\text{ cm}^{-1}$  is found at  $T = 482.5^{\circ}\text{C}$ .

There are several ZnO peaks ( $720\text{ cm}^{-1}$ ,  $715\text{ cm}^{-1}$ ,  $710\text{ cm}^{-1}$ ) which seem to be one shifting peak. Whereas the peak at  $720\text{ cm}^{-1}$  is first seen at  $T = -56.5^{\circ}\text{C}$  and is last seen at  $T = 328.5^{\circ}\text{C}$  the peak at  $715\text{ cm}^{-1}$  starts at  $T = 335.5^{\circ}\text{C}$  which is the following scanpoint. The peak at  $715\text{ cm}^{-1}$  shifts to  $710\text{ cm}^{-1}$  at  $T = 377.5^{\circ}\text{C}$ . Hence the peak at  $715\text{ cm}^{-1}$  is seen in the same temperature range as the  $\text{CO}_2$ -peak at  $1870\text{ cm}^{-1}$ .

Figure 5.8(a) shows the first spectrum at  $T = -84.5^{\circ}\text{C}$  with peaks at  $2920\text{ cm}^{-1}$ ,  $2850\text{ cm}^{-1}$ ,  $1260\text{ cm}^{-1}$ ,  $900\text{ cm}^{-1}$ . Figure 5.8(b) shows the area between wavenumber  $3000\text{ cm}^{-1}$  and  $2300\text{ cm}^{-1}$  for a better view of the first two peaks.

| Wavenumber | Vibration                | Compound                             |
|------------|--------------------------|--------------------------------------|
| 2960       | CH-stretch               | OH or CO <sub>2</sub> H              |
| 2920       | CH <sub>3</sub> -stretch | CH <sub>3</sub> OH                   |
| 2850       | CH-stretch               | CH <sub>3</sub> OH                   |
| 1870       | CO <sub>2</sub> -stretch | CO <sub>2</sub>                      |
| 1860       | CO <sub>2</sub> -stretch | CO <sub>2</sub>                      |
| 1840       | CO <sub>2</sub> -stretch | CO <sub>2</sub>                      |
| 1830       | CO <sub>2</sub> -stretch | CO <sub>2</sub>                      |
| 1540       | CCO-stretch              | CH <sub>2</sub> CHO                  |
| 1260       | rocking vibration        | CO <sub>2</sub> or CH <sub>2</sub> O |
| 910        | CH <sub>2</sub> -wagging | CH <sub>2</sub> O                    |
| 900        | CH <sub>2</sub> -wagging | CH <sub>2</sub> O                    |
| 890        | -                        | ZnO                                  |
| 720        | asym. stretch            | ZnO ?                                |
| 715        | asym. stretch            | ZnO ?                                |
| 710        | -                        | ZnO ?                                |

Table 5.4.: Detected wavenumbers and possible compounds during the methanol desorption from Pd/Zn; 3<sup>rd</sup> experiment

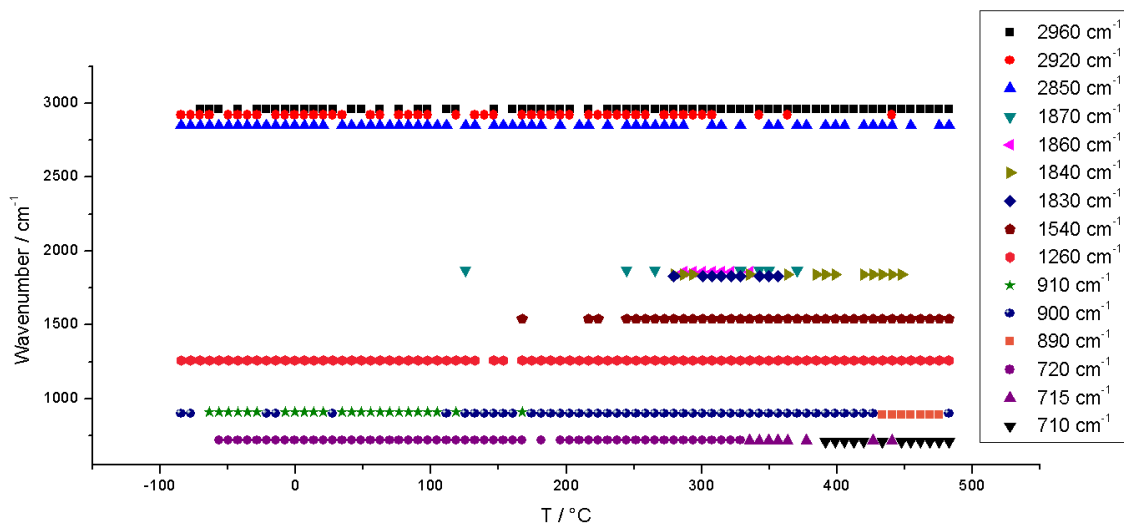


Figure 5.7.: Detected wavenumbers over temperature during methanol desorption from Pd/Zn; 3<sup>rd</sup> experiment

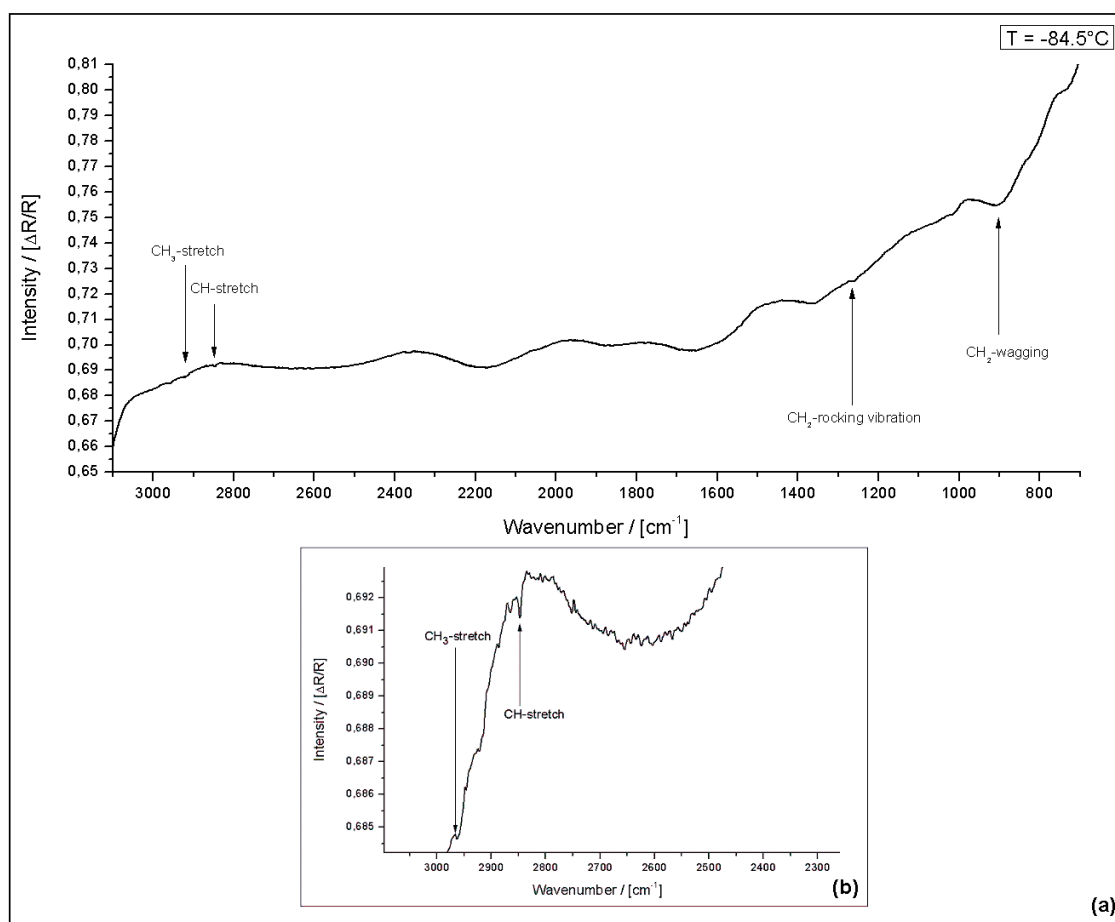


Figure 5.8.: First IR-spectrum of methanol adsorbed on Pd/Zn; 0.8 ML Zn-coverage at  $T = -84.5^{\circ}\text{C}$

#### 4<sup>th</sup> experiment

In the last experiment with Pd/Zn the sample was cooled down to  $T = -86^{\circ}\text{C}$  ( $\approx 187\text{ K}$ ). A Zn coverage of 0.7 ML was given. Table 5.5 shows the wavenumbers of the detected peaks with their corresponding compounds on the sample and figure 5.9 gives an overview at which temperature each peak was detected.

Again we have peaks at  $2960\text{ cm}^{-1}$  (= formate) and  $2920\text{ cm}^{-1}$  (= methanol) but they are seen at different temperatures than in the last experiment. The peak at  $2960\text{ cm}^{-1}$  is seen between  $T = -86^{\circ}\text{C}$  and  $T = 40^{\circ}\text{C}$  as well as between  $T = 166^{\circ}\text{C}$  and  $T = 299^{\circ}\text{C}$ . The peak at  $2920\text{ cm}^{-1}$  is found between  $T = -86^{\circ}\text{C}$  and  $T = 54^{\circ}\text{C}$  and a last time at  $T = 201^{\circ}\text{C}$ . A second methanol - peak at  $1010\text{ cm}^{-1}$  can be found between  $T = -86^{\circ}\text{C}$  and  $T = -23^{\circ}\text{C}$ . Carbon dioxide ( $1840\text{ cm}^{-1}$ ) can be found from time to time between  $T = -44^{\circ}\text{C}$  and  $T = 390^{\circ}\text{C}$ . Another methanol peak ( $2845\text{ cm}^{-1}$ ) can be seen among  $T = -86^{\circ}\text{C}$  and  $T = 61^{\circ}\text{C}$

Formaldehyde ( $1350\text{ cm}^{-1}$ ) is detected between  $T = -86^{\circ}\text{C}$  and  $T = 131^{\circ}\text{C}$  before it shifts to  $1340\text{ cm}^{-1}$  and remains there till  $T = 285^{\circ}\text{C}$ . There it shifts back to  $1350\text{ cm}^{-1}$  and goes back to  $1340\text{ cm}^{-1}$  at  $T = 369^{\circ}\text{C}$ . At  $T = 446^{\circ}\text{C}$  and  $T = 453^{\circ}\text{C}$  this peak can be located at  $1350\text{ cm}^{-1}$  again. As in the third experiment, a peak for  $\text{CO}_2$  or  $\text{CH}_2\text{O}$  can be found over the whole temperature range at a wavenumber of  $1260\text{ cm}^{-1}$ .

Corresponding ZnO - peaks are found at:

- $880\text{ cm}^{-1}$  and  $870\text{ cm}^{-1}$  (seen alternately between  $T = -86^{\circ}\text{C}$  and  $T = 453^{\circ}\text{C}$ )
- $830\text{ cm}^{-1}$  and  $820\text{ cm}^{-1}$  (seen alternately till  $T = 215^{\circ}\text{C}$ . Henceforward only  $820\text{ cm}^{-1}$  is seen till  $T = 382^{\circ}\text{C}$ )
- $730\text{ cm}^{-1}$  and  $720\text{ cm}^{-1}$

The peak at  $730\text{ cm}^{-1}$  is seen between  $T = -30^{\circ}\text{C}$  and  $T = 5^{\circ}\text{C}$  as well as between  $T = 138^{\circ}\text{C}$  and  $T = 411^{\circ}\text{C}$ . Among  $T = 12^{\circ}\text{C}$  and  $T = 131^{\circ}\text{C}$  just as between  $T = 425^{\circ}\text{C}$  and  $T = 453^{\circ}\text{C}$  this peaks shifts down to  $720\text{ cm}^{-1}$ .

Figure 5.10(a) shows the first spectrum of this experiment at  $T = -86^{\circ}\text{C}$  with peaks at  $2960\text{ cm}^{-1}$ ,  $2920\text{ cm}^{-1}$ ,  $2845\text{ cm}^{-1}$ ,  $2030\text{ cm}^{-1}$ ,  $1350\text{ cm}^{-1}$ ,  $1260\text{ cm}^{-1}$ ,  $1010\text{ cm}^{-1}$ ,  $880\text{ cm}^{-1}$ . Between  $1750\text{ cm}^{-1}$  and  $1350\text{ cm}^{-1}$  only noise is seen. This derives from water which is condensed on the window between measurement chamber and detector. Figure 5.10(b) shows the area between wavenumber  $3000\text{ cm}^{-1}$  and  $2200\text{ cm}^{-1}$  for a better view of the first three peaks. Figure 5.10(c) shows the area between  $1600\text{ cm}^{-1}$  and  $1000\text{ cm}^{-1}$ .

| Wavenumber | Compound                 |                                      |
|------------|--------------------------|--------------------------------------|
| 2960       | CH-stretch               | CO <sub>2</sub> H                    |
| 2920       | CH <sub>3</sub> -stretch | CH <sub>3</sub> OH                   |
| 2845       | CH-stretch               | CH <sub>3</sub> OH                   |
| 2030       | -                        | ?                                    |
| 1840       | CO <sub>2</sub> -stretch | CO <sub>2</sub>                      |
| 1540       | CCO-stretch              | CH <sub>2</sub> CHO                  |
| 1350       | CO-stretch               | CO <sub>2</sub> H                    |
| 1340       | CO-stretch               | CO <sub>2</sub> H                    |
| 1260       | rocking vibration        | CO <sub>2</sub> or CH <sub>2</sub> O |
| 1010       | CO-stretch               | CH <sub>3</sub> OH                   |
| 880        | -                        | ZnO                                  |
| 870        | -                        | ZnO                                  |
| 830        | -                        | ZnO                                  |
| 820        | -                        | ZnO                                  |
| 730        | asym. stretch            | ZnO                                  |
| 720        | asym. stretch            | ZnO ?                                |

Table 5.5.: Detected wavenumbers and possible compounds during the methanol desorption from Pd/Zn; 4<sup>th</sup> experiment

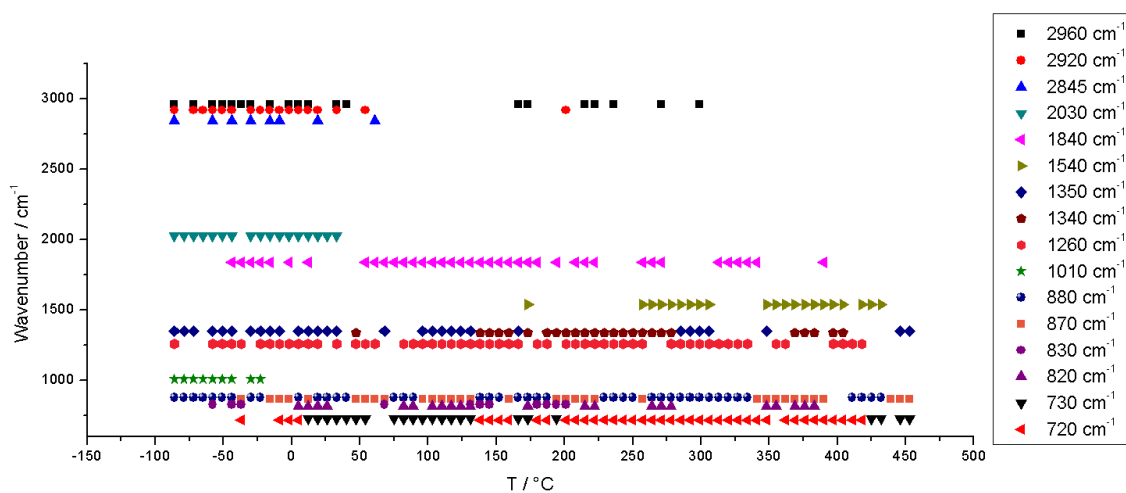


Figure 5.9.: Detected wavenumbers over temperature during methanol desorption from Pd/Zn; 4<sup>th</sup> experiment

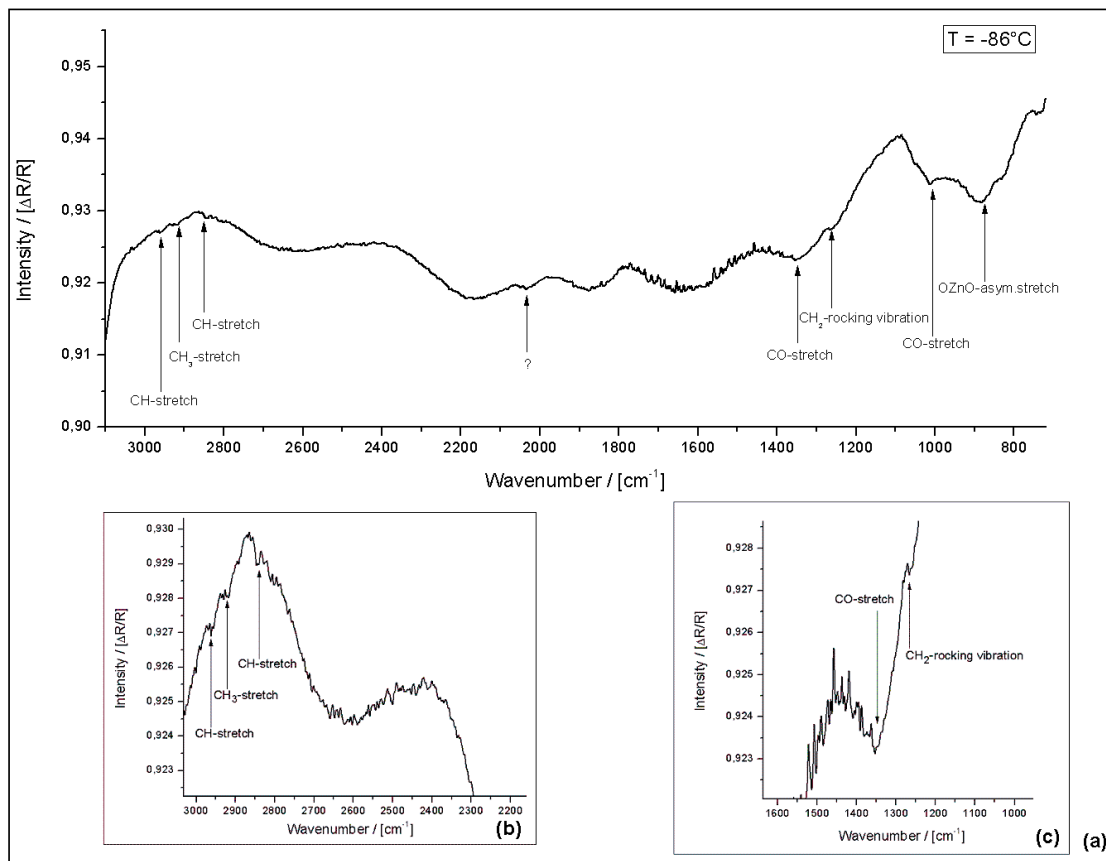


Figure 5.10.: First IR-spectrum of methanol adsorbed on Pd/Zn; 0.7 ML Zn-coverage at  $T = -86^\circ\text{C}$

### Discussion of the Pd(111)- and Pd/Zn-measurements

As it can be seen in this measurement series, methanol desorption from Pd and Pd/Zn is subject to a complex process. Comparing figures 5.2, 5.4, 5.6, 5.8, 5.10 show that the whole process is heavily dependent from the temperature at which methanol adsorption takes place. This is why always a different amount of peaks is detected at different wavenumbers. Another fact to consider is that at each experiment a different surface structure is given. Even if there is the same amount of Zn on the sample a different surface structure could be present according to [25]. This also affects the reaction paths.

Methanol desorption from Pd(111) shows ZnO-peaks ( $800\text{ cm}^{-1}$  and  $700\text{ cm}^{-1}$ ) over the whole temperature range. So it seems that the sample was not clean. This is an explanation why there is formaldehyde seen, too. There is a formate peak ( $2960\text{ cm}^{-1}$ ) which is always seen at the same time as the ZnO-peaks. This fits very well with the TDS-results. Methanol-peaks are seen over the whole temperature range. Because methanol adsorbs on Pd(111) at 100 K (see [33]) and desorbs below 200 K (see [36], [39]) this cannot be methanol on the sample. So several reference spectra (spectra of clean Pd) were divided to check if these methanol-peaks arise from the background. These divisions always give a flat line so there is no background signal which influences the results. Another reason why there is methanol detected at temperatures where no methanol should be is that the IR-beam grazes the measurement chamber. The MTC-detector is mounted on the chamber by a flange. So it could be that the IR-beam hits this flange before striking the detector. If this assumption is correct there is additionally to methanol from the sample, methanol from the chamber detected. The measurement chamber always has room temperature (around  $25^\circ\text{C}$ ). So even if there is no methanol on the sample left, it is possible that there is still methanol on the chamber surface.

Methanol desorption from Pd/Zn always looks different. In the first experiment (0.7 ML Zn-coverage) a temperature of  $T = -87^\circ\text{C}$  is reached. No methanol is seen. Maybe the sample was not cold enough so that all methanol was desorbed even before the measurement was started. But in the last experiment methanol is seen. There nearly the same conditions were given (0.7 ML Zn-coverage,  $T = -86^\circ\text{C}$ ). Why in one case methanol is seen and in another one not is unclear. The differences may arise from the different surface structures which are given in every experiment. Another reason may be that the oxygen amount in the ZnO layer is not exactly the same in each measurement, which arises from experimental reasons (manual opening and closing of the inlet valve). Methanol-peaks are always seen at  $2920\text{ cm}^{-1}$ . In some experiments there are additional peaks at  $2850\text{ cm}^{-1}$  and around  $1010\text{ cm}^{-1}$ . Formate is found in the 3<sup>rd</sup> (at  $2960\text{ cm}^{-1}$ ) and 4<sup>th</sup> experiment ( $2960\text{ cm}^{-1}$  and  $1350\text{-}1340\text{ cm}^{-1}$ ).

In all experiments, except of the second Pd/Zn experiment, ZnO is seen. So the adsorbed Zn was oxidized. This oxygen maybe comes from the sample itself. Because of the sample cleaning process oxygen could be dissolved in the sample. So there is a sub-surface of PdO which is the origin of this oxygen. It turned out that the inlet valve for

oxygen was a little bit leaky. This is another reason why there is seen ZnO instead of Zn on the Pd surface. The only species which is seen in all experiments is CO<sub>2</sub> (1840 cm<sup>-1</sup>). It is always seen over the whole temperature range. Nearly the same applies for CH<sub>2</sub>O (1260 cm<sup>-1</sup>) which is seen in all experiments except of the second Pd/Zn measurement.

### 5.1.3. Methanol desorption from Pd/ZnO

At last Pd/ZnO was investigated. Six experiments under different conditions (different ZnO-coverages and temperatures) were done.

#### 1<sup>st</sup> experiment - high O<sub>2</sub> pressure

In the first experiment with Pd/ZnO the sample was cooled down to  $T = -74.4^{\circ}\text{C}$  ( $\approx 199\text{ K}$ ) and a ZnO - layer thickness of 0.6 ML was given. The ZnO-layer was built under a high oxygen pressure ( $1 \cdot 10^{-5}\text{mbar}$ ). Table 5.6 shows the wavenumbers of the detected peaks with their corresponding compounds on the sample and figure 5.11 gives an overview at which temperature each peak was detected.

There are two peaks representing methanol:  $2920\text{ cm}^{-1}$  and  $2850\text{ cm}^{-1}$ . The peak at  $2920\text{ cm}^{-1}$  can be found for the first time at  $T = -54.4^{\circ}\text{C}$  while the peak at  $2850\text{ cm}^{-1}$  is seen at  $T = -74.4^{\circ}\text{C}$ . Both peaks appear till  $T = 436.6^{\circ}\text{C}$ .

For CO<sub>2</sub> there are two peaks as well but they seem to be one shifting peak again. They are at  $1840\text{ cm}^{-1}$  and at  $1830\text{ cm}^{-1}$ . The peak at  $1840\text{ cm}^{-1}$  is seen at  $T = 135.6^{\circ}\text{C}$  till  $T = 156.6^{\circ}\text{C}$  where it shifts to  $1830\text{ cm}^{-1}$ . At  $T = 198.6^{\circ}\text{C}$  it shifts back to  $1840\text{ cm}^{-1}$  till it shifts to  $1830\text{ cm}^{-1}$  at  $T = 226.6^{\circ}\text{C}$  again. There it remains till  $T = 254.6^{\circ}\text{C}$ . At  $T = 352.6^{\circ}\text{C}$  this peak shifts to  $1830\text{ cm}^{-1}$  again till  $T = 373.6^{\circ}\text{C}$  where it has its last shift to  $1840\text{ cm}^{-1}$ .

A more simple behavior is found for the water peak ( $1560\text{ cm}^{-1}$ ) which is seen between  $T = -74.4^{\circ}\text{C}$  and  $T = 422.6^{\circ}\text{C}$ .

There are four peaks representing formaldehyde ( $1270\text{ cm}^{-1}$ ,  $1200\text{ cm}^{-1}$ ,  $910\text{ cm}^{-1}$ ,  $900\text{ cm}^{-1}$ ) whereof the peaks at  $910\text{ cm}^{-1}$  and  $900\text{ cm}^{-1}$  seem to be one shifting peak. The peak at  $1270\text{ cm}^{-1}$  can be found between  $T = -74.4^{\circ}\text{C}$  and  $T = -18.4^{\circ}\text{C}$  and the peak at  $1200\text{ cm}^{-1}$  can be seen between  $T = -74.4^{\circ}\text{C}$  and  $T = 65.6^{\circ}\text{C}$ . At  $910\text{ cm}^{-1}$  there is a peak only three times, at  $T = -74.4^{\circ}\text{C}$ ,  $2.6^{\circ}\text{C}$  and  $65.6^{\circ}\text{C}$ . The peak at  $900\text{ cm}^{-1}$  is seen between  $T = -53.4^{\circ}\text{C}$  and  $T = -18.4^{\circ}\text{C}$  and at last at  $T = 16.6^{\circ}\text{C}$ .

As it is shown in table 5.6, there are several ZnO-peaks. There is a shifting peak at  $880\text{ cm}^{-1}$  -  $870\text{ cm}^{-1}$ . The peak appears for the first time at  $880\text{ cm}^{-1}$  at the same temperature than the formaldehyde peak at  $910\text{ cm}^{-1}$ :  $T = 2.6^{\circ}\text{C}$  and  $T = 16.6^{\circ}\text{C}$ . Then the peak is seen insular at  $880\text{ cm}^{-1}$  and  $870\text{ cm}^{-1}$  till it shifts to  $880\text{ cm}^{-1}$  at  $T = 198.6^{\circ}\text{C}$ . At  $T = 254.6^{\circ}\text{C}$  it shifts to  $870\text{ cm}^{-1}$  where it remains till  $T = 324.6^{\circ}\text{C}$ . After that this peak can be found alternately at  $880\text{ cm}^{-1}$  and  $870\text{ cm}^{-1}$  ( $T = 331.6^{\circ}\text{C}$  till  $T = 394.6^{\circ}\text{C}$ ). From  $T = 394.6^{\circ}\text{C}$  till  $T = 436.6^{\circ}\text{C}$  it shifts back to  $880\text{ cm}^{-1}$ . The next ZnO-peak at  $815\text{ cm}^{-1}$  can be found in a temperature range between  $T = -60.4^{\circ}\text{C}$  and  $T = 16.6^{\circ}\text{C}$ . At last it is seen at  $T = 51.6^{\circ}\text{C}$ . The following peak is a shifting peak again ( $790\text{ cm}^{-1}$  -  $780\text{ cm}^{-1}$ ). It first appears at  $T = 72.6^{\circ}\text{C}$  ( $790\text{ cm}^{-1}$ ) and is

seen again at this wavenumber between  $T = 135.6^\circ\text{C}$  till  $T = 331.6^\circ\text{C}$ . In this temperature range only two shifts can be found: at  $T = 198.6^\circ\text{C}$  and  $T = 261.5^\circ\text{C}$  this peak shifts to  $780\text{ cm}^{-1}$ . At  $T = 331.6^\circ\text{C}$  this peak shifts to  $780\text{ cm}^{-1}$  where it remains till  $T = 387.6^\circ\text{C}$ . At  $T = 387.6^\circ\text{C}$  this peak can be found at  $790\text{ cm}^{-1}$  again till  $T = 429.6^\circ\text{C}$ .

At last there are ZnO-peaks between  $750\text{ cm}^{-1}$  and  $730\text{ cm}^{-1}$ . First there is a peak at  $750\text{ cm}^{-1}$ . It can be seen between  $T = -74.4^\circ\text{C}$  and  $T = 65.6^\circ\text{C}$ . Then this peak shifts to  $745\text{ cm}^{-1}$ . There it remains till  $T = 107.6^\circ\text{C}$ . At higher temperature several alternating peaks are seen between  $745\text{ cm}^{-1}$  and  $730\text{ cm}^{-1}$  till they disappear at  $T = 352.6^\circ\text{C}$ .

Figure 5.12 shows the first IR-spectrum of this experiment. There are peaks at  $2850\text{ cm}^{-1}$ ,  $1560\text{ cm}^{-1}$ ,  $1270\text{ cm}^{-1}$ ,  $910\text{ cm}^{-1}$  and  $750\text{ cm}^{-1}$ . To have a better view there are two zooms of the peaks. As it can be seen in the first zoom on the left hand side, there are thermal shifts of the IR spectrometer seen, too (broad peak around  $2150\text{ cm}^{-1}$ ). This makes it difficult to identify real peaks.

| Wavenumber | Vibration                | Compound           |
|------------|--------------------------|--------------------|
| 2920       | CH <sub>3</sub> -stretch | CH <sub>3</sub> OH |
| 2850       | CH-stretch               | CH <sub>2</sub> O  |
| 1840       | CO <sub>2</sub> -stretch | CO <sub>2</sub>    |
| 1830       | CO <sub>2</sub> -stretch | CO <sub>2</sub>    |
| 1560       | bend                     | H <sub>2</sub> O   |
| 1270       | rocking vibration        | CH <sub>2</sub> O  |
| 1200       | CO-stretch               | CH <sub>2</sub> O  |
| 910        | CH <sub>2</sub> -wagging | CH <sub>2</sub> O  |
| 900        | CH <sub>2</sub> -wagging | CH <sub>2</sub> O  |
| 880        | -                        | ZnO                |
| 870        | -                        | ZnO                |
| 815        | -                        | ZnO                |
| 790        | -                        | ZnO                |
| 780        | -                        | ZnO                |
| 750        | asym. stretch            | ZnO                |
| 745        | asym. stretch            | ZnO                |
| 740        | asym. stretch            | ZnO                |
| 735        | asym. stretch            | ZnO                |
| 730        | asym. stretch            | ZnO                |
| 665        | -                        | ?                  |
| 660        | -                        | ?                  |

Table 5.6.: Detected wavenumbers and possible compounds during the methanol desorption from Pd/ZnO; 1<sup>st</sup> experiment

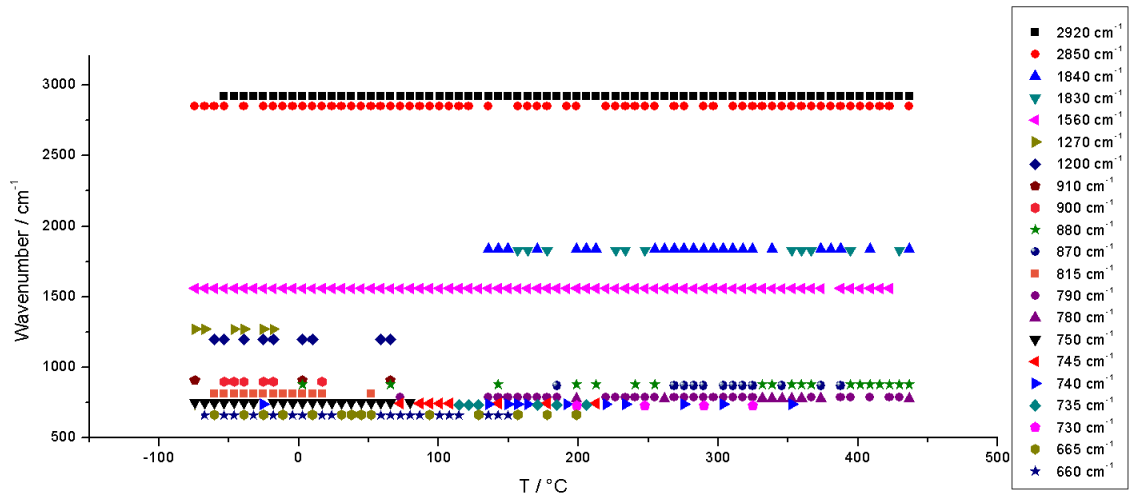


Figure 5.11.: Detected wavenumbers over temperature during methanol desorption from Pd/ZnO; 1<sup>st</sup> experiment

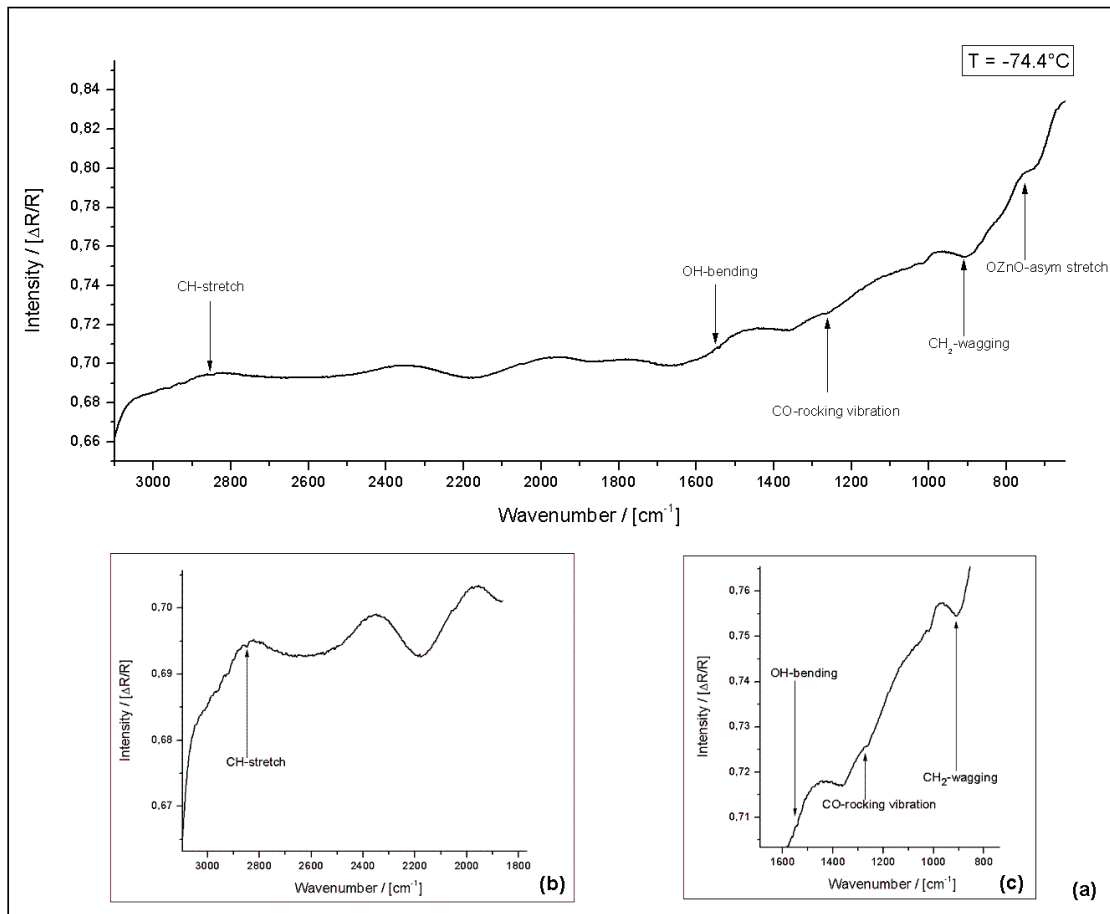


Figure 5.12.: First IR-spectrum of methanol adsorbed on Pd/ZnO; 0.7 ML ZnO-coverage; oxygen pressure during Zn-evaporation:  $1 \cdot 10^{-5}$  mbar;  $T = -74.4^\circ\text{C}$

## 2<sup>nd</sup> experiment - low O<sub>2</sub> pressure

The sample was covered by 0.5 ML ZnO and was cooled down to  $T = -74.7^{\circ}\text{C}$  ( $\approx 198\text{ K}$ ). The ZnO-layer was built under a low oxygen pressure ( $5 \cdot 10^{-7}\text{ mbar}$ ). Table 5.7 shows the wavenumbers of the detected peaks with their corresponding compounds on the sample and figure 5.13 gives an overview at which temperature each peak was detected.

In this experiment four methanol peaks can be found:  $2920\text{ cm}^{-1}$ ,  $2850\text{ cm}^{-1}$ ,  $1010\text{ cm}^{-1}$  and  $1000\text{ cm}^{-1}$ . The peaks at  $2920\text{ cm}^{-1}$  and  $2850\text{ cm}^{-1}$  are seen both between  $T = -74.7^{\circ}\text{C}$  and  $T = 471.3^{\circ}\text{C}$ .

The peaks at  $1010\text{ cm}^{-1}$  and  $1000\text{ cm}^{-1}$  seem to be one shifting peak. First this peak is seen  $T = -74.7^{\circ}\text{C}$  till  $T = 30.3^{\circ}\text{C}$  at  $1010\text{ cm}^{-1}$ . Then it shifts to  $1000\text{ cm}^{-1}$  where it can be found till  $T = 100.3^{\circ}\text{C}$ .

Two formate peaks are seen. The first one at  $2960\text{ cm}^{-1}$  also can be an OH-peak. It is seen fractional between  $T = -4.7^{\circ}\text{C}$  and  $T = 171.3^{\circ}\text{C}$ . Henceforward it can be found till  $T = 282.3^{\circ}\text{C}$ . At higher temperature it is seen only from time to time again. This peak disappears at  $T = 450.3^{\circ}\text{C}$ . The second formate peak seems to be a shifting peak. It can be found alternating between  $1300\text{ cm}^{-1}$  and  $1290\text{ cm}^{-1}$  in a temperature range between  $T = 401.3^{\circ}\text{C}$  and  $T = 471.3^{\circ}\text{C}$ .

There are four formaldehyde-peaks. The first one shifts between  $1470\text{ cm}^{-1}$  and  $1450\text{ cm}^{-1}$ . It is seen among  $T = -67.7^{\circ}\text{C}$  and  $T = -4.7^{\circ}\text{C}$  at a wavenumber of  $1470\text{ cm}^{-1}$ . In this temperature range there is sometimes a peak at  $1450\text{ cm}^{-1}$  too. At higher temperatures this peak can be found alternately at  $1470\text{ cm}^{-1}$ ,  $1460\text{ cm}^{-1}$  and  $1450\text{ cm}^{-1}$  till  $T = 163.3^{\circ}\text{C}$ . At  $T = 86.3^{\circ}\text{C}$  it is at  $1450\text{ cm}^{-1}$  for the last time, at  $T = 366.3^{\circ}\text{C}$  there is the last peak at  $1470\text{ cm}^{-1}$  and the last peak at  $1460\text{ cm}^{-1}$  can be found at  $T = 471.3^{\circ}\text{C}$ . It is to say that at temperatures below  $T = 163.3^{\circ}\text{C}$  this peak is only seen seldom. The next formaldehyde peak is a shifting peak again. It can be found at  $1250\text{ cm}^{-1}$ ,  $1240\text{ cm}^{-1}$  and  $1230\text{ cm}^{-1}$ . It is first seen at  $1250\text{ cm}^{-1}$  at  $T = -53.7^{\circ}\text{C}$  till  $T = -11.7^{\circ}\text{C}$  and again between  $T = 443.3^{\circ}\text{C}$  and  $T = 471.3^{\circ}\text{C}$ . Around  $T = -25.7^{\circ}\text{C}$  this peak starts to shift to lower wavenumbers ( $1240\text{ cm}^{-1}$  and  $1230\text{ cm}^{-1}$ ) where it can be found alternating between these two wavenumbers till  $T = 86.3^{\circ}\text{C}$ . From  $T = 93.3^{\circ}\text{C}$  until  $T = 450.3^{\circ}\text{C}$  it remains at  $1230\text{ cm}^{-1}$ . Only for three times it can be found at  $1240\text{ cm}^{-1}$  again: at  $T = 314.3^{\circ}\text{C}$ ,  $436.3^{\circ}\text{C}$  and  $471.3^{\circ}\text{C}$ .

The third peak is seen at  $1190\text{ cm}^{-1}$  and  $1180\text{ cm}^{-1}$ . These peaks alternate between these two wavenumbers between  $T = -61.7^{\circ}\text{C}$  and  $T = 51.3^{\circ}\text{C}$ . At higher temperatures this peak remains at  $1180\text{ cm}^{-1}$  till  $T = 471.3^{\circ}\text{C}$ .

The last formaldehyde-peak is shifting too (between  $920\text{ cm}^{-1}$  and  $905\text{ cm}^{-1}$ ). This peak is first seen at  $920\text{ cm}^{-1}$  at  $T = -74.7^{\circ}\text{C}$  until it shifts to  $915\text{ cm}^{-1}$  at  $T = -18.7^{\circ}\text{C}$ . There it can be found till  $T = 44.3^{\circ}\text{C}$ . At  $910\text{ cm}^{-1}$  it can be found between  $T = -32.7^{\circ}\text{C}$

and  $T = 141.3^\circ\text{C}$ . Between  $T = 51.3^\circ\text{C}$  and  $T = 219.3^\circ\text{C}$  it also can be seen at  $905\text{ cm}^{-1}$ . It is to say that in the temperature range between  $T = -32.7^\circ\text{C}$  and  $T = 51.3^\circ\text{C}$  this peak shifts between  $910\text{ cm}^{-1}$  and  $915\text{ cm}^{-1}$ .

Three  $\text{CO}_2$ -peaks can be found. One  $\text{CO}_2$ -peak can be seen fractional between  $T = 310.3^\circ\text{C}$  and  $T = 457.3^\circ\text{C}$ . Another one at  $1850\text{ cm}^{-1}$  is seen from  $T = -74.7^\circ\text{C}$  till  $T = 2.3^\circ\text{C}$ . The last one is at  $1840\text{ cm}^{-1}$  (fractional between  $T = 170.3^\circ\text{C}$  and  $T = 408.3^\circ\text{C}$ ).

There is a shifting peak representing water which is first seen at  $1510\text{ cm}^{-1}$  from  $T = -74.7^\circ\text{C}$  until  $T = 86.3^\circ\text{C}$ . From there it is alternating between  $1515\text{ cm}^{-1}$  and  $1510\text{ cm}^{-1}$  till  $T = 261.3^\circ\text{C}$  where it shifts back to  $1510\text{ cm}^{-1}$ . There it remains till  $T = 471.3^\circ\text{C}$ .

At last there are ZnO-peaks between  $840\text{ cm}^{-1}$  and  $730\text{ cm}^{-1}$ . The first one starts at  $840\text{ cm}^{-1}$  at  $T = -74.7^\circ\text{C}$ . It is seen until  $T = -39.7^\circ\text{C}$ . At  $T = -25.7^\circ\text{C}$  it starts to shift to  $830\text{ cm}^{-1}$  where it remains until  $T = 142.3^\circ\text{C}$ . From there it is found alternating between  $830\text{ cm}^{-1}$  and  $825\text{ cm}^{-1}$  till  $T = 471.3^\circ\text{C}$ . The last one starts at  $750\text{ cm}^{-1}$  at  $T = -74.7^\circ\text{C}$ . At  $T = 37.3^\circ\text{C}$  it shifts to  $745\text{ cm}^{-1}$  before it shifts to  $740\text{ cm}^{-1}$  at  $T = 352.3^\circ\text{C}$ . At higher temperatures it is alternating between  $740\text{ cm}^{-1}$  and  $730\text{ cm}^{-1}$ .

Figure 5.14 shows the first IR-spectrum of this experiment at  $T = -74.7^\circ\text{C}$ . There are peaks at  $2920\text{ cm}^{-1}$ ,  $2850\text{ cm}^{-1}$ ,  $1850\text{ cm}^{-1}$ ,  $1600\text{ cm}^{-1}$ ,  $1510\text{ cm}^{-1}$ ,  $1470\text{ cm}^{-1}$ ,  $1010\text{ cm}^{-1}$ ,  $920\text{ cm}^{-1}$ ,  $840\text{ cm}^{-1}$ , and  $750\text{ cm}^{-1}$ . In contrast to the spectra of the other experiments, all peaks can be seen very clearly in this spectrum.

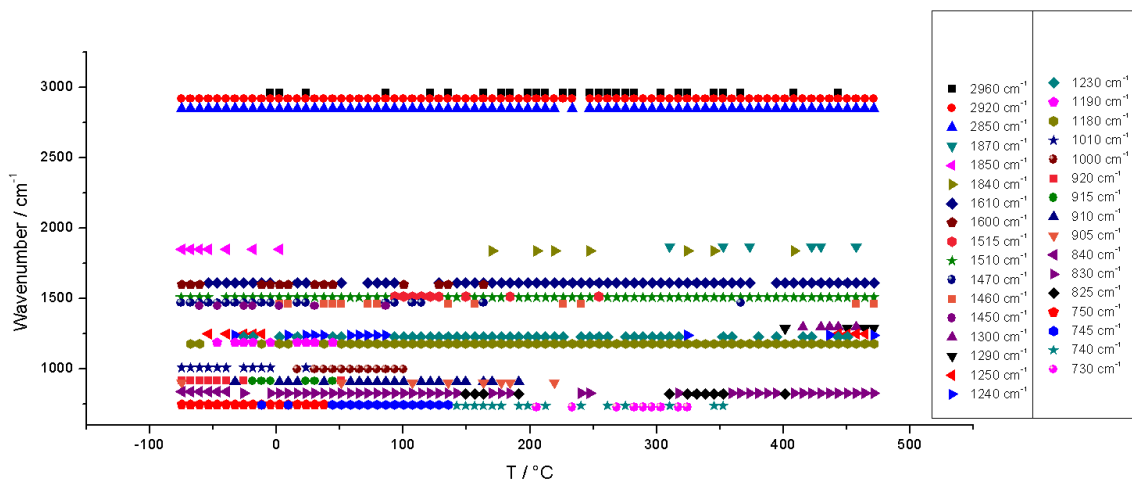


Figure 5.13.: Detected wavenumbers over temperature during methanol desorption from Pd/ZnO; 2<sup>nd</sup> experiment

| Wavenumber | Compound                 |                         |
|------------|--------------------------|-------------------------|
| 2960       | CH-stretch               | OH or CO <sub>2</sub> H |
| 2920       | CH <sub>3</sub> -stretch | CH <sub>3</sub> OH      |
| 2850       | CH-stretch               | CH <sub>3</sub> OH      |
| 1870       | CO <sub>2</sub> -stretch | CO <sub>2</sub>         |
| 1850       | CO <sub>2</sub> -stretch | CO <sub>2</sub>         |
| 1840       | CO <sub>2</sub> -stretch | CO <sub>2</sub>         |
| 1610       | CO-stretch               | CH <sub>3</sub> CO ?    |
| 1600       | CO-stretch               | CH <sub>3</sub> CO ?    |
| 1515       | bend                     | H <sub>2</sub> O        |
| 1510       | bend                     | H <sub>2</sub> O        |
| 1470       | CO-stretch               | CH <sub>2</sub> O       |
| 1460       | CO-stretch               | CH <sub>2</sub> O       |
| 1450       | CO-stretch               | CH <sub>2</sub> O       |
| 1300       | CO-stretch               | CO <sub>2</sub> H       |
| 1290       | -                        | ?                       |
| 1250       | -                        | CH <sub>2</sub> O       |
| 1240       | -                        | CH <sub>2</sub> O       |
| 1230       | -                        | CH <sub>2</sub> O       |
| 1190       | rocking vibration        | CH <sub>2</sub> O       |
| 1180       | rocking vibration        | CH <sub>2</sub> O       |
| 1010       | CO-stretch               | CH <sub>3</sub> OH      |
| 1000       | CO-stretch               | CH <sub>3</sub> OH      |
| 920        | CH <sub>2</sub> -wagging | CH <sub>2</sub> O       |
| 915        | CH <sub>2</sub> -wagging | CH <sub>2</sub> O       |
| 910        | CH <sub>2</sub> -wagging | CH <sub>2</sub> O       |
| 905        | CH <sub>2</sub> -wagging | CH <sub>2</sub> O       |
| 840        | -                        | ZnO                     |
| 830        | -                        | ZnO                     |
| 825        | -                        | ZnO                     |
| 750        | asym. stretch            | ZnO                     |
| 745        | asym. stretch            | ZnO                     |
| 740        | asym. stretch            | ZnO                     |
| 730        | asym. stretch            | ZnO                     |

Table 5.7.: Detected wavenumbers and possible compounds during the methanol desorption from Pd/ZnO; 2<sup>nd</sup> experiment

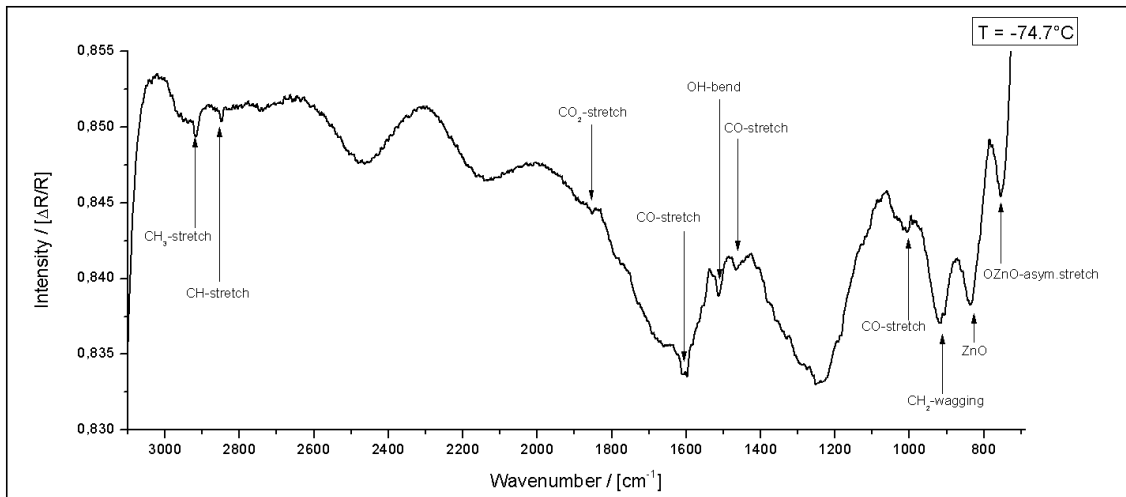


Figure 5.14.: First IR-spectrum of methanol adsorbed on Pd/ZnO; 0.5 ML ZnO-coverage; oxygen pressure during Zn-evaporation:  $5 \cdot 10^{-7}$  mbar;  $T = -74.7^\circ\text{C}$

### 3<sup>rd</sup> experiment - low O<sub>2</sub> pressure

The third ZnO-experiment was done with a ZnO coverage of 0.6 ML. The ZnO-layer was deposited under a low oxygen pressure again. The sample was cooled down to  $T = -92^\circ\text{C}$  ( $\approx 181$  K) before the measurement was started. Table 5.8 shows the wavenumbers of the detected peaks with their corresponding compounds on the sample and figure 5.15 gives an overview at which temperature each peak was detected.

Two methanol-peaks can be found. The first one is a shifting peak at  $2920\text{ cm}^{-1}$  and accordingly  $2915\text{ cm}^{-1}$ . Both wavenumbers are seen alternately between  $T = -64^\circ\text{C}$  and  $T = -8^\circ\text{C}$ . After that  $2920\text{ cm}^{-1}$  is seen at  $T = 20^\circ\text{C}$  and  $T = 27^\circ\text{C}$ . This peak is seen again fractional among  $T = 209^\circ\text{C}$  and  $T = 342^\circ\text{C}$ . The second methanol-peak is at  $1000\text{ cm}^{-1}$ . There it can be found from  $T = 27^\circ\text{C}$  until  $T = 482^\circ\text{C}$ . But as it can be seen at figure 5.15 there are breaks where this peak could not be found. So there is no  $1000\text{ cm}^{-1}$  peak between  $T = 132^\circ\text{C}$  and  $T = 167^\circ\text{C}$ , as well as between  $T = 349^\circ\text{C}$  and  $T = 433^\circ\text{C}$ . There is also a break where this peak is not seen from  $T = 440^\circ\text{C}$  till  $T = 482^\circ\text{C}$  where this peak appears for the last time.

There are two formaldehyde-peaks. The first one shifts between  $1495\text{ cm}^{-1}$  and  $1490\text{ cm}^{-1}$ . It is seen alternating among these two wavenumbers from  $T = -92^\circ\text{C}$  till  $T = -8^\circ\text{C}$ . Then this peak disappears and is not seen until  $T = 76^\circ\text{C}$  and  $T = 83^\circ\text{C}$  (at  $1495\text{ cm}^{-1}$  at both temperatures). There is also one peak at  $T = 104^\circ\text{C}$  ( $1490\text{ cm}^{-1}$ ). This peak appears again at  $T = 174^\circ\text{C}$  where it can be found alternating between both wavenumbers again till  $T = 489^\circ\text{C}$ . The second formaldehyde-peak can be found at  $905\text{ cm}^{-1}$  or rather  $900\text{ cm}^{-1}$ . It is seen first at  $900\text{ cm}^{-1}$  at  $T = 153^\circ\text{C}$ . At  $T = 258^\circ\text{C}$  it shifts to  $900\text{ cm}^{-1}$  and at higher temperatures it is alternating between these two wavenumbers till  $T = 489^\circ\text{C}$ .

One formate-peak can be found shifting between  $1350\text{ cm}^{-1}$  and  $1340\text{ cm}^{-1}$ . It can be found (with breaks) from  $T = -57^\circ\text{C}$  till  $T = 489^\circ\text{C}$ .

In this experiment two  $\text{CO}_2$ -peaks are seen. The first one seems to be a shifting one, but it is seen rarely. It can be found at  $1870\text{ cm}^{-1}$  ( $T = 90^\circ\text{C}$ ,  $111^\circ\text{C}$ ,  $125^\circ\text{C}$ ,  $132^\circ\text{C}$ ,  $167^\circ\text{C}$  and  $223^\circ\text{C}$ ) and at  $1860\text{ cm}^{-1}$  ( $T = 6^\circ\text{C}$ ,  $41^\circ\text{C}$ ,  $48^\circ\text{C}$  and  $146^\circ\text{C}$ ). The second one is alternating between  $1840\text{ cm}^{-1}$  and  $1830\text{ cm}^{-1}$ . From  $T = -78^\circ\text{C}$  until  $T = 167^\circ\text{C}$  it can be found at these two wavenumbers. A very last peak at  $1840\text{ cm}^{-1}$  is at  $T = 209^\circ\text{C}$ .

Before talking about the ZnO-peaks let us have a look at the water-peak at  $1595\text{ cm}^{-1}$  or rather  $1590\text{ cm}^{-1}$ . It can be found at  $1590\text{ cm}^{-1}$  at  $T = 76^\circ\text{C}$ ,  $83^\circ\text{C}$  and between  $T = 160^\circ\text{C}$  and  $T = 321^\circ\text{C}$ . Then it shifts to  $1595\text{ cm}^{-1}$  where it can be seen from  $T = 328^\circ\text{C}$  till  $T = 489^\circ\text{C}$ .

At last, there are two ZnO-peaks. One at  $890\text{ cm}^{-1}$  can be found from  $T = -92^\circ\text{C}$  till  $T = 216^\circ\text{C}$ . The other one is first seen at  $730\text{ cm}^{-1}$  between  $T = -85^\circ\text{C}$  and  $T = -57^\circ\text{C}$ . Then it shifts up to  $740\text{ cm}^{-1}$  where it can be found from  $T = -50^\circ\text{C}$  until  $T = 83^\circ\text{C}$ . But this peak is not staying at  $740\text{ cm}^{-1}$  all the time. Sometimes it shifts back to  $730\text{ cm}^{-1}$ . At  $T = 90^\circ\text{C}$  it shifts up to  $750\text{ cm}^{-1}$  /  $745\text{ cm}^{-1}$  where it can be found alternating at higher temperatures. Initiating from  $T = 370^\circ\text{C}$  up to higher temperatures this peak is seen around  $745\text{ cm}^{-1}$ .

Figure 5.16 shows the first IR-spectrum of this experiment at  $T = -92^\circ\text{C}$ . There are peaks at  $1495\text{ cm}^{-1}$ ,  $890\text{ cm}^{-1}$ ,  $745\text{ cm}^{-1}$ , and  $660\text{ cm}^{-1}$  whereof the peak at  $660\text{ cm}^{-1}$  could be noise as well because this wavenumber lies near to the detection limit of the used detector.

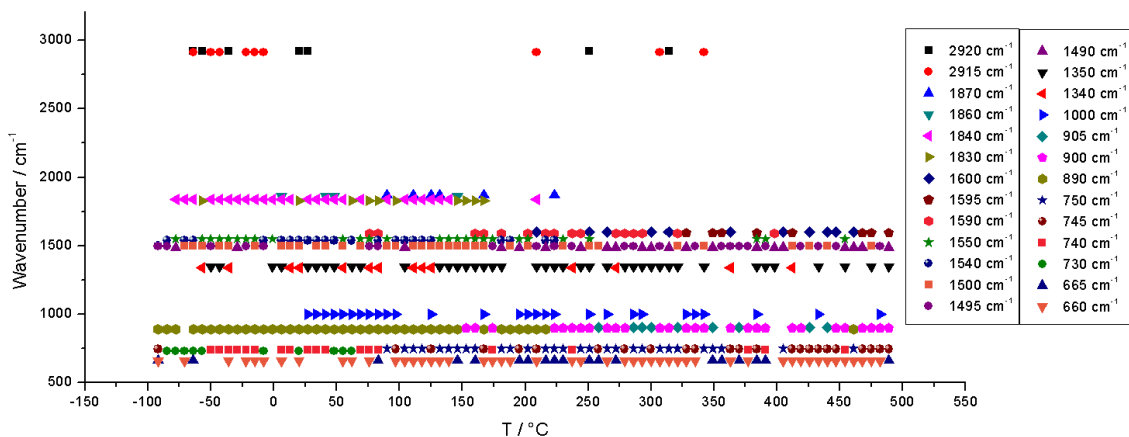


Figure 5.15.: Detected wavenumbers over temperature during methanol desorption from Pd/ZnO; 3<sup>rd</sup> experiment

| Wavenumber | Vibration                | Compound            |
|------------|--------------------------|---------------------|
| 2920       | CH <sub>3</sub> -stretch | CH <sub>3</sub> OH  |
| 2915       | CH <sub>3</sub> -stretch | CH <sub>3</sub> OH  |
| 1870       | CO <sub>2</sub> -stretch | CO <sub>2</sub>     |
| 1860       | CO <sub>2</sub> -stretch | CO <sub>2</sub>     |
| 1840       | CO <sub>2</sub> -stretch | CO <sub>2</sub>     |
| 1830       | CO <sub>2</sub> -stretch | CO <sub>2</sub>     |
| 1600       | -                        | ?                   |
| 1595       | bend                     | H <sub>2</sub> O    |
| 1590       | bend                     | H <sub>2</sub> O    |
| 1550       | CCO-stretch              | CH <sub>2</sub> CHO |
| 1540       | CCO-stretch              | CH <sub>2</sub> CHO |
| 1500       | -                        | ?                   |
| 1495       | CO-stretch               | CH <sub>2</sub> O   |
| 1490       | CO-stretch               | CH <sub>2</sub> O   |
| 1350       | CO-stretch               | CO <sub>2</sub> H   |
| 1340       | CO-stretch               | CO <sub>2</sub> H   |
| 1000       | CO-stretch               | CH <sub>3</sub> OH  |
| 905        | CH <sub>2</sub> -wagging | CH <sub>2</sub> O   |
| 900        | CH <sub>2</sub> -wagging | CH <sub>2</sub> O   |
| 890        | -                        | ZnO                 |
| 750        | asym. stretch            | ZnO                 |
| 745        | asym. stretch            | ZnO                 |
| 740        | asym. stretch            | ZnO                 |
| 730        | asym. stretch            | ZnO                 |
| 665        | -                        | ?                   |
| 660        | -                        | ?                   |

Table 5.8.: Detected wavenumbers and possible compounds during the methanol desorption from Pd/ZnO; 3<sup>rd</sup> experiment

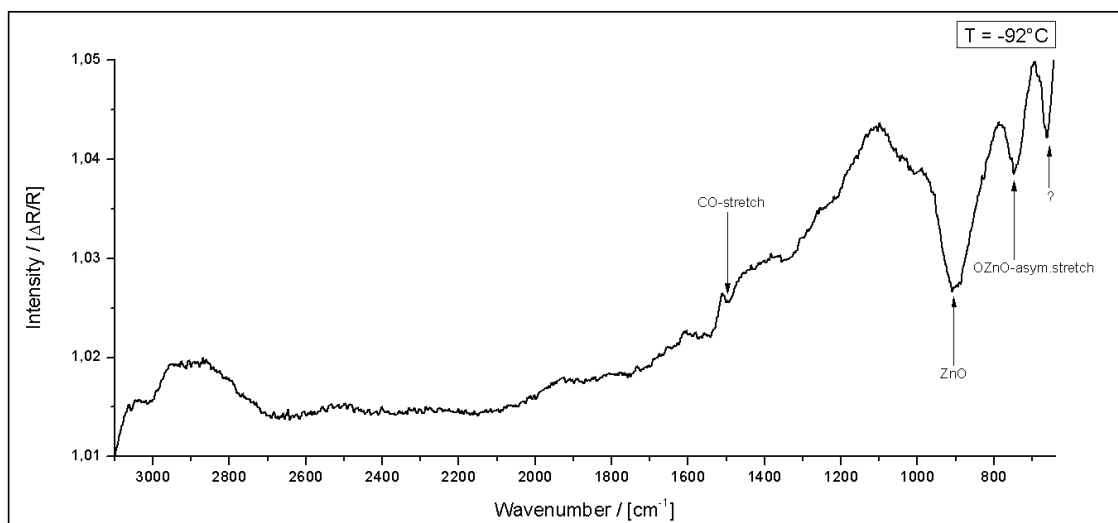


Figure 5.16.: First IR-spectrum of methanol adsorbed on Pd/ZnO; 0.6 ML ZnO-coverage; oxygen pressure during Zn-evaporation:  $5 \cdot 10^{-7}$  mbar;  $T = -92^\circ\text{C}$

#### 4<sup>th</sup> experiment - high O<sub>2</sub> pressure

The sample with a coverage of 0.6 ML of ZnO was cooled down to  $T = -66^{\circ}\text{C}$  ( $\approx 207\text{ K}$ ). The ZnO-layer was built under a high oxygen pressure. Table 5.9 shows the wavenumbers of the detected peaks with their corresponding compounds on the sample and figure 5.17 gives an overview at which temperature each peak was detected.

A methanol-peak is seen shifting between  $1070\text{ cm}^{-1}$  and  $1060\text{ cm}^{-1}$ . It can be found at  $1070\text{ cm}^{-1}$  at  $T = -66^{\circ}\text{C}$ ,  $-38^{\circ}\text{C}$  and  $-17^{\circ}\text{C}$ . From  $T = -59^{\circ}\text{C}$  till  $T = -49^{\circ}\text{C}$  it can also be found at  $1060\text{ cm}^{-1}$ .

A formate-peak can be found between  $1370\text{ cm}^{-1}$  and  $1360\text{ cm}^{-1}$ . This peak is located at  $1370\text{ cm}^{-1}$  between  $T = -66^{\circ}\text{C}$  and  $T = -59^{\circ}\text{C}$ , from  $T = 4^{\circ}\text{C}$  till  $T = 25^{\circ}\text{C}$  and from  $T = 60^{\circ}\text{C}$  until  $T = 459^{\circ}\text{C}$ . This peak shifts at  $T = 228^{\circ}\text{C}$ . Henceforward it can be found alternating between  $1370\text{ cm}^{-1}$  and  $1365\text{ cm}^{-1}$ . The second shift is seen at  $T = 291^{\circ}\text{C}$ . Here it starts to alternate between  $1370\text{ cm}^{-1}$  and  $1360\text{ cm}^{-1}$ .

There are two formaldehyde-peaks. The first one can be found at  $1460\text{ cm}^{-1}$  from  $T = -66^{\circ}\text{C}$  till  $T = 368^{\circ}\text{C}$ . The second one is shifting between  $925\text{ cm}^{-1}$  and  $920\text{ cm}^{-1}$ . First it is at  $920\text{ cm}^{-1}$  at  $T = 326^{\circ}\text{C}$ . Then it can be found at  $925\text{ cm}^{-1}$  between  $T = 347^{\circ}\text{C}$  and  $T = 424^{\circ}\text{C}$ . At  $T = 410^{\circ}\text{C}$  it starts to shift back to  $920\text{ cm}^{-1}$  where it can be found between  $T = 410^{\circ}\text{C}$  and  $T = 466^{\circ}\text{C}$ .

In this experiment a CO<sub>2</sub>-peak at  $1850\text{ cm}^{-1}$  is seen again. Between  $T = -66^{\circ}\text{C}$  and  $T = 305^{\circ}\text{C}$  it is shifting between  $1850\text{ cm}^{-1}$  and  $1845\text{ cm}^{-1}$ . There are gaps where this peak cannot be found from  $T = 144^{\circ}\text{C}$  till  $T = 165^{\circ}\text{C}$ , from  $T = 235^{\circ}\text{C}$  until  $T = 263^{\circ}\text{C}$  and from  $T = 277^{\circ}\text{C}$  till  $T = 298^{\circ}\text{C}$ .

A water-peak can be found in the range between  $1520\text{ cm}^{-1}$  and  $1510\text{ cm}^{-1}$ . It is first seen at  $1515\text{ cm}^{-1}$  between  $T = -66^{\circ}\text{C}$  and  $T = 4^{\circ}\text{C}$ . There is a shift up to  $1520\text{ cm}^{-1}$  where it is seen from  $T = -10^{\circ}\text{C}$  till  $T = 88^{\circ}\text{C}$ . At  $T = 95^{\circ}\text{C}$  this peak shifts back to  $1515\text{ cm}^{-1}$  /  $1510\text{ cm}^{-1}$  where it is alternating till  $T = 207^{\circ}\text{C}$ . Between  $T = 214^{\circ}\text{C}$  and  $T = 431^{\circ}\text{C}$  it can be found at  $1510\text{ cm}^{-1}$  again.

At last there are two ZnO-peaks. The first is shifting between  $850\text{ cm}^{-1}$  and  $840\text{ cm}^{-1}$ . Between  $T = -66^{\circ}\text{C}$  and  $T = 88^{\circ}\text{C}$  it can be found alternating between  $850\text{ cm}^{-1}$ ,  $845\text{ cm}^{-1}$  and  $840\text{ cm}^{-1}$ . At higher temperatures the peak is not seen at  $850\text{ cm}^{-1}$  anymore. At  $T = 305^{\circ}\text{C}$  and higher temperatures the peak remains at  $840\text{ cm}^{-1}$ . The second ZnO-peak can be found at  $760\text{ cm}^{-1}$  between  $T = 39^{\circ}\text{C}$  and  $T = 130^{\circ}\text{C}$ . Then it begins to shift and is seen alternating between  $760\text{ cm}^{-1}$  and  $755\text{ cm}^{-1}$  till  $T = 270^{\circ}\text{C}$ . At  $T = 277^{\circ}\text{C}$  the peak alternates between  $760\text{ cm}^{-1}$ ,  $755\text{ cm}^{-1}$  and  $750\text{ cm}^{-1}$ . From  $T = 410^{\circ}\text{C}$  it remains at  $750\text{ cm}^{-1}$ .

Figure 5.18 shows the first IR-spectrum of this experiment at  $T = -66^{\circ}\text{C}$ . There are

peaks at  $1850\text{ cm}^{-1}$ ,  $1605\text{ cm}^{-1}$ ,  $1515\text{ cm}^{-1}$ ,  $1460\text{ cm}^{-1}$ ,  $1370\text{ cm}^{-1}$ ,  $1070\text{ cm}^{-1}$ ,  $930\text{ cm}^{-1}$ ,  $840\text{ cm}^{-1}$  and  $665\text{ cm}^{-1}$ . Again the peak at  $665\text{ cm}^{-1}$  also can be noise.

| Wavenumber | Vibration                | Compound           |
|------------|--------------------------|--------------------|
| 1850       | CO <sub>2</sub> -stretch | CO <sub>2</sub>    |
| 1845       | CO <sub>2</sub> -stretch | CO <sub>2</sub>    |
| 1610       | CO-stretch               | CH <sub>3</sub> CO |
| 1605       | CO-stretch               | CH <sub>3</sub> O  |
| 1600       | CO-stretch               | CH <sub>3</sub> O  |
| 1520       | bend                     | H <sub>2</sub> O   |
| 1515       | bend                     | H <sub>2</sub> O   |
| 1510       | bend                     | H <sub>2</sub> O   |
| 1460       | CO-stretch               | CH <sub>2</sub> O  |
| 1370       | CO-stretch               | CO <sub>2</sub> H  |
| 1365       | CO-stretch               | CO <sub>2</sub> H  |
| 1360       | CO-stretch               | CO <sub>2</sub> H  |
| 1290       | umbrella                 | CH <sub>3</sub> O  |
| 1280       | umbrella                 | CH <sub>3</sub> O  |
| 1070       | CO-stretch               | CH <sub>3</sub> OH |
| 1060       | CO-stretch               | CH <sub>3</sub> OH |
| 940        | -                        | ?                  |
| 935        | -                        | ?                  |
| 930        | -                        | ?                  |
| 925        | CH <sub>2</sub> -wagging | CH <sub>2</sub> O  |
| 920        | CH <sub>2</sub> -wagging | CH <sub>2</sub> O  |
| 850        | -                        | ZnO                |
| 845        | -                        | ZnO                |
| 840        | -                        | ZnO                |
| 760        | asym. stretch            | ZnO                |
| 755        | asym. stretch            | ZnO                |
| 750        | asym. stretch            | ZnO                |
| 670        | -                        | ?                  |
| 665        | -                        | ?                  |
| 660        | -                        | ?                  |

Table 5.9.: Detected wavenumbers and possible compounds during the methanol desorption from Pd/ZnO; 4<sup>th</sup> experiment

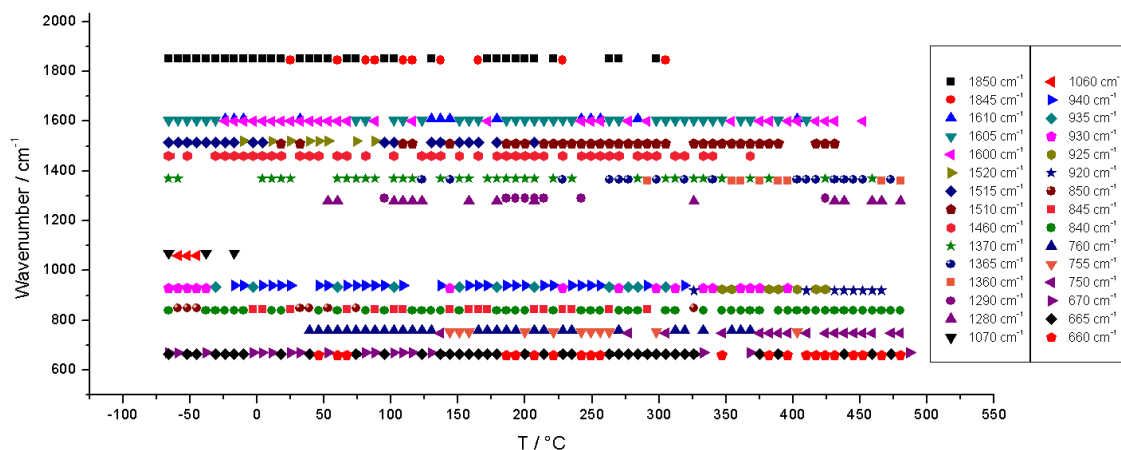


Figure 5.17.: Detected wavenumbers over temperature during methanol desorption from Pd/ZnO; 4<sup>th</sup> experiment

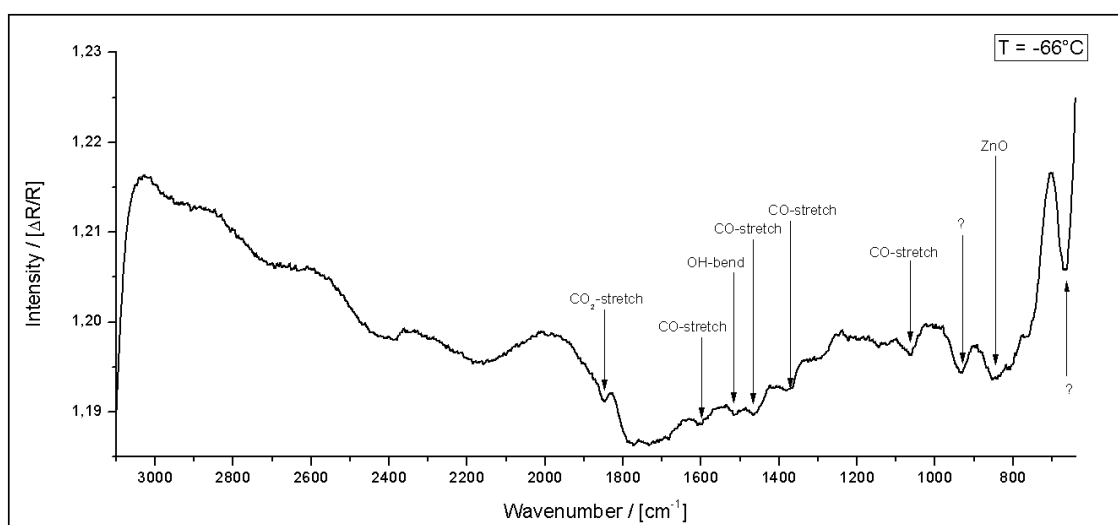


Figure 5.18.: First IR-spectrum of methanol adsorbed on Pd/ZnO; 0.6 ML ZnO-coverage; oxygen pressure during Zn-evaporation:  $1 \cdot 10^{-5}$  mbar;  $T = -66^\circ\text{C}$

### 5<sup>th</sup> experiment - high O<sub>2</sub> pressure

In this experiment a ZnO coverage of 0.3 ML was given and the sample was cooled down to  $T = -72.5^{\circ}\text{C}$  ( $\approx 200.5\text{ K}$ ). The ZnO-layer was deposited under a high oxygen pressure again. Table 5.10 shows the wavenumbers of the detected peaks with their corresponding compounds on the sample and figure 5.19 gives an overview at which temperature each peak was detected.

Two methanol-peaks can be found. The first one is at  $2915\text{ cm}^{-1}$  between  $T = -51.5^{\circ}\text{C}$  and  $T = 32.5^{\circ}\text{C}$ . A very last peak is at  $T = 174.5^{\circ}\text{C}$ . The second methanol-peak shifts between  $1020\text{ cm}^{-1}$  and  $1005\text{ cm}^{-1}$ . The first peak is at  $1005\text{ cm}^{-1}$  at a temperature of  $T = 67.5^{\circ}\text{C}$ . Then it can be found alternating between this wavenumber and  $1010\text{ cm}^{-1}$  from  $T = 172.5^{\circ}\text{C}$  till  $T = 284.5^{\circ}\text{C}$ . At  $1010\text{ cm}^{-1}$  it can be found between  $T = 179.5^{\circ}\text{C}$  and  $T = 333.5^{\circ}\text{C}$ . This peak shifts to  $1020\text{ cm}^{-1}$  where it can be seen from  $T = 361.5^{\circ}\text{C}$  until  $T = 431.5^{\circ}\text{C}$ . The last two peaks are at  $T = 438.5^{\circ}\text{C}$  ( $1010\text{ cm}^{-1}$ ) and  $T = 480.5^{\circ}\text{C}$  ( $1005\text{ cm}^{-1}$ ).

In this experiment one can find two formate-peaks. The first one at  $2960\text{ cm}^{-1}$  may also be an OH-peak. It can be seen between  $T = -58.5^{\circ}\text{C}$  and  $T = 11.5^{\circ}\text{C}$ . The second one shifts from  $1320\text{ cm}^{-1}$  up to  $1340\text{ cm}^{-1}$ . First it is seen at  $1330\text{ cm}^{-1}$  at  $T = -65.5^{\circ}\text{C}$ . Then it lies at  $1320\text{ cm}^{-1}$  from  $T = 172.5^{\circ}\text{C}$  until  $T = 207.5^{\circ}\text{C}$  where it shifts to  $1330\text{ cm}^{-1}$ . It is alternating between  $1320\text{ cm}^{-1}$  and  $1330\text{ cm}^{-1}$  till  $T = 298.5^{\circ}\text{C}$ . There it shifts to  $1340\text{ cm}^{-1}$  where it can be found till  $T = 480.5^{\circ}\text{C}$ . There is a gap from  $T = 389.5^{\circ}\text{C}$  till  $T = 445.5^{\circ}\text{C}$  where this peak disappears.

At  $1260\text{ cm}^{-1}$  there is a peak between  $T = -72.5^{\circ}\text{C}$  and  $T = 18.5^{\circ}\text{C}$  which can be a CO<sub>2</sub> - or a formaldehyde-peak. There is definitely a formaldehyde-peak at  $905\text{ cm}^{-1}$  at low temperature ( $T = -72.5^{\circ}\text{C}$  till  $T = 32.5^{\circ}\text{C}$ ) which shifts to  $910\text{ cm}^{-1}$  where it can be found till  $T = 333.5^{\circ}\text{C}$ . Then it shifts again at  $T = 347.5^{\circ}\text{C}$  and can be seen alternating between  $920\text{ cm}^{-1}$  and  $925\text{ cm}^{-1}$  until  $T = 445.5^{\circ}\text{C}$ . The last two peaks are at  $T = 473.5^{\circ}\text{C}$  ( $905\text{ cm}^{-1}$ ) and  $T = 480.5^{\circ}\text{C}$  ( $910\text{ cm}^{-1}$ ).

A CO<sub>2</sub>-peak can be found shifting between  $1840\text{ cm}^{-1}$  and  $1835\text{ cm}^{-1}$  in a temperature range from  $T = -58.5^{\circ}\text{C}$  till  $T = 109.5^{\circ}\text{C}$ .

ZnO can be found between  $745\text{ cm}^{-1}$  and  $715\text{ cm}^{-1}$ . At low temperature ( $T = -72.5^{\circ}\text{C}$  till  $T = 32.5^{\circ}\text{C}$ ) the ZnO-peak lies at  $715\text{ cm}^{-1}$  /  $720\text{ cm}^{-1}$ . Then there is a shift and this peak is seen at  $725\text{ cm}^{-1}$  /  $730\text{ cm}^{-1}$  between  $T = 53.5^{\circ}\text{C}$  and  $T = 193.5^{\circ}\text{C}$ . Then there is a second shift up to  $730\text{ cm}^{-1}$  /  $735\text{ cm}^{-1}$  till this peak is found at  $740\text{ cm}^{-1}$  at  $T = 438.5^{\circ}\text{C}$ . There it remains till  $T = 466.5^{\circ}\text{C}$ .

Figure 5.20 shows the first IR-spectrum of this experiment at  $T = -72.5^{\circ}\text{C}$ . There are peaks at  $2960\text{ cm}^{-1}$ ,  $1260\text{ cm}^{-1}$ ,  $905\text{ cm}^{-1}$ ,  $720\text{ cm}^{-1}$ . The rest seems to be noise.

| Wavenumber | Vibration                | Compound                             |
|------------|--------------------------|--------------------------------------|
| 2960       | CH-stretch               | CO <sub>2</sub> H                    |
| 2915       | CH <sub>3</sub> -stretch | CH <sub>3</sub> OH                   |
| 1840       | CO <sub>2</sub> -stretch | CO <sub>2</sub>                      |
| 1835       | CO <sub>2</sub> -stretch | CO <sub>2</sub>                      |
| 1340       | CO-stretch               | CO <sub>2</sub> H                    |
| 1330       | CO-stretch               | CO <sub>2</sub> H                    |
| 1320       | CO-stretch               | CO <sub>2</sub> H                    |
| 1260       | rocking vibration        | CO <sub>2</sub> or CH <sub>2</sub> O |
| 1020       | CO-stretch               | CH <sub>3</sub> OH                   |
| 1010       | CO-stretch               | CH <sub>3</sub> OH                   |
| 1005       | CO-stretch               | CH <sub>3</sub> OH                   |
| 925        | CH <sub>2</sub> -wagging | CH <sub>2</sub> O                    |
| 920        | CH <sub>2</sub> -wagging | CH <sub>2</sub> O                    |
| 910        | CH <sub>2</sub> -wagging | CH <sub>2</sub> O                    |
| 905        | CH <sub>2</sub> -wagging | CH <sub>2</sub> O                    |
| 745        | asym. stretch            | ZnO                                  |
| 735        | asym. stretch            | ZnO                                  |
| 730        | asym. stretch            | ZnO                                  |
| 725        | asym. stretch            | ZnO                                  |
| 720        | asym. stretch            | ZnO                                  |
| 715        | asym. stretch            | ZnO                                  |

Table 5.10.: Detected wavenumbers and possible compounds during the methanol desorption from Pd/ZnO; 5<sup>th</sup> experiment

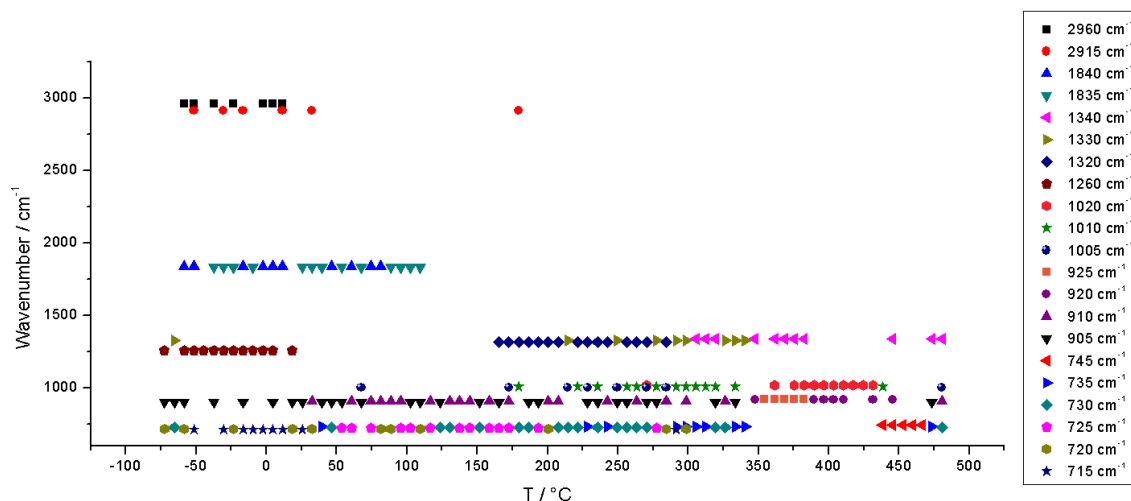


Figure 5.19.: Detected wavenumbers over temperature during methanol desorption from Pd/ZnO; 5<sup>th</sup> experiment

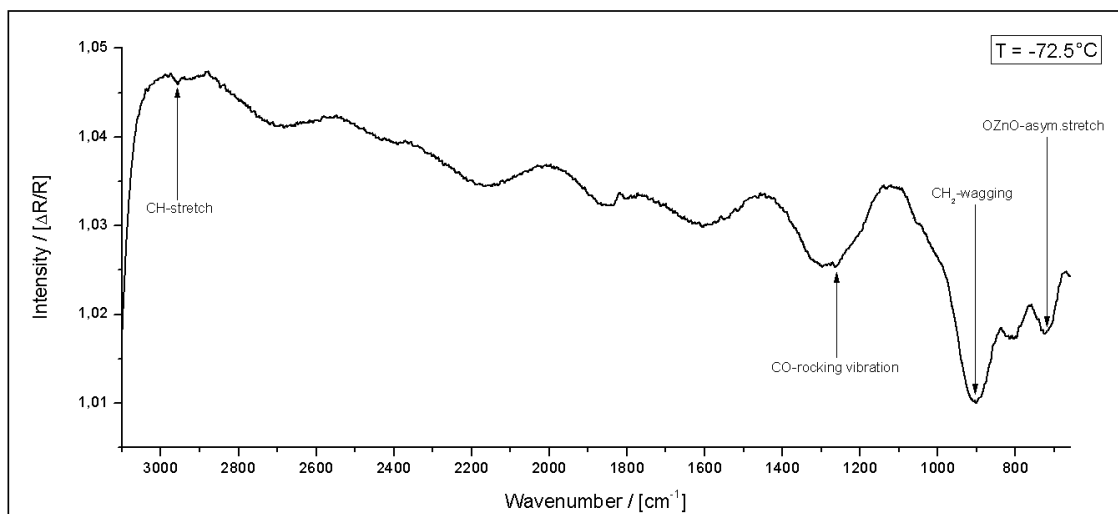


Figure 5.20.: First IR-spectrum of methanol adsorbed on Pd/ZnO; 0.3 ML ZnO-coverage; oxygen pressure during Zn-evaporation:  $1 \cdot 10^{-5}$  mbar;  $T = -72.5^\circ\text{C}$

### 6<sup>th</sup> experiment - high O<sub>2</sub> pressure

In the last experiment the sample had a ZnO coverage of 0.3 ML and was cooled down to  $T = -104.7^\circ\text{C}$  ( $\approx 168\text{ K}$ ). The ZnO-layer was deposited under a high oxygen pressure. Table 5.11 shows the wavenumbers of the detected peaks with their corresponding compounds on the sample and figure 5.21 gives an overview at which temperature each peak was detected.

Three methanol-peaks can be found. The first one shifts between  $3015\text{ cm}^{-1}$  and  $3000\text{ cm}^{-1}$ . It can be seen from  $T = -104.7^\circ\text{C}$  till  $T = 294.3^\circ\text{C}$ . The peak shifts from  $3000\text{ cm}^{-1}$  (low temperature) to  $3015\text{ cm}^{-1}$  (high temperature). The second methanol-peak at  $2940\text{ cm}^{-1}$  can be found between  $T = -104.7^\circ\text{C}$  and  $T = -76.7^\circ\text{C}$ . At last there is a methanol-peak alternating between  $1005\text{ cm}^{-1}$  and  $1000\text{ cm}^{-1}$  whereas it is seen at  $1000\text{ cm}^{-1}$  at  $T = 98.3^\circ\text{C}$  for the first time. A peak representing formate is seen alternating among  $1340\text{ cm}^{-1}$  and  $1350\text{ cm}^{-1}$ . This shifting peak can be found over the whole temperature range.

From  $T = -97.7^\circ\text{C}$  till  $T = 147.3$  there is a formaldehyde-peak which shifts from  $915\text{ cm}^{-1}$  (low temperature) to  $905\text{ cm}^{-1}$  (high temperature). Above  $T = 77.3^\circ\text{C}$  it remains at  $905\text{ cm}^{-1}$ . There are also peaks at  $910\text{ cm}^{-1}$  at  $T = 231.3^\circ\text{C}$  and  $T = 483.3^\circ\text{C}$  as well as at  $905\text{ cm}^{-1}$  at  $T = 441.3^\circ\text{C}$  and  $T = 476.3^\circ\text{C}$ . A gap is given between  $T = 154.3^\circ\text{C}$  and  $T = 231.3^\circ\text{C}$  and between  $T = 238.3^\circ\text{C}$  and  $T = 441.3^\circ\text{C}$ .

A CO<sub>2</sub>-peak is seen at  $1860\text{ cm}^{-1}$  which shifts up to  $1870\text{ cm}^{-1}$ . It is found at  $1860\text{ cm}^{-1}$  from  $T = -104.7^\circ\text{C}$  until  $T = 63.3^\circ\text{C}$ . Between  $T = -83.7^\circ\text{C}$  and  $T = -48.7^\circ\text{C}$  as well as from  $T = 70.3^\circ\text{C}$  till  $T = 259.3^\circ\text{C}$  it is seen at  $1870\text{ cm}^{-1}$ .

At last there are two ZnO-Peaks. The first one shifts from  $840\text{ cm}^{-1}$  (seen from  $T = -104.7^\circ\text{C}$  till  $T = 231.3^\circ\text{C}$ ) down to  $835\text{ cm}^{-1}$  (from  $T = -83.7^\circ\text{C}$  till  $T = 315.3^\circ\text{C}$ ) and at last down to  $830\text{ cm}^{-1}$  (from  $T = 183.3^\circ\text{C}$  till  $T = 476.3^\circ\text{C}$ ). So there is a shift from  $840\text{ cm}^{-1}$  at low temperature down to  $830\text{ cm}^{-1}$  at high temperature. The second ZnO-peak shows nearly the same behavior. It shifts from  $750\text{ cm}^{-1}$  at low temperature down to  $740\text{ cm}^{-1}$  at high temperature. In detail it is seen at  $750\text{ cm}^{-1}$  from  $T = -104.7^\circ\text{C}$  till  $T = 259.3^\circ\text{C}$ , at  $745\text{ cm}^{-1}$  from  $T = 196.3^\circ\text{C}$  till  $T = 329.3^\circ\text{C}$  and at  $740\text{ cm}^{-1}$  from  $T = 315.3^\circ\text{C}$  till  $T = 483.3^\circ\text{C}$ .

Figure 5.22(a) shows the first IR-spectrum of this experiment at  $T = -104.7^\circ\text{C}$ . There are peaks at  $3015\text{ cm}^{-1}$ ,  $2940\text{ cm}^{-1}$ ,  $1860\text{ cm}^{-1}$ ,  $1335\text{ cm}^{-1}$ ,  $1005\text{ cm}^{-1}$ ,  $910\text{ cm}^{-1}$ ,  $840\text{ cm}^{-1}$ ,  $740\text{ cm}^{-1}$  and  $665\text{ cm}^{-1}$ . Figure 5.22(b) shows the area between  $3100\text{ cm}^{-1}$  and  $2400\text{ cm}^{-1}$  in more detail to have a better view of the first two peaks. Figure 5.22(c) shows the area between  $2000\text{ cm}^{-1}$  and  $1000\text{ cm}^{-1}$ . As it can be seen in figure 5.22(a) and (c) there is lots of noise between wavenumber  $1800\text{ cm}^{-1}$  and  $1350\text{ cm}^{-1}$  which arises again from water on the window between measurement chamber and detector. This makes it difficult to identify peaks in this area.

| Wavenumber | Vibration                | Compound           |
|------------|--------------------------|--------------------|
| 3015       | CH <sub>3</sub> -stretch | CH <sub>3</sub> OH |
| 3010       | CH <sub>3</sub> -stretch | CH <sub>3</sub> OH |
| 3000       | CH <sub>3</sub> -stretch | CH <sub>3</sub> OH |
| 2940       | CH <sub>3</sub> -stretch | CH <sub>3</sub> OH |
| 1870       | CO <sub>2</sub> -stretch | CO <sub>2</sub>    |
| 1860       | CO <sub>2</sub> -stretch | CO <sub>2</sub>    |
| 1340       | CO-stretch               | CO <sub>2</sub> H  |
| 1335       | CO-stretch               | CO <sub>2</sub> H  |
| 1330       | CO-stretch               | CO <sub>2</sub> H  |
| 1005       | CO-stretch               | CH <sub>3</sub> OH |
| 1000       | CO-stretch               | CH <sub>3</sub> OH |
| 915        | CH <sub>2</sub> -wagging | CH <sub>2</sub> O  |
| 910        | CH <sub>2</sub> -wagging | CH <sub>2</sub> O  |
| 905        | CH <sub>2</sub> -wagging | CH <sub>2</sub> O  |
| 840        | -                        | ZnO                |
| 835        | -                        | ZnO                |
| 830        | -                        | ZnO                |
| 750        | asym. stretch            | ZnO                |
| 745        | asym. stretch            | ZnO                |
| 740        | asym. stretch            | ZnO                |
| 670        | -                        | ?                  |
| 665        | -                        | ?                  |
| 660        | -                        | ?                  |

Table 5.11.: Detected wavenumbers and possible compounds during the methanol desorption from Pd/ZnO; 6<sup>th</sup> experiment

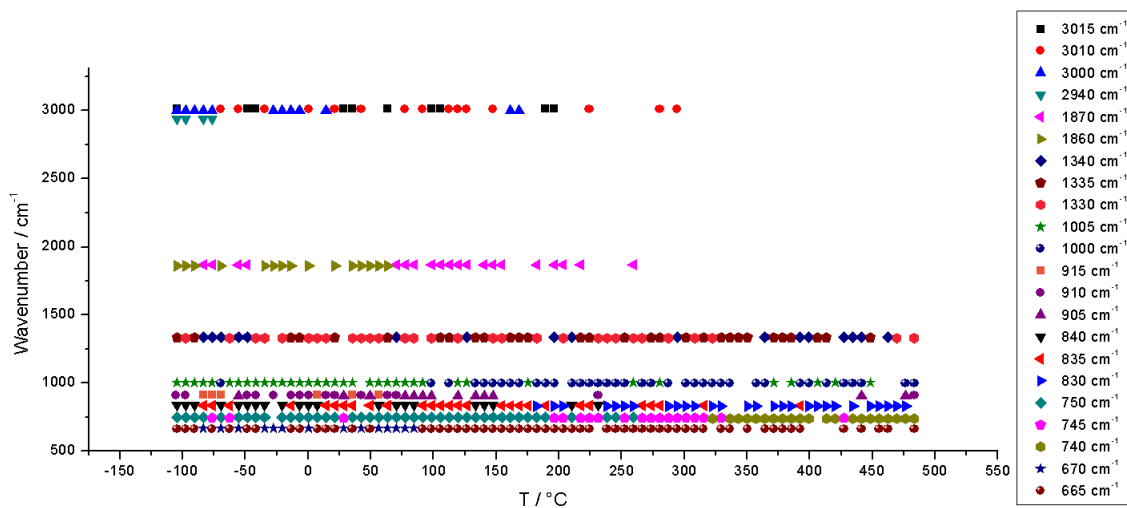


Figure 5.21.: Detected wavenumbers over temperature during methanol desorption from Pd/ZnO; 6<sup>th</sup> experiment

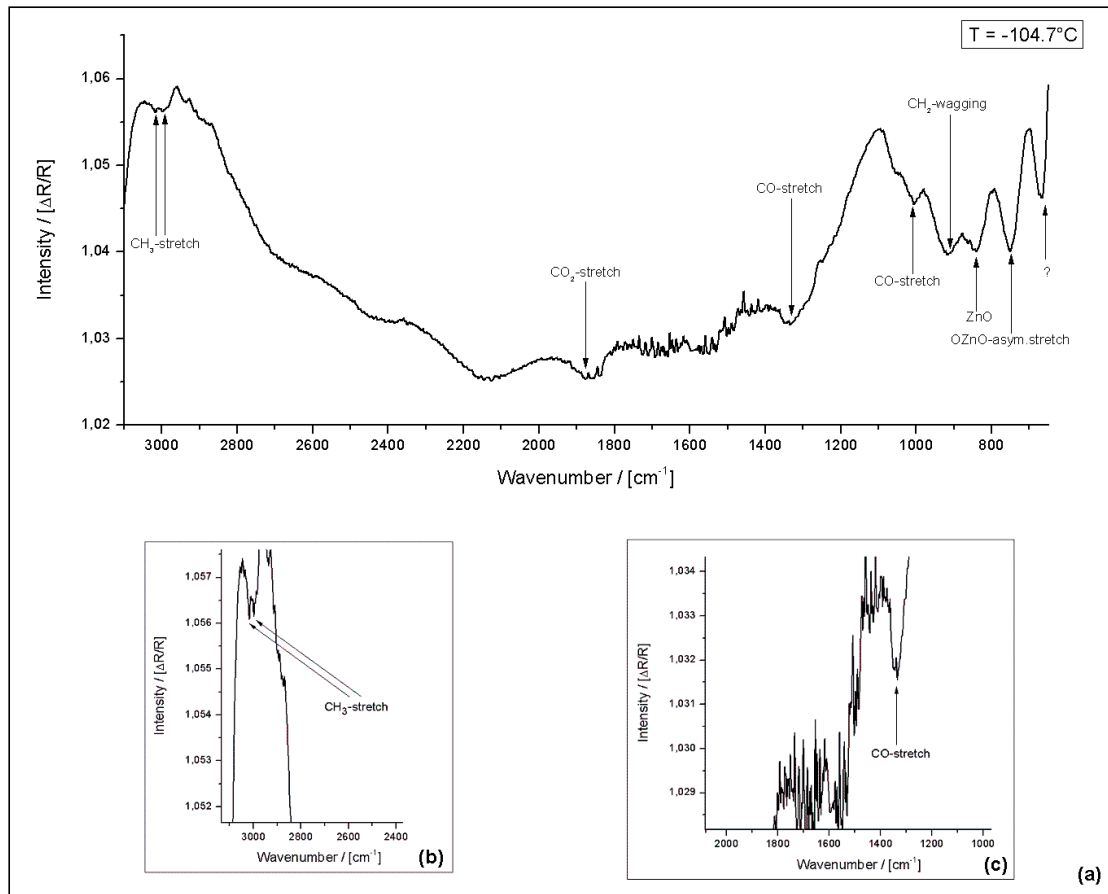


Figure 5.22.: First IR-spectrum of methanol adsorbed on Pd/ZnO; 0.3 ML ZnO-coverage; oxygen pressure during Zn-evaporation:  $1 \cdot 10^{-5}$  mbar;  $T = -104.7^\circ\text{C}$

### Discussion - Pd/ZnO-measurements

In this measurement series methanol desorption from Pd/ZnO was investigated. Four experiments with high oxidized and two experiments with low oxidized ZnO were done. The results are similar to the Pd/Zn measurement series. Again, methanol desorption from Pd/ZnO seems to be a complex process which is heavily dependent from the temperature at which methanol exposition takes place. As one can see in figures 5.12, 5.14, 5.16, 5.18, 5.20 and 5.22 the first IR-spectrum at lowest temperature always looks different. A reason for this is the temperature which is reached for methanol exposition. A second reason is that at each experiment a different surface structure is given.

In all experiments except for the first one, the CO stretching vibration around  $1000\text{ cm}^{-1}$  is seen. This peak indicates together with peaks around  $2920\text{ cm}^{-1}$  the presence of methanol. The peak around  $2920\text{ cm}^{-1}$  which stems from the for  $\text{CH}_3$ -stretch vibration is seen over the whole temperature range in the first two experiments. Only at low temperature it is seen in experiment 3, 5 and 6. It is never seen at experiment 4. In the 4<sup>th</sup> experiment only a temperature of  $T = -66^\circ\text{C}$  is reached. Maybe this is the reason why no peak at  $2920\text{ cm}^{-1}$  is seen. Why there is sometimes methanol seen at high temperatures is unclear. Maybe the IR-beam hits the measurement chamber before striking the detector. Figure 5.23 shows the measurement configuration for the IR experiments. In this figure the window between the measurement chamber (window 1) and the detector window (window 2) are shown. Possible adsorbats are water at the detector window (window 2) and methanol on the window between the chambers (window 1). So methanol which is adsorbed at window 1 is the second reason why there is sometimes methanol seen at high temperature in the IR-spectrum. These two reasons could affect the results in this measurement series.

Another species which is seen in all experiments is formaldehyde. There are  $\text{CH}_2$ -wagging vibrations around  $910\text{ cm}^{-1}$  which can be seen at low temperature as well as at high temperature. Together with formate, which is also seen over the whole temperature range, this could be an evidence that there is methanol adsorbed on the window between the measurement chamber and the detector (see window 1 in figure 5.23) or that the IR-beam grazes the chamber wall.

In all experiments there is one or more peaks seen around  $1830\text{ cm}^{-1}$  which represent  $\text{CO}_2$  stretch vibrations. These peaks always show a different behavior. For example it is seen only at low temperatures in the 4<sup>th</sup>, 5<sup>th</sup> and 6<sup>th</sup> experiment. In the first experiment it is seen only at high temperatures and in the second one it is seen over the whole temperature range. In all experiments different ZnO coverages are given because the desorption rate was not measurable with the QMB. Although the sample was nitrogen cooled the temperature which was reached during sample cooling was also different in each experiment. The reasons for this are unknown. Because these terms of condition (temperature, ZnO coverage) are always different it is very difficult to say what the reasons for this behavior are.

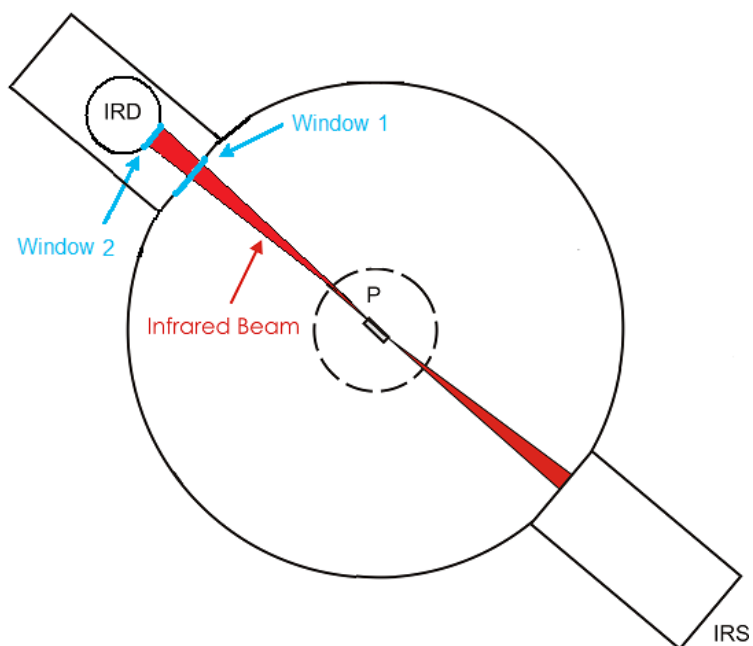


Figure 5.23.: Illustration of the measurement chamber the infrared detector and the windows; adapted from [6]  
IRS - Infrared source  
P - Sample  
IRD - Infrared detector  
Window 1 - Window between chamber and detector  
Window 2 - Detector window

## 5.2. IR - Summary

RAIRS measurements were done to get an overview of the reaction paths of methanol dissociation on Pd(111), Pd/Zn and Pd/ZnO with low and high oxidized ZnO layers. For this reason methanol desorption from Pd(111), Pd/Zn and Pd/ZnO was studied via IR-spectroscopy in situ. It turned out that the reaction process on Pd/ZnO is much more complicated than expected. Because methanol is only weakly bound on the surface the whole process is sensitive to the temperature where methanol adsorption takes place. Due to the characteristic of ZnO layers the surface structure is never the same. So even if the conditions (coverage, temperature) are the same in two experiments, the surface structure is different. This also effects the bonding mechanism of methanol on the surface.

# 6. IR/TDS - Comparison

## 6.1. Introduction

In order to get a better understanding of the reaction processes on the sample surface the IR and TDS results have to be compared. To do this, it is necessary that the experiments which are compared were done under the same conditions. Because these terms could not be well controlled, only two experiments offer nearly the same temperature and ZnO coverage:

1<sup>st</sup> ZnO experiment of the 1<sup>st</sup> TDS measurements series with 0.4 ML of high oxidized ZnO at  $T = -109.5^{\circ}\text{C}$  (see figure 4.3) and the 6<sup>th</sup> IR experiment of methanol desorption from high oxidized ZnO with 0.3 ML coverage at  $T = -104.7^{\circ}\text{C}$  (see figures 5.21 and 5.22).

These two experiments are compared to gain more information on the reactions on the sample surface. In both experiments the sample was heated but with different heating rates. In the TDS experiments a heating rate of 1 K/s was given, and in the IR experiments there was a heating rate of 0.1 K/s. So in the IR experiments the heating rate was much smaller. To compare both experiments one has to consider that a smaller heating rate leads to a broadening of the peak. In the same way a smaller heating rate leads to a shift of the peak maxima to lower temperatures. To get an idea how much the peak is affected by the different heating rates a Matlab program (see appendix A) was used. This program was written by Dr. DI. Hans Peter Koch and modified for this application [40].

Figure 6.1 shows the simulation of the thermo desorption spectra of methanol which was obtained in the experiment (see figure 4.3(b)). The desorption energy  $E_d$  was calculated via equation 2.16 with the following parameters, which were given in the experiment:  $T_m$  was set to 270 K and  $\beta = 1$  K/s. Using these parameters one obtains a desorption energy of  $E_d = 71594$  Joule. This desorption energy was used to calculate the desorption rate according to the Polanyi Wigner equation in the matlab routine. In figure 6.1 the desorption of methanol from PdZnO with different heating rates is shown. The blue line shows the desorption using a heating rate of 1 K/s, the red one shows the desorption using a heating rate of 0.1 K/s. Figure 6.1(a) shows the desorption rate vs. the temperature. There one can see how the peak shifts using different heating rates. The peak maxima of the blue line lies at 269 K ( $= 4^{\circ}\text{C}$ ) which fits very well with the experiment (peak maxima at  $T = 3^{\circ}\text{C}$ , see figure 4.3(b)). This peak shifts to 251.6 K if a heating rate of 0.1 K/s is used. So there is a shift of  $T = 17.4$  K. The Full Width at

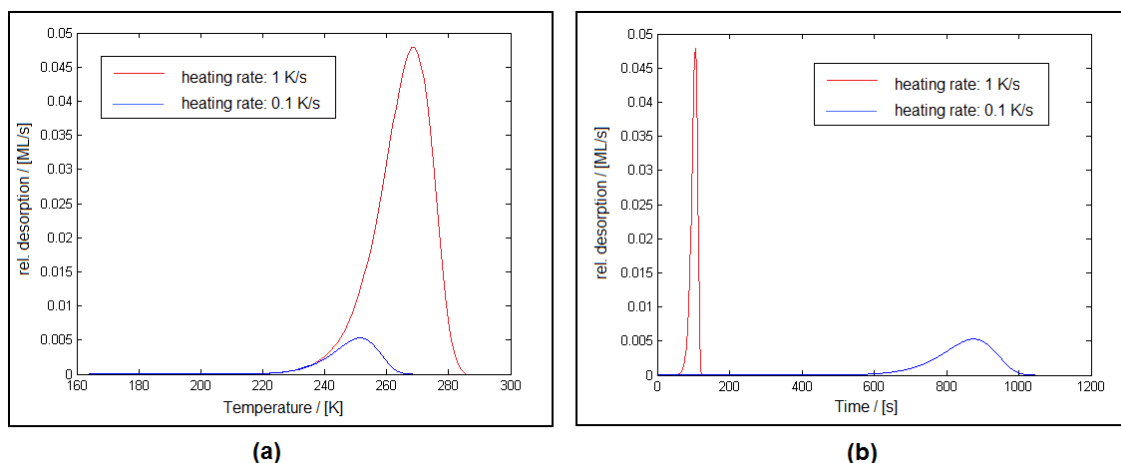


Figure 6.1.: Calculated TDS of methanol from PdZnO using different heating rates; (a) rel. desorption rate vs. temperature, (b) rel. desorption rate vs. time

Half Maximum (FWHM) which is calculated by the matlab routine, too is given to 17.2 (blue line) and 19.1 (red line). Figure 6.1(b) shows the desorption rate vs. the time. There one can see that using a higher heating rate will lead to an earlier desorption of the adsorbate. Using a heating rate of 1 K/s the peak maximum is reached after 106 seconds. By contrast the maximum is reached after 888 seconds using a heating rate of 0.1 K/s.

The results of the calculation are as follows:

Using a heating rate of 0.1 K/s instead of 1 K/s leads to a shift of  $T = 17.4^{\circ}\text{C}$  to higher temperatures. In contrast, the FWHM is affected by the different heating rate just a little bit. There is a change of the FWHM of 1.9 which can be neglected. This means that species which are seen in the TDS are seen in the IR-spectra around temperatures 17.4 K lower than in the TDS. With this knowledge it is possible to compare the TDS- and IR-measurements in spite of the different heating rates.

## 6.2. Discussion

### 6.2.1. IR/TDS-results: Methanol

There are peaks representing methanol at  $3015\text{ cm}^{-1}$ ,  $3010\text{ cm}^{-1}$ ,  $3000\text{ cm}^{-1}$ ,  $2940\text{ cm}^{-1}$ ,  $1005\text{ cm}^{-1}$  and  $1000\text{ cm}^{-1}$  (shown in figure 5.22). The peaks around  $3000\text{ cm}^{-1}$  are seen from  $T = -104.7^{\circ}\text{C}$  till  $T = 200^{\circ}\text{C}$ . These peaks would shift to  $T = 217^{\circ}\text{C}$  if a heating rate of 1 K/s would have been used instead of 0.1 K/s. In the TDS-measurement the first methanol peak was seen from  $T = -109.5^{\circ}\text{C}$  till  $T = 216^{\circ}\text{C}$ . The peak maximum lies at  $T = 3^{\circ}\text{C}$ . This temperature reign fits very well with the temperature reign where methanol is seen in the IR-experiment.

The peaks around  $3000\text{ cm}^{-1}$  are seen again at higher temperature. The last peak lies at  $T = 294.3^\circ\text{C}$ . The second methanol-peak in the TDS is seen at  $T = 409^\circ\text{C}$ . It starts at  $T = 216^\circ\text{C}$  and goes till  $700^\circ\text{C}$ . So there are two possible reasons:

1. The second TDS peak does not arise from the sample itself but from the sample holder. This is the reason why no methanol is seen in the IR at this temperature
2. The TDS peak arises from the sample surface. It is not seen in the IR-spectrum because the peaks around  $3000\text{ cm}^{-1}$  are very small. So it is possible that they are not seen because of the bad signal-to-noise ratio.

Around  $200^\circ\text{C}$  there should not be any methanol on the sample left, so the first argument is more probable than the second one. The CO-stretch peaks around  $1000\text{ cm}^{-1}$  are seen over the whole temperature range (see figure 5.21). The reasons therefore are manifold. As already mentioned maybe methanol or methanol fragments are adsorbed on the window between measurement chamber and detector as well. This would affect the results and could be the reason why this peak at  $1000\text{ cm}^{-1}$  is seen all the time.

### 6.2.2. IR/TDS-results: Formaldehyde

As already said in chapter 4, no formaldehyde which arises from methanol dissociation is seen in the TDS. The detected mass 29 is a methanol fragment which is formed in the QMS. The desorption curve of mass 29 looks like the methanol desorption curve. So the first peak lies between  $T = -109.5^\circ\text{C}$  and  $T = 216^\circ\text{C}$  with its maximum at  $T = 3^\circ\text{C}$ . In the IR-spectrum  $\text{CH}_2$ -wagging vibration peaks are seen around  $910\text{ cm}^{-1}$  (from  $T = -97.7^\circ\text{C}$  till  $T = 147.3^\circ\text{C}$ ). So it is seen in the same range than the first TDS-peak of mass 29. Unlike to the TDS-peak the IR peak disappears at  $T = 147.3^\circ\text{C}$  which results in  $T = 165.1^\circ\text{C}$  if a heating rate of  $1\text{ K/s}$  would have been used. This value lies beyond the measurement error. So maybe real formaldehyde is seen in the IR-measurement. This would mean that formaldehyde is a reaction intermediate on the surface, which does not desorb.

There are also some  $\text{CH}_2$ -wagging vibration peaks seen at higher temperature which may rise again from methanol fragments adsorbed on the sample or maybe from fragments adsorbed on the window between measurement chamber and detector. No IR-peaks are seen in the temperature range where the second TDS-peak is found.

### 6.2.3. IR/TDS-results: Formate

Formate is seen around  $1335\text{ cm}^{-1}$  over the whole temperature range. At first glance it seems again that methanol or rather methanol fragments were adsorbed on the window between chamber and detector (window1 in figure 5.23) or that the IR-beam grazes somewhere at the chamber surface. This would mean that there is formate adsorbed on the chamber walls. In figure 4.3(d) the desorption curve of formate is shown. On closer examination one can see that after the formate peak disappears at  $T = 70^\circ\text{C}$  there is a

slight increase of the signal again. Hence the formate-peaks in the IR-spectra seem to be real formate peaks.

#### 6.2.4. IR/TDS-results: Carbon dioxide

Carbon dioxide peaks around  $1870\text{ cm}^{-1}$  are seen from  $T = -104.7^\circ\text{C}$  till  $T = 259.3^\circ\text{C}$  (at higher temperature they are only seen fractional before they disappear). The exponential decay of the background (see figure 4.3(c)) makes it difficult to compare these peaks with the TDS results. Carbon dioxide is seen till  $T = 409^\circ\text{C}$  in TDS which does not fit with the IR-results even if the different heating rate is considered. Additionally carbon dioxide is seen from  $T = 409^\circ\text{C}$  till  $T = 800^\circ\text{C}$  in TDS. This slope at high temperature could again be  $\text{CO}_2$  desorption from the sample holder which affects the TDS-results. The difference between the IR- and TDS-results in the mid. temperature range could arise of the large background which is seen in TDS. This background leads to a deformation of the desorption peaks. Therefore the results look different even if they are not.

#### 6.2.5. IR/TDS-results: Remaining species

No water was seen in this IR-experiment. ZnO was seen over the whole temperature range which is obvious because Zn desorption starts only around  $600^\circ\text{C}$  (see [20]).

# 7. Summary

## 7.1. Pyridine adsorption on Pd/ZnO

In order to check if the surface of Pd/ZnO shows different oxide-terminations, pyridine adsorption on Pd/ZnO was investigated by IR-spectroscopy as well as pyridine desorption from different ZnO layers on Pd(111) by TDS. Up to now it was assumed that ZnO shows a wurzit-structure on Pd(111). This would be a reason why there were 2 ML ZnO islands with different height seen in the STM. So two different ZnO layers were formed on Pd(111):

1. low oxidized ZnO: Zn evaporation at an oxygen pressure of  $5 \cdot 10^{-8}$  mbar (first surface layer probably consists of Zn and O)
2. high oxidized ZnO: Zn evaporation at an oxygen pressure of  $1 \cdot 10^{-5}$  mbar (first surface layer consists of O - the whole surface is oxygen covered)

In the first case there should be a different termination, if ZnO shows a wurzit-structure on Pd(111). In the second experiment (high oxidized ZnO) there should be the whole surface covered by oxygen. After the ZnO layers were formed pyridine was adsorbed on the sample because it goes into physisorption with oxygen and into chemisorption with metal-atoms. This different type of bond with its different bond strength has to lead to a shift of the peaks in the IR- and TPD-spectrum. After pyridine was adsorbed to the sample an IR-spectrum was made before the pyridine desorption was investigated by TDS.

The investigations have shown that ZnO does not form a wurzit-structure on Pd(111) because there were no differences in the IR- or TDS-spectra rather there was low or high oxidized ZnO. So it is assumed that there is no different termination. This result fits very well with the newest calculations [41] which have shown that ZnO forms a boron-nitride-structure on Pd(111) up to 4 ML. The difference in height of the 2 ML islands, which was seen in STM, might occur because of OH-groups on the surface.

## 7.2. Methanol desorption from Pd(111), Pd/Zn and Pd/ZnO

Methanol dissociation and desorption from Pd(111), Pd/Zn and Pd/ZnO (low and high oxidized) was investigated by IR-spectroscopy and TDS to get an overview of the chemical reaction processes. Therefore several experiments were done which have shown that the reaction processes are very complex. It was not possible to gain general information of the reaction paths on the different samples because the conditions were always different (coverage, temperature). The amount of Zn which was evaporated onto the sample could not be controlled by a QMB (see chapter 2.8). Additionally, it was not possible to reach the same minimum temperature in all experiments. As a result of this the spectra always look different and it is difficult to compare experiments with each other. Nevertheless, some conclusions can be drawn.

Below 1 ML coverage (whether Zn or ZnO) formate desorption at low temperatures was seen in TDS. At the same temperature there was Zn desorption seen, too. So the formate desorption leads to a zinc desorption at temperatures where no zinc desorption is expected. This effect was not seen at a Zn-coverage above 1 ML. So it seems that this reaction occurs at the Pd/Zn or rather Pd/ZnO interfaces. An effect which was only seen above 1 ML ZnO coverage was oxygen desorption at  $T = 738^{\circ}\text{C}$ . Because of the large methanol-background no formaldehyde, which arises from methanol dissociation, was seen.

More difficult to interpret are the IR-spectroscopy results. In nearly all experiments methanol was seen at temperatures where no methanol is expected on the sample. It is impossible that there is methanol on the sample left at temperatures around  $400^{\circ}\text{C}$ . The same was seen for formate. So it seems that there was methanol adsorbed on the window between measurement chamber and detector as well which affected the results. In addition, maybe the IR-beam grazes the chamber wall before it hits the detector. This would be another reason for these results. It is seen again, that the whole reaction process is extremely sensitive to the temperature where methanol adsorption takes place.

The two IR- and TDS-experiments which were comparable have shown some correlations.

Formaldehyde was seen in the IR-spectrometer. So it could be that formaldehyde is a reaction intermediate on the surface which does not desorb. This is why it was not seen in TDS. Formate was seen in both experiments, IR and TDS, at low temperatures. So this could be a real reaction product of the methanol dissociation. These results are evidences that the species seen in IR and in TDS really are players in the reaction pathway.

# Bibliography

- [1] <http://de.wikipedia.org/wiki/Brennstoffzelle>; downloaded on 25.02.2010.
- [2] N. Iwasa, T. Akazawa, S. Ohyama, K. Fujikawa, N. Takezawa. Dehydrogenation of methanol to methyl format over supported Ni, Pd and Pt catalyst. Anomalous catalytic functions of PdZn and PtZn alloys. *Reaction Kinetics and Catalysis Letters*, 55:245, 1995.
- [3] N. Iwasa, S. Kudo, H. Takahashi, S. Masuda, N. Takezawa. Highly selective supported Pd catalysts for steam reforming of methanol. *Catalysis Letters*, 19:221, 1993.
- [4] C. Fukuhara, Y. Kamata, A. Igarashi. Catalytic performance of plate-type Pd/Zn based catalysts for steam reforming of methanol, prepared by electroless plating. *Applied Catalysis A: General*, 330:108, 2007.
- [5] N. Iwasa, S. Masuda, N. Ogawa, N. Takezawa. Steam reforming of methanol over Pd/ZnO: Effect of the formation of PdZn alloys upon the reaction. *Applied Catalysis A: General*, 125:145 – 157, 1995.
- [6] H.P. Koch. *Experimental and Theoretical Investigation of the Interaction of simple Molecules with Rhodium, Copper and Palladium/Zinc Surfaces*. PhD thesis, Graz University of Technology, 2009.
- [7] G. Krenn. *Die Wechselwirkung von Methanol, Kohlenmonoxid und Wasserstoff mit Rh(111) und Rhodium-Vanadium-Legierungsoberflächen*. PhD thesis, Graz University of Technology, 2005.
- [8] *Specs ErLEED User Manual 1.3*.
- [9] G. Ertl, J. Küppers. *Low Energy Electrons and Surfacechemistry Vol.4*. Verlag Chemie, 1974.
- [10] <http://en.wikipedia.org/wiki/File:Slide1.PNG>; downloaded on 24.07.2009.
- [11] [http://www.specs.de/cms/upload/PDFs/SPECS\\_Prospekte/Leed\\_EQ.pdf](http://www.specs.de/cms/upload/PDFs/SPECS_Prospekte/Leed_EQ.pdf); downloaded on 24.07.2009.
- [12] C.D. Wagner, W.M. Riggs, L.E. Davis, J.F. Moulder, G.E. Muilenberg. *Handbook of X-ray photoelectron spectroscopy*. Perkin-Elmer Corporation, 1978.

- [13] <http://elchem.kaist.ac.kr/vt/chem-ed/ms/graphics/quad-sch.gif>; downloaded on 03.08.2009.
- [14] A.J.B. Robertson. *Mass Spectrometry*. Methian Co. Ltd., London, 1954.
- [15] H.P. Koch. RAIRS investigation of methanol dehydrogenation on Rh and Rh/V surfaces. Master thesis, Graz University of Technology, 2005.
- [16] P.A. Redhead. Thermal desorption of gases. *Vacuum*, 12:203, 1962.
- [17] C.M. Chan, R. Aris, W.H. Weinberg. An analysis of thermal desorption mass spectra 1. *Applications of Surface Science*, 1:360 – 376, 1978.
- [18] C.M. Chan, W.H. Weinberg. An analysis of thermal desorption mass spectra 2. *Applications of Surface Science*, 1:377 – 387, 1978.
- [19] A. Tamtögl. Adsorption and Desorption Processes on Clean and Zn-Modified Pd(111). Master thesis, Graz University of Technology, 2008.
- [20] H. Gabasch, A. Knop-Gericke, R. Schlögl, S. Penner, B. Jenewein, K. Hayek, B. Klötzer. Zn Adsorption on Pd(111): ZnO and PdZn alloy formation. *The Journal of Physical Chemistry B*, 110:11391 – 11398, 2006.
- [21] H.P. Koch, I. Bako, G. Weirum, M. Kratzer, R. Schennach. A theoretical study of Zn adsorption and desorption on a Pd(111) substrate. *Surface Science*, 2010. DOI:10.1016/j.susc.2010.02.022.
- [22] M. Kratzer. *Reaction Kinetics & Dynamics of H<sub>2</sub>, O<sub>2</sub> and CO on modified Pd(111) surfaces*. PhD thesis, Graz University of Technology, 2009.
- [23] M.Kratzer, A.Tamtögl, J.Killmann, R.Schennach, A.Winkler. Preparation and calibration of ultrathin Zn layers on Pd(1 1 1). *Applied Surface Science*, 255:5755–5759, 2009, DOI:10.1016/j.apsusc.2008.12.083.
- [24] G. Weirum, S. Surnev. STM study of Pd/ZnO.
- [25] G. Weirum, G. Barcaro, A. Fortunelli, R. Schennach, S. Surnev, F.P. Netzer. Growth and stability of Zn oxide layers on a Pd(111) surface. in preparation.
- [26] [http://www.ksi-meinsberg.de/finished\\_projects/glasmetallisierung/bild\\_11e8a298.png](http://www.ksi-meinsberg.de/finished_projects/glasmetallisierung/bild_11e8a298.png) downloaded on 16.11.2009.
- [27] L.M. Parker, D.M. Bibby, G.R. Burns. Fourier-transform Infrared Study of Pyridine sorbed on Zeolite HY. *J. Chem. SOC., Faraday Trans.*, 87 (19):3319–3323, 1991.
- [28] K.B. Wiberg, V.A. Walters, K.N. Wong, S.D. Colson. Azines: vibrational force field and intensities for pyridine. *The Journal of Physical Chemistry*, 88 (24):6067–6075, 1984.

- [29] M.P. Andersson, P. Uvdal. Transformation of Pyridine to O-Pyridyl on W(110) As Probed by Vibrational Spectroscopy: Experiments and Calculations. *The Journal of Physical Chemistry B*, 105:9458–9462, 2001.
- [30] V.H. Grassian, E.L. Muettterties. Vibrational electron energy loss spectroscopic study of benzene, toluene, and pyridine adsorbed on palladium(111) at 180 K. *The Journal of Physical Chemistry*, 91(2):389 – 396, 1987.
- [31] [http://www.plamsa.de/de/plasma\\_wissenswertes/part2.html](http://www.plamsa.de/de/plasma_wissenswertes/part2.html); downloaded on 20.08.2009.
- [32] S. Surnev. private communications.
- [33] R. Schennach, A. Eichler, K.D. Rendulic. Adsorption and Desorption on Pd(111) and on Pd/V Surface Alloy. *The Journal of Physical Chemistry B*, 107:2552 – 2558, 2003.
- [34] E. Jeroro, J.M. Vohs. Zn Modification of the Reactivity of Pd(111) Toward Methanol and Formaldehyde. *Journal of American Chemical Society*, 130:10199 – 10207, 2008.
- [35] E. Demirci, A. Winkler. Quantitative determination of reaction products by in-line thermal desorption spectroscopy: The system methanol/Pd(111). *Journal of Vacuum Science & Technology A*, 26:78 – 82, Jan/Feb 2008.
- [36] J.J. Chen, Z.C. Jiang, Y. Zhou, B.R. Chakraborty, N. Winograd. Spectroscopic study of methanol decomposition on Pd(111). *Surface Science*, 328:248 – 262, 1995.
- [37] H.P. Koch, I. Bako, R. Schennach. Adsorption of small molecules on a (2x1) PdZn surface alloy on Pd(111). *Surface Science*, 640:595–607, 2010.
- [38] <http://webbook.nist.gov/chemistry/vib-ser.html>.
- [39] E. Jeroro, J.M. Vohs. Zn Modification of the Reactivity of Pd(111) toward Methanol and formaldehyde. *Journal of American Chemical Society*, 130:10199 – 10207, 2008.
- [40] H.P. Koch. private communications.
- [41] A. Fortunelli. private communications.

# List of Figures

|       |  |    |
|-------|--|----|
| 1.1.  | Schematic description of a PEMFC . . . . .   | 2  |
| 2.1.  | UHV-chamber; Red line divides the machine into lower and higher level .  | 5  |
| 2.2.  | UHV chamber and measuring instruments at lower level; adapdet from [6]   | 7  |
| 2.3.  | UHV Chamber and measuring instruments at upper level; adapdet from [6]   | 8  |
| 2.4.  | The Pd(111) sample, mounted on the manipulator . . . . .   | 9  |
| 2.5.  | Schematic diagram of an LEED; adapted from [10] . . . . .  | 10 |
| 2.6.  | Block diagram of the ErLEED . . . . .  | 11 |
| 2.7.  | Schematic view of the ErLEED150 optics and the LEED flange; adapted from [11] . . . . .                                | 12 |
| 2.8.  | Scattering of a plane wave at a one-dimensional periodic lattice; adapted from [9] . . . . .                           | 12 |
| 2.9.  | Schematic diagram of the experimental arrangement for photoelectron spectroscopy of solids; adapted from [9] . . . . . | 14 |
| 2.10. | Energy level diagram for XPS; adapted from [9] . . . . .   | 15 |
| 2.11. | X-ray spectrum of Pd . . . . .   | 15 |
| 2.12. | Schematic view of a Quadrupole Mass-Spectrometer; adapted from [13] .  | 16 |
| 2.13. | Schematic view of the optical path of the infrared light; adapted from [15]  | 18 |
| 2.14. | Scheme of a Michelson interferometer . . . . .   | 18 |
| 2.15. | Schematic description how to get an FT-IR spectrum . . . . .   | 20 |
| 2.16. | Illustration of the different kinds of desorption spectra . . . . .  | 21 |
| 2.17. | TDS which was used to calculate the area of 1 ML zinc coverage . . . . .   | 22 |
| 3.1.  | LEED-pattern of a clean Pd(111) surface with corresponding crystallographic directions . . . . .                       | 24 |
| 3.2.  | ZnO island formation on Pd(111) . . . . .  | 25 |
| 3.3.  | STM- and LEED- picture of the (6x6) structure of ZnO; 0.7 ML coverage; adapted from [24] . . . . .                     | 26 |
| 3.4.  | STM- and LEED- picture of the (4x4) structure of ZnO; 0.7 ML coverage; adapted from [24] . . . . .                     | 26 |
| 3.5.  | STM picture of ZnO and the apparent height of the islands; 1.5 ML coverage   | 28 |
| 3.6.  | Wurzit-structure; adapted from [26] . . . . .  | 28 |
| 3.7.  | Schematic illustration of the two possible terminations of ZnO in the wurzit-structure . . . . .                       | 29 |
| 3.8.  | The two possible bond-typs of pyridine on ZnO depending on the termination . . . . .                                   | 29 |
| 3.9.  | IR- and TPD- spectra of pyridine on ZnO high and low oxidized . . . . .  | 30 |

|   |    |
|---|----|
| 3.10. Boron-nitride-structur of ZnO; adapted from [31] . . . . .  | 30 |
| 4.1. Methanol spectrum during adsorbtion . . . . .  | 33 |
| 4.2. Thermal desorption spectra of methanol desorption from Pd/Zn (Zinc coverage: 0.6 ML) . . . . .   | 35 |
| 4.3. Thermal desorption spectra of methanol desorption from Pd/ZnO (ZnO coverage: 0.4 ML; oxygen pressure during Zn-evaporation: $1 \cdot 10^{-5}$ mbar) .  | 37 |
| 4.4. Thermal desorption spectra of methanol desorption from Pd/ZnO (ZnO coverage: 0.6 ML oxygen pressure during Zn-evaporation: $5 \cdot 10^{-7}$ mbar) .   | 39 |
| 4.5. Thermal desorption spectra of methanol desorption from Pd - 1 <sup>st</sup> experiment   | 41 |
| 4.6. Thermal desorption spectra of methanol desorption from Pd - 2 <sup>nd</sup> experiment . . . . .   | 43 |
| 4.7. TDS of mass 64 desorption from Pd; Comparison of the two Pd-methanol-TDS-experiments . . . . .   | 44 |
| 4.8. The Pd(111) sample mounted on the copper holder; . . . . .   | 46 |
| 4.9. TDS of the 1 <sup>st</sup> Measurement series . . . . .  | 48 |
| 4.10. Thermal desorption spectra of methanol desorption from Pd/ZnO (ZnO coverage: 0.8 ML; oxygen pressure during Zn-evaporation: $1 \cdot 10^{-5}$ mbar) . | 50 |
| 4.11. Thermal desorption spectra of methanol desorption from Pd/ZnO (ZnO coverage: 2.2 ML; oxygen pressure during Zn-evaporation: $1 \cdot 10^{-5}$ mbar) . | 52 |
| 4.12. TDS of the 2 <sup>st</sup> Measurement series . . . . .   | 55 |
| 4.13. Thermal desorption spectra of methanol desorption from Pd - 3 <sup>rd</sup> Measurement series . . . . .  | 57 |
| 4.14. Thermal desorption spectra of methanol desorption from Pd/ZnO (ZnO coverage: 0.3 ML; oxygen pressure during Zn-evaporation: $1 \cdot 10^{-5}$ mbar) . | 59 |
| 4.15. TDS of the 3 <sup>rd</sup> Measurement series . . . . .   | 61 |
| 5.1. Detected wavenumbers over temperature during methanol desorption from Pd . . . . .   | 65 |
| 5.2. First IR-spectrum of methanol adsorbed on Pd at T = -97°C . . . . .  | 65 |
| 5.3. Detected wavenumbers over temperature during methanol desorption from Pd/Zn; 1 <sup>st</sup> experiment . . . . .                                      | 67 |
| 5.4. First IR-spectrum of methanol adsorbed on Pd/Zn; 0.7 ML; T = -87°C .   | 67 |
| 5.5. Detected wavenumbers over temperature during methanol desorption from Pd/Zn; 2 <sup>nd</sup> experiment . . . . .                                      | 69 |
| 5.6. First IR-spectrum of methanol adsorbed on Pd/Zn; 0.4 ML Zn; T = -100°C   | 70 |
| 5.7. Detected wavenumbers over temperature during methanol desorption from Pd/Zn; 3 <sup>nd</sup> experiment . . . . .                                      | 72 |
| 5.8. First IR-spectrum of methanol adsorbed on Pd/Zn; 0.8 ML Zn; T = -84.5°C  | 73 |
| 5.9. Detected wavenumbers over temperature during methanol desorption from Pd/Zn; 4 <sup>th</sup> experiment . . . . .                                      | 75 |
| 5.10. First IR-spectrum of methanol adsorbed on Pd/Zn; 0.7 ML Zn; T = -86°C   | 76 |
| 5.11. Detected wavenumbers over temperature during methanol desorption from Pd/ZnO; 1 <sup>st</sup> experiment . . . . .                                    | 81 |

---

|  |     |
|--|-----|
| 5.12. First IR-spectrum of methanol adsorbed on Pd/ZnO; 0.7 ML ZnO-coverage; oxygen pressure during Zn-evaporation: $1 \cdot 10^{-5}$ mbar; $T = -74.4^{\circ}\text{C}$ . . . .  | 82  |
| 5.13. Detected wavenumbers over temperature during methanol desorption from Pd/ZnO; 2 <sup>nd</sup> experiment . . . . .   | 84  |
| 5.14. First IR-spectrum of methanol adsorbed on Pd/ZnO; 0.5 ML ZnO-coverage; oxygen pressure during Zn-evaporation: $5 \cdot 10^{-7}$ mbar; $T = -74.7^{\circ}\text{C}$ . . . .  | 86  |
| 5.15. Detected wavenumbers over temperature during methanol desorption from Pd/ZnO; 3 <sup>rd</sup> experiment . . . . .   | 87  |
| 5.16. First IR-spectrum of methanol adsorbed on Pd/ZnO; 0.6 ML ZnO-coverage; oxygen pressure during Zn-evaporation: $5 \cdot 10^{-7}$ mbar; $T = -92^{\circ}\text{C}$ . . . .    | 89  |
| 5.17. Detected wavenumbers over temperature during methanol desorption from Pd/ZnO; 4 <sup>th</sup> experiment . . . . .   | 92  |
| 5.18. First IR-spectrum of methanol adsorbed on Pd/ZnO; 0.6 ML ZnO-coverage; oxygen pressure during Zn-evaporation: $1 \cdot 10^{-5}$ mbar; $T = -66^{\circ}\text{C}$ . . . .    | 92  |
| 5.19. Detected wavenumbers over temperature during methanol desorption from Pd/ZnO; 5 <sup>th</sup> experiment . . . . .   | 94  |
| 5.20. First IR-spectrum of methanol adsorbed on Pd/ZnO; 0.3 ML ZnO-coverage; oxygen pressure during Zn-evaporation: $1 \cdot 10^{-5}$ mbar; $T = -72.5^{\circ}\text{C}$ . . . .  | 95  |
| 5.21. Detected wavenumbers over temperature during methanol desorption from Pd/ZnO; 6 <sup>th</sup> experiment . . . . .   | 97  |
| 5.22. First IR-spectrum of methanol adsorbed on Pd/ZnO; 0.3 ML ZnO-coverage; oxygen pressure during Zn-evaporation: $1 \cdot 10^{-5}$ mbar; $T = -104.7^{\circ}\text{C}$ . . . . | 98  |
| 5.23. . . . .  | 100 |
| 6.1. Calculated TDS of methanol from PdZnO using different heating rates .   | 103 |

# List of Tables

|       |  |    |
|-------|--|----|
| 4.1.  | Detected mass and corresponding species in each TDS . . . . .  | 33 |
| 4.2.  | Start- and end-temperature of the formate and the zinc peak in the first series of measurement . . . . .                     | 47 |
| 5.1.  | Detected wavenumbers and possible compounds during the methanol desorption from Pd . . . . .                                 | 64 |
| 5.2.  | Detected wavenumbers and possible compounds during the methanol desorption from Pd/Zn; 1 <sup>st</sup> experiment . . . . .  | 66 |
| 5.3.  | Detected wavenumbers and possible compounds during the methanol desorption from Pd/Zn; 2 <sup>nd</sup> experiment . . . . .  | 69 |
| 5.4.  | Detected wavenumbers and possible compounds during the methanol desorption from Pd/Zn; 3 <sup>rd</sup> experiment . . . . .  | 72 |
| 5.5.  | Detected wavenumbers and possible compounds during the methanol desorption from Pd/Zn; 4 <sup>th</sup> experiment . . . . .  | 75 |
| 5.6.  | Detected wavenumbers and possible compounds during the methanol desorption from Pd/ZnO; 1 <sup>st</sup> experiment . . . . . | 80 |
| 5.7.  | Detected wavenumbers and possible compounds during the methanol desorption from Pd/ZnO; 2 <sup>nd</sup> experiment . . . . . | 85 |
| 5.8.  | Detected wavenumbers and possible compounds during the methanol desorption from Pd/ZnO; 3 <sup>rd</sup> experiment . . . . . | 88 |
| 5.9.  | Detected wavenumbers and possible compounds during the methanol desorption from Pd/ZnO; 4 <sup>th</sup> experiment . . . . . | 91 |
| 5.10. | Detected wavenumbers and possible compounds during the methanol desorption from Pd/ZnO; 5 <sup>th</sup> experiment . . . . . | 94 |
| 5.11. | Detected wavenumbers and possible compounds during the methanol desorption from Pd/ZnO; 6 <sup>th</sup> experiment . . . . . | 97 |

# A. Appendix - Matlab Program and Calculated Values

The matlab program calculates the desorption rate according to the Polanyi Wigner equation (2.15) for the given parameters. The desorption rate is computed for two different heating rates (1 K/s and 0.1 K/s). The used desorption energy was calculated according to the Redhead equation (2.16) for first order of desorption. The starting temperature of desorption is set to 270 K and a coverage of 1 ML is given. Together with the calculated desorption energy the program simulates the first methanol-peak shown in figure 4.3(b) for different heating rates.

The program will calculate the desorption rate for the given parameters and will plot it versus the temperature (saved in  $T_{vector}$ ) and versus time (saved in  $numb(k)$ ). The temperature is raised in each step according to the heating rate ( $T = T + \beta$ ). In the same way the coverage falls ( $coverage = coverage - r_{des}$ ). The temperature where the peaks have their maximum is calculated and displayed too.

The second part of the program calculates the FWHM of the desorption curves. Using linear interpolation, the points  $x_1$  ( $T_{unten}$ ) and  $x_2$  ( $T_{oben}$ ) where the function has reached the half of its maximum are found. The FWHM is then given by the difference  $T_{oben}$  minus  $T_{unten}$ .

## The Program Code

```
#####  
% Desorption_END.m  
% Author: Hans Peter Koch  
% Last modified: 01.03.2010 by Frederik Weber  
#####  
clear all; close all;  
% y-achse: rel. desorption rate  
% x-achse: Temperature or Time  
N_0=10^15; %number of particles on the surface  
coverage=1; %Coverage
```

```

#####
%Input-Parameters of the Polanyi-Wigner Equation
#####
E_des=71594; %Desorptionsenergy, calculated by the Redhead equation
nu_1=10^13; %Frequency-Parameter
R=8.314472; %Joule per mol Kelvin
T_initial=164;%Starting temperatre
betav=[0.1,1];%Heating rate

jmax=0; % counter variable
numb=zeros(1,length(betav));

#####
%Polanyi Wigner Equation, first order
#####
jmax=0;%Zählvaribale
numb=zeros(1,length(betav));
for k=1:length(betav)
    T=T_initial;
    beta=betav(k);
    j=1;

    while (coverage>=100000000000/N_0)

        %Polanyi Wigner Equation
        r_des=coverage.^1.*nu_1*exp(-E_des./(R.*T));
        %write everything in one vector - temperaure vector:
        T_vector(j+jmax)=T;
        T=T+beta;
        %write everything in one vector - coverage vector;
        coverage=coverage-r_des;
        R_des(j+jmax)=r_des;
        j=j+1;

    end
    jmax=jmax+j-1;
    numb(k)=j-1;
end
#####
% Plot 1: Temperature as x-axis
#####
n1=1;
n2=0;
figure(1);
for m=1:length(betav)

```

```

n2=numb(m)+n2;
plot(T_vector(n1:n2),R_des(n1:n2));hold on
n1=numb(m)+n1;
end

#####
% Plot 2: time as x-axis
#####
n1=1;
n2=0;
figure(2);
for m=1:length(betav)
n2=numb(m)+n2;
plot(1:numb(m),R_des(n1:n2));hold on
n1=numb(m)+n1;
end

#####
%Peak-Maximum of desorption
#####
n1=1;
n2=0;
for m=1:length(betav)
n2=numb(m)+n2;
rmax=max(R_des(n1:n2));
for i=n1:n2
    if (rmax==R_des(i))
        T_max(m)=T_vector(i);%Peakmaxima
    end
end
n1=numb(m)+n1;
end
T_max % T_max display
#####
%Modification, for FWHM calculation
#####
n1=1;
n2=0;

for m=1:length(betav)
    n2=numb(m)+n2;

    count=0;

    for i=n1:n2

```

```
%intaploation between the values
T_vector_neu=linspace(T_vector(n1),T_vector(n2),30000);
R_des_inter=interp1(T_vector(n1:n2),R_des(n1:n2),T_vector_neu);
%search for values
for j=1:length(R_des_inter)
    if (R_des_inter(j)<max(R_des_inter)/2) && (count==0)
        T_unten=T_vector_neu(j);
    elseif (R_des_inter(j)>=max(R_des_inter)/2) && (count==0)
        T_unten1=T_vector_neu(j);
        count=1;
    elseif (R_des_inter(j)>=max(R_des_inter)/2) && (count==1)
        T_oben=T_vector_neu(j);
    elseif count==1
        T_oben1=T_vector_neu(j);
        count=2;
    else
        break
    end
end

end

end

#####
%Calculation of FWHM
#####
    T_halbwertsbreite(m)=T_oben-T_unten1;
    T_halbwertsbreite1(m)=T_oben1-T_unten;
    n1=numb(m)+n1;

end

T_halbwertsbreite
T_halbwertsbreite1
```